Coral species-specific loss and physiological legacy effects are elicited by extended marine heatwave

Strand, E.L.[1*], Wong, K.H.[1,2], Farraj, A.[1], Gray, S.[1], McMenamin, A.[1], Putnam, H.M.[1]

[1] University of Rhode Island
[2] Department of Marine Biology and Ecology, University of Miami Rosenstiel School of Marine and Atmospheric Science, 4600 Rickenbacker Causeway, Miami, FL, 33149, USA.
[*]corresponding author

Key Words

- Physiological legacy
- Double-stressor experiment
- Thermal and ocean acidification tolerance
- Coral-algal symbiosis
- Multivariate statistics
- Symbiodiniaceae communities
- Stress and recovery periods

Abstract

Marine heatwaves are increasing in frequency and intensity, with potentially catastrophic consequences for marine ecosystems such as coral reefs. An extended heatwave and recovery time-series that incorporates multiple stressors and is environmentally realistic can provide enhanced predictive capacity for performance under climate change conditions. We exposed common reef-building corals in Hawai‘i, *Montipora capitata* and *Pocillopora acuta*, to a 2-month period of high temperature and high pCO_2 conditions or ambient conditions in a factorial design, followed by 2 months of ambient conditions. High temperature, rather than high pCO_2, drove multivariate physiology shifts through time in both species, including decreases in respiration rates and endosymbiont densities. *Pocillopora acuta* exhibited more significantly negatively altered physiology, and substantially higher bleaching and mortality than *M. capitata*. The sensitivity of *P. acuta* appears to be driven by higher baseline rates of photosynthesis paired with

lower host antioxidant capacity, creating an increased sensitivity to oxidative stress. Thermal tolerance of *M. capitata* may be partly due to harboring a mixture of *Cladocopium* and *Durusdinium* spp., whereas *P. acuta* was dominated by other distinct *Cladocopium* spp. Only *M. capitata* survived the experiment, but physiological state in heatwave exposed *M. capitata* remained significantly diverged at the end of recovery relative to individuals that experienced ambient conditions. In future climate scenarios, particularly marine heatwaves, our results indicate a species-specific loss of corals that is driven by baseline host and symbiont physiological differences as well as Symbiodiniaceae community compositions, with the surviving species experiencing physiological legacies that are likely to influence future stress responses.

Introduction

Coral holobionts, a meta-organism composed of an animal coral host, endosymbiont dinoflagellates and associated microbial community (Rohwer et al., 2002), make up the structure of one of the most ecologically diverse and economically valuable ecosystems in the world: coral reefs. The function and health of the coral holobiont, and therefore coral reefs, is dependent on this multipartner symbiotic relationship that cycles nutrients and provides each partner with otherwise limited or unavailable nutritional resources (Bourne et al., 2016). However, climate change is impacting the marine environment through increasing ocean temperatures (IPCC, 2018), specifically marine heatwaves (Oliver et al., 2021) and ocean acidification (Gattuso et al., 2015), among other local stressors, challenging the symbiotic function, physiological processes and, ultimately, the survival of reef-building corals. Although ocean acidification will place a chronic energetic strain on coral calcification (Mollica et al., 2018) and cellular acid–base balance (Tresguerres et al., 2017; Gibbin et al., 2014), the dominant physiological stress is currently in the form of increasingly frequent, intense marine heatwaves (Oliver et al., 2018; Sweet and Brown, 2016). This thermal stress triggers dysbiosis known as ‘coral bleaching’, or the disruption of the

symbiotic relationship between a coral host and their photosynthetic endosymbionts, Symbodinicaeae. This results in the coral host expelling the endosymbionts, leaving a stark white (‘bleached’) appearance and the coral host depleted of their primary carbon source (Gates et al., 1992; Boilard et al., 2020). Mass coral bleaching events resulting from marine heatwaves have increased in frequency and intensity in recent years (Oliver et al., 2021), and this trend is on track to continue, with catastrophic consequences projected for coral reef ecosystems (Heron et al., 2016; Le Nohaïc et al., 2017; van Woesik and Kratochwill, 2022).

The current understanding of the mechanistic cascade of bleaching is linked to the response of the host and/or endosymbionts to increased reactive oxygen species (ROS) levels produced under higher temperature that consequently increase oxidative stress and cause a breakdown of photosynthetic processes within the symbiont cells (Weis, 2008; Gates et al., 1992). This breakdown causes the symbiont cells to be either digested or expelled via several mechanisms including exocytosis, apoptosis, necrosis and host cell detachment (Weis, 2008; Lesser, 2004; Gates et al., 1992). A review of recent studies has shown that oxidative stress can occur in the host first (Oakley and Davy, 2018), suggesting that host antioxidant capacity may be critical in tolerating higher levels of temperature stress. However, host response to changing environment conditions has been shown to be highly species-specific (Bahr et al., 2016). In Kāne‘ohe Bay, O’ahu, Hawai’i, two common reef-building coral species display differential thermal tolerance: *Montipora capitata* is more resistant and *Pocillopora acuta* is more sensitive to environmental stress (Bahr et al., 2015; Gibbin et al., 2015). The underlying mechanisms to differential tolerance are known to be complex, ranging from genetic influences, epigenetic patterns, and associated endosymbiont and bacterial communities (Putnam, 2021), to host morphological structure and tissue thickness differences (Loya et al., 2001), but are not fully understood. Thus, multivariate analyses of key processes and traits can provide the capacity to quantify temporal variation in host, symbiont and holobiont responses, and are necessary to more

fully elucidate the bleaching cascade (Gardner et al., 2017; Wall et al., 2021; McLachlan et al., 2021).

Although extensive research has been conducted on the effects of increased temperature on coral (Mydlarz et al., 2010; Sweet and Brown, 2016; McLachlan et al., 2020; Cziesielski et al., 2019; Lesser, 2011; van Oppen and Lough, 2018), there are fewer experimental studies that simultaneously address critical environmentally relevant aspects that reflect a coral's natural conditions. Specifically, there are few studies that concurrently: (1) mimic daily and seasonal environmental fluctuations (van Woesik et al., 2022; Ziegler et al., 2021; Putnam and Edmunds, 2011), while (2) accounting for simultaneous, multivariate stressors (Pendleton et al., 2016; van Woesik et al., 2022), (3) sampling with high frequency to capture short and long-term temporal stress and recovery dynamics (Claar et al., 2020; Gardner et al., 2017), (4) during environmentally realistic times of the year (vanWoesik et al., 2022; Ziegler et al., 2021) and (5) tracking the survivors following the stress exposure (Claar et al., 2020; Gardner et al., 2017). These factors are particularly important, as exposure to diurnal temperature and pCO_2 fluctuations elicit different responses than stable, or less variable conditions (Putnam and Edmunds, 2011; Dufault et al., 2012; Schoepf et al., 2022; Barshis et al., 2013; Wall et al., 2021). Further, high-frequency sampling of a variety of variables was able to elucidate that symbiont expulsion and bleaching precedes severe holobiont physiological responses and health decline in later stress time points (Gardner et al., 2017). Additionally, seasonal studies of influences on coral physiology (Jurriaans and Hoogenboom, 2020; Scheufen et al., 2017; Thornhill et al., 2011; Edmunds and Putnam, 2020) highlight the variation in traits based on recent environmental conditions, supporting the need to study bleaching under seasonally realistic conditions to more accurately predict an organism's stress response (e.g. conducting bleaching studies at the timing of the peak of temperature for that region). Thus, high-frequency sampling of coral multivariate phenotypes

through time and following bleaching stress is necessary to understand the mechanisms and sequential timing of the symbiotic state during stress and subsequent recovery.

Here, we tested the effect of an environmentally realistic extended heatwave in the context of diurnally fluctuating temperature and ocean acidification on coral physiology to improve our understanding of coral stress biology and forecasting reef futures. Specifically,we conducted a 4-month multi-stressor time-series experiment during the fall warming season in Kāneʻohe Bay, O'ahu, Hawai'i, to assess the temporal dynamics during exposure to increased temperature and partial pressure of CO_2 (pCO_2) in addition to seasonal change, to compare differential stress response in a resilient and a sensitive coral species, and to investigate temporal dynamics during recovery and the potential for physiological legacies after an environmental perturbation.

Methods

Coral Collections

Coral fragments (one ~3×3 cm fragment per colony from 75 colonies of *Montipora capitata* Dana 1846 and 75 colonies of Pocillopora acuta Lamarck 1816) were collected via clippers at ~3–4.5 m depth from each of six reef areas ranging across the north to south span of Kāneʻohe Bay including both fringing and patch reefs [Lilipuna Fringe: 21°25'45.9"N 157°47'28.0"W; Hawaiʻi Institute of Marine Biology (HIMB): 21°26′ 09.8″ N 157°47′ 12.7″ W; Reef.11.3: 21°27′ 02.9″ N 157°47′ 41.8″ W; Reef.18: 21°27′ 02.9″ N 157°48′ 40.1″ W; Reef.35.36: 21°28′ 26.0″ N 157°50′ 01.2″ W; Reef.42.43: 21°28′ 37.9″ N 157°49′ 36.8″ W] under Hawaiʻi Department of Aquatic Resources Special Activity Permit 2019-60, between 4 and 10 September 2018 (Fig. 1A,B). This collection approach, ensuring each fragment was >10 m apart from each other, was designed to target a diverse collection of genotypes that represent the coral population for *M. capitata* and *P. acuta* in Kāneʻohe Bay. Coral fragments were

128 brought back to HIMB and affixed in an upright position to individually numbered plastic coral
129 fragment mounting plugs by hot gluing the base of the skeleton to the plug (McMaster-Carr, Hot-
130 Melt Glue #7518A54). Coral fragments were allowed to acclimate for ~14 days in outdoor
131 mesocosm tanks and then were randomly allocated in an even distribution (n=405 *P. acuta* and
132 n=440 *M. capitata*) to 12 replicate tanks for 2 months (weeks 1–8) of temperature and pCO_2
133 stress exposure and 2 months of ambient condition recovery (weeks 9–16) as described below.
134 The goal of our coral collection design was to examine the population of corals in Kāneʻohe Bay.
135 Therefore, the coral fragments were randomly allocated to the tanks, so the site of collection
136 was not included statistically.
137
138 *Experimental Timeline*
139 Coral fragments were exposed to one of four experimental conditions – (1) ambient
140 temperature+ambient pCO_2 (ATAC), (2) ambient temperature+high pCO_2 (ATHC), (3) high
141 temperature+ambient pCO_2 (HTAC) and (4) high temperature+high pCO_2 (HTHC) – for 2
142 months (22 September–17 November 2018; Fig. 1C). Treatment conditions (n=3 replicate tanks
143 per treatment) were randomly assigned to 12 outdoor flow-through mesocosm tanks
144 (122×122×30 cm; 510 l) supplied with sand-filtered seawater from Kāneʻohe Bay. Flow rates,
145 measured daily with a graduated cylinder and timer, averaged 84.36±1.20 ml s^{-1} (n=826),
146 providing full mesocosm tank turnover every ~2 h. Mesocosm tanks were 60% shaded from full
147 irradiance, and photosynthetically active radiation (PAR) was measured continuously with an
148 Apex cosine corrected PAR Sensor (PMK, Neptune Systems, accuracy =±5%) that was cross-
149 calibrated to the Li-Cor cosine corrected PAR sensor (LI-193 spherical underwater quantum
150 sensor, LI-COR Biosciences). Additionally, light values (roughly 100–700 PAR) from six different
151 positions in each tank were compared to determine spatial differences within each tank. There
152 was no significant difference in light between positions in each tank (n=4 per position per tank;
153 position P=0.978; tank P=0.143). Based on these results, light was measured in the center of

the tank approximately daily for the duration of the experiment using the LI-193 spherical underwater quantum sensor. To further reduce any potential position effects with respect to incoming water, heater position or bubble stream, the positions of the coral fragments in the tank were changed weekly. During this process, coral fragments were gently cleaned with toothbrushes and tanks were scrubbed to remove excess algal growth.

Experimental temperature conditions

Temperature treatment conditions were programmed to mimic the natural daily fluctuations of the environment at the collection sites in Kāneʻohe Bay, Hawaiʻi (NOAA Moku o Loʻe Buoy data from September 2018, https://www.ndbc.noaa.gov/station_page.php?station=mokh1; Fig. 1G; Fig. S1). Based on these data, the high temperature treatment fluctuated between ~29 and 30°C to reflect previous marine heatwaves in Kāneʻohe Bay, Hawaiʻi (+2°C above ambient temperature). Temperature was monitored with Apex Extended Life Temperature Probes (accuracy =±0.05°C, Neptune Systems) and temperature loggers (HOBO Water Temp Pro v2, accuracy=±0.21°C, resolution=0.02°C, Onset Computer Corp.) that were placed in each tank at the same height as the coral fragments for the duration of the experiment and logged temperature at 10 min intervals. Temperature was separately controlled by submersible heaters (ProHeat D-1500 Heater Controllers, precision ±1°C). Ambient temperature treatments reflected the natural conditions of Kāneʻohe Bay owing to the flow-through nature of the tanks.

Experimental pCO_2 conditions

Experimental pCO_2 treatment conditions were based on measurements of ambient conditions in Kāneʻohe Bay, Hawaiʻi (Drupp et al., 2011), and projected future lower pH conditions in embayments, which can have lower mean pH and higher diel fluctuations owing to calcification, photosynthesis and respiration of the benthic community and increased residence

time in the embayment (Jury et al., 2013; Shaw et al., 2016). The target pH range was based on values reported from low pH measured on the HIMB patch reef in Kāneʻohe Bay (Guadayol et al., 2014). The daily fluctuating pH levels in the high pCO_2 treatment tanks were maintained between 7.6 and 7.7 (pH NBS scale) with an independent pH-stat feedback system in each tank, and ambient conditions fluctuated between 7.9 and 8.0 (pH NBS scale; Fig. 1E,F). To generate the high pCO_2 treatment, two 99.99% food-grade CO_2 cylinders were connected to an automatic gas cylinder changeover system (Assurance Valve Systems, Automatic Gas Changeover Eliminator Valves #6091) to prevent an abrupt shortage of CO_2 supply. CO_2 was added into the seawater on-demand through gas flow solenoids (Milwaukee MA955), based on the pH reading (NBS) of a lab-grade pH probe (Apex pH, Neptune Systems) in each tank. CO_2 was delivered via airlines plumbed into a Venturi injector (Forfuture-go G1/2 Garden Irrigation Device Venturi Fertilizer Injector), which was connected to a water circulating pump (Pondmaster Pond-mag Magnetic Drive Water Pump Model 5). Gas injected into the system was either CO_2 or ambient air depending on treatment, and was injected through a Venturi injector connected to a pressure-driven pump, resulting in constant bubbling and moving water. An Apex AquaController (Neptune Systems) environmental control system with a wifi base unit (Apex Controller Base Unit, Neptune Systems) was linked to 12 individual monitoring units (Apex PM1 pH/ORP Probe Module, Neptune Systems) with Apex lab-grade pH Probes (accuracy=±0.01 pH NBS scale, Neptune Systems), which were used for microprocessor-control of a power strip (Apex Energy Bar 832, Neptune Systems) containing 12 individual solenoids. This pH-stat feedback system constantly monitored seawater temperature and pH conditions. Once sampling and treatments were completed, the pCO_2 injections were shut off immediately in all tanks and the temperature gradually decreased over the course of a week (Fig. 1G), and fragments were exposed to ambient temperature and ambient pCO_2 conditions for~2months (18November 2018–12 January 2019), identified here as the recovery period.

Total Alkalinity and Carbonate Chemistry

Tank parameters [temperature (°C), pH (total scale) and salinity (psu)] were measured 2–3 times daily using a handheld digital thermometer (Fisherbrand, Traceable Platinum Ultra-Accurate Digital Thermometer, accuracy=±0.05°C, resolution=0.001°C) and a portable multiparameter meter (Thermo Fisher Scientific, Orion Star A series A325). A pH probe (Mettler Toledo, InLab Expert Pro pH probe #51343101; accuracy=±0.2 mV, resolution=0.1 mV) and conductivity probe (Orion, DuraProbe 4-Electrode Conductivity Cell Model 013010MD; accuracy=0.5% of psu reading, resolution=0.01 psu) were used with an Orion A Star meter to measure pH (mV) and salinity (psu), respectively. pH (total scale) was calculated from standard curves of pH (mV) across a range of temperature (°C) in a tris standard (Dickson Laboratory, Tris batch T27 bottles 269 and 236, and batch T26 bottle 198). Water samples (125 ml) were taken from each tank twice a week to measure total alkalinity and, along with the pH on the total scale, as described above, to calculate carbonate chemistry. An automated titrator (Mettler Toledo T50) was used to titrate water samples with salinity-adjusted 0.1 mol l−1 hydrochloric acid (Dickson Laboratory Titrant A3, A14). A non-linear, least-squares procedure of the Gran approach (SOP 3b; Dickson et al., 2007) was used to calculate total alkalinity (TA; μmol kg^{-1} seawater). Accuracy of the titrations was determined using certified reference material [Dickson Laboratory CO_2 Certified Reference Material (CRM) batch 132 (salinity=33.441, TA=2229.24±1.03 μmol kg^{-1}), batch 137 (salinity=33.607, TA=2231.59±0.62 μmol kg^{-1}), batch 176 (salinity=33.532, TA=2226.38±0.53 μmol kg−1); NOAA Ocean Carbon and Acidification Data System]. Tank total alkalinity values were only accepted if the total alkalinity value of the CRM from that day was within 1%of the reported CRM. Carbonate values, including aragonite saturation (Ω), carbon dioxide (CO_2), carbonate (CO_2^{-3}), dissolved inorganic carbon (DIC), bicarbonate (HCO^{3-}), partial pressure of carbon dioxide (pCO_2) and pH, were calculated using SEACARB (v3.2.16 in R Studio; https://CRAN.R-project.org/package=seacarb) with the following parameters: calculated total pH, calculated TA, flag=8 [pH and ALK given], P=0, Pt=0,

232 Sit=0, pHscale='T', kf='pf', k1k2='l' and ks='d'. The equilibrium constant of hydrogen fluoride
233 (mol kg−1) (kf='pf') was set to 'pf' for salinities ranging from 10 to 40 psu and temperature
234 ranging from 9 to 33°C (Perez and Fraga, 1987) and recommended by Dickson et al. (2007).
235 The first (K1) and second (K2) dissociation constants of carbonic acid (mol kg−1) were set to 'l'
236 (k1k2='l') for salinities ranging from 19 to 43 psu and temperature ranging from 2 to 35°C
237 (k1k2='l'; Lueker et al., 2000). The stability constant of hydrogen sulfate (mol kg−1) (Ks) was set
238 to 'd' (Dickson, 1990) for salinities ranging from 5 to 45 psu and temperature ranging from 0 to
239 45°C. Salinity and temperature inputs were the measurements taken at the time of the water
240 sample collection.
241
242
243 ***Physiological Response Variables***
244 Physiological sampling occurred at the following time points: 1, 2, 4, 6, 8, 12 and 16 weeks
245 (Fig. 1D). Physiological samples were immediately snap-frozen in liquid nitrogen after
246 photosynthetic and respiration rates were measured (described below; n=2 per tank×3 tanks per
247 treatment=6 fragments per treatment per species per time point). All samples were stored at
248 −80°C until subsequent processing.
249
250 *Survivorship, growth rates, and color score*
251 Survivorship was tracked daily throughout the 2-month exposure and 2-month recovery
252 periods using a binary score for dead versus alive. Alive was defined as any fragment with live
253 tissue. Growth over time was determined by the buoyant weight technique (Davies, 1989; Jokiel
254 et al., 1978) using air, freshwater and saltwater standard curves as a function of temperature.
255 Each coral fragment was buoyant weighed in its respective treatment temperature and pCO_2
256 conditions. Wet buoyant mass was converted to dry mass using the aragonite density of 2.03 g
257 cm^{-3} for Montipora spp. (Anthony and Hoegh-Guldberg, 2003) and 2.93 g cm^{-3} for *P. acuta*

(Jokiel et al., 1978). Rates were normalized to surface area, determined by a single-dip wax dipping technique (Veal et al., 2010), and reported in units of mg $CaCO_3$ cm^{-2} day^{-1}. To assess tissue color change over time as a proxy for cell density and pigmentation sensu Edmunds et al. (2003), each coral fragment was photographed once a week (16 time points across the 4-month experiment) with a red, green, blue color standard. ImageJ was used to extract the mean red, green and blue color score for each coral fragment and these values were normalized to the mean of the red, green and blue color standards, respectively. The color scorewas quantified as principal component 1 (PC1; using the princomp function in R) from the principal component analysis (PCA) (sensu Edmunds et al., 2003).

Photosynthesis and Respiration Rates

Prior to experimental exposures, 10 coral fragments (5 per species) were used to generate a photosynthetic irradiance (PI) curve to determine saturating irradiance for assessing rates of photosynthesis. Fragments were exposed to 10 light levels: 0, 15, 30, 60, 91, 136, 227, 416, 529 and 756 µmol photons m^{-2} s^{-1} (as measured by the Apex PAR sensor described above) generated by two LEDs (Aqua Illumination Hydra FiftyTwo) hung above the incubation chambers (described below). Rates of oxygen consumption or evolution were extracted using local linear regressions in the LoLinR package (Olito et al., 2017) in µmol O_2 l^{-1} s^{-1}. Rates were corrected to chamber volume including coral displacement. Rates of the blank chambers were subtracted from the rates of the coral fragments within each run to account for background photosynthesis or respiration owing to phytoplankton, zooplankton and bacteria. Rates of oxygen flux were normalized to surface area for final units of µmolO_2 cm^{-2} h^{-1}. Curve fitting of a non-linear least squares fit for a non-rectangular hyperbola (Marshall and Biscoe, 1980; Heberling and Fridley, 2013) was used to identify PI curve characteristics of each species. To calculate net photosynthesis (Pnet; µmol O_2 h^{-1}), the following PI curve fit equation was used:

$$Pnet = \frac{\phi PPFD + \sqrt{(\phi PPFD + P_{max})2 - 4\Theta\phi PPFD + P_{max}}}{2\Theta} - Rd \quad [1]$$

where PPFD (photosynthetic photon flux density) is the irradiance (µmol photons m^{-2} s^{-1}), areal Pnet is net photosynthesis normalized to tissue area covered (cm^2) and cellular Pnet is net photosynthesis normalized to symbiont cell density (number of cells), Pmax is the maximum gross photosynthetic rate (µmol O2 cm^{-2} h^{-1}), φ is the apparent quantum yield (mol O_2 mol photons^{-1}) and Rd is the light-enhanced dark respiration rate (Edmunds and Davies, 1988) (µmol O2 cm^{-2} h^{-1}).

Photoinhibition, as represented by Ik,was calculated as Pmax divided by the apparent quantum yield. PI curves were performed four times throughout the experiment to ensure the coral fragments were not reaching photoinhibition (Fig. S4). Fragments were placed in individual respiration chambers (~610 ml), with individual temperature (Pt1000 temperature sensor, PreSens Precision Sensing GmbH) and fiber-optic oxygen probes (Oxygen Dipping Probes DPPSt7, accuracy=±0.05% O_2, PreSens Precision Sensing GmbH) connected to a 10-channel oxygen meter (OXY-10 ST, accuracy= ±1.0°C, resolution=0.1°C, PreSens Precision Sensing GmbH) to evaluate photosynthesis (under saturating light conditions, as determined by PI curves described above) and light-enhanced dark respiration (Edmunds and Davies, 1988). The respirometry setup consisted of 10 chambers with stir bars and respective treatment water. Samples were measured in a series of runs that consisted of eight fragments (n=4 per species) and two blank chambers per run exposed to PAR irradiance of ~500 µmol photons m^{-2} s^{-1} for 15 min to assess photosynthetic rates. Immediately afterwards, these fragments were exposed to dark conditions (0 µmol photons m^{-2} s^{-1}) for 20min to assess light-enhanced dark respiration. Following respirometry, fragments were immediately snap-frozen in liquid nitrogen and stored at −80°C. Raw oxygen flux data (temperature corrected) were thinned every 40 s and rates of

308 oxygen flux were calculated with local linear regression as described above. Net photosynthesis
309 was calculated by subtracting the oxygen change of the dark runs (a
310 negative value) from the oxygen change of the light runs (a positive value), to isolate
311 photosynthetic rates of the symbionts from the light enhanced dark respiration of the coral
312 holobiont.
313
314 *Tissue removal, surface area, and endosymbiont density*
315 Coral tissue was removed from the coral skeletons by airbrushing (Iwata Eclipse HP-
316 BCS) with ice-cold 1× phosphate buffered saline (PBS) solution, and the total volumewas
317 recorded. The tissue slurry was then homogenized for 15 s at high speed (PRO Scientific Bio-
318 Gen PRO200 Homogenizer, 10 mm Homogenizer Probe). Of the total tissue slurry, aliquots of
319 500 µl were taken for endosymbiont density, 500 µl for host soluble protein and host total
320 antioxidant capacity (TAC), 1 ml for chlorophyll a (*chl a*) concentration assays, and 5 ml for ash
321 free dry weight (AFDW). The skeleton was rinsed in freshwater and soaked in 20% bleach for
322 24 h and dried at room temperature for 24 h. Symbiodiniaceae cell concentration was quantified
323 with six technical separately loaded replicate counts on a hemocytometer (Hausser Scientific,
324 Bright-Line Counting Chamber) after homogenizing the tissue slurry for 1 min. The host
325 tissue was homogenized so that the symbiont cells were free of host tissue and clearly visible
326 on the counting slide. The average count (cells ml^{-1}) was standardized to the airbrushed
327 homogenate volume and surface area to produce cell density values in cells cm^{-2}.
328
329 *Host soluble protein and total antioxidant capacity*
330 To quantify host soluble protein and host TAC, the host tissue was isolated from
331 symbionts by centrifugation at 10,000 g for 10 min at 4°C. Soluble host protein of the
332 supernatant was measured using the Pierce BCA Protein Assay Kit (Pierce Biotechnology,
333 Waltham, MA, USA, catalog no. 23225) with two duplicates per sample measured by a 96-well

334 microplate reader (BioTek Synergy HTX Multi-Mode Reader Model S1LFA) at a wavelength of
335 562 nm. Resulting values were calculated from a bovine serum albumin standard curve and
336 standardized to homogenate volume and surface area to obtain host soluble protein values (mg
337 cm^{-2}). Host TAC was quantified in duplicate per sample with the Cell BioLabs OxiSelect Total
338 Antioxidant Capacity (TAC) Assay Kit (catalog no. STA-360) according to the manufacturer's
339 instructions and compared with a uric acid standard curve. Antioxidants in the sample reduce
340 Copper II to Copper I, resulting in positive correlation between copper reducing equivalents
341 (CRE, mmol l^{-1}) and antioxidant levels. CRE values were standardized to total soluble protein
342 for final values in units of CRE µmol mg^{-1}.
343
344 *Chlorophyll-a concentration*
345 To isolate symbiont cells for *chl a* concentration measurements, a 1 ml aliquot of tissue
346 homogenate was centrifuged at 13,000 g for 3 min and the supernatant was discarded. Then, 1
347 ml of 100% acetone was added to the symbiont pellet, mixed for 15 s on a lab vortex mixer, and
348 incubated in the dark at 4°C for 24 h. Samples and acetone blanks were read in duplicate (200
349 µl each) on a 96-well microplate reader at λ=630 and 663 nm. *Chl a* concentrations were
350 calculated with the following dinoflagellate equation for 100% acetone: *chl a*=11.43E663–
351 0.64E630 (Jeffrey and Humphrey, 1975). Concentration values were multiplied by 0.584 to
352 correct for the path length of the plate for units of µg ml^{-1} and standardized to the airbrushed
353 homogenate volume, normalized by surface area (µg cm^{-2}) and per symbiont cell (µg $cell^{-1}$).
354
355 *Tissue Biomass*
356 Tissue biomass was quantified using the AFDW method. Specifically, 5 ml of tissue
357 slurry was centrifuged at 13,000 g for 3 min. A volume of 4 ml of the supernatant host tissue
358 was removed and placed in preburned aluminum pan weighed on an analytical balance (Mettler

359 Toledo, model ML203T/00) and the symbiont pellet was resuspended in 1 ml PBS solution and
360 added to separate pre-weighed burned aluminum pans. The samples were placed in a drying
361 oven (Thermo Fisher Scientific, Heratherm General Protocol Oven, catalog no. 51028112) for
362 24 h at 60°C, weighed, and then placed in a muffle furnace for 4 h at 500°C (Thermo Fisher
363 Scientific, Lindberg Blue M Muffle Furnace, catalog no. BF51728C-1). AFDW (mg cm^{-2}) of the
364 host and symbiont fractions was calculated as the post-drying oven mass (dry mass)–post-
365 muffle furnace mass, and final values were standardized to the airbrushed homogenate volume
366 and normalized to surface area. Symbiont to host (S:H) biomass ratios were calculated by
367 dividing the symbiont AFDW by the host AFDW.
368
369 *Univariate statistical analysis*
370 Owing to the near-complete mortality during the recovery period in *P. acuta*, only the
371 exposure period was analyzed for the following physiological variables: tissue biomass, *chl a*,
372 endosymbiont density, respiration rates, photosynthetic rates, host TAC and host soluble
373 protein. *Montipora capitata* responses were analyzed in the exposure and recovery period
374 separately to assess the effect of treatment on physiological state and the effect of treatment
375 history on physiological state during a recovery period. Net photosynthetic rates per cm^2 from
376 the exposure period in *M. capitata* and color score for both species were square root
377 transformed to meet assumptions of analysis. Gross photosynthetic rates per cm^2 and growth
378 rates in *M. capitata*, and growth rates and *chl a* per cell in *P. acuta* were log10 transformed for
379 the exposure periods. Endosymbiont density, symbiont AFDW per cell, host soluble protein and
380 host TAC were log transformed in both *M. capitata* and *P. acuta*. All physiological responses
381 (tissue biomass, *chl a* concentration, endosymbiont density, respiration rates, photosynthetic
382 rates, host TAC and host soluble protein) were analyzed with linear mixed-effects models (lme4
383 package version 1.1-27.1; Bates et al., 2015) with time, temperature and pCO_2 as fixed factors,

384 tank number as a random factor, and sum effect coding (Kugler et al., 2018) to test for
385 interaction effects. The goal of our coral collection design was to examine the population of
386 corals in Kāneʻohe Bay. Therefore, the coral fragments were randomly allocated to the tanks, so
387 site of collection was not included statistically, as there was not a balanced design across the
388 tanks. Color score and growth rates were analyzed using linear mixed-effects models with time,
389 temperature and pCO_2 as fixed factors and plug ID nested within tank number as a random
390 repeated measures factor. Survivorship probability was calculated with a Cox proportional
391 hazards mixed effects model fit by maximum likelihood using the coxpH function in the coxme
392 package (version 2.2-16; Therneau and Grambsch, 2013) with temperature and pCO_2
393 treatments as fixed effects and plug ID as a random factor. Type III Wald $\chi 2$ ANOVA tests were
394 performed on all models to assess significance of fixed effects. The normality and variance
395 assumptions of the ANOVA test were assessed with quantile–quantile plots and Levene's test.
396 To determine baseline differences at week 1 in physiology at between the two species,
397 treatment replicates were grouped for each response variable (n=6 per treatment×4
398 treatments=24 per species), prior to significant physiological change, and a Welch two-sample t-
399 test was used for each univariate measurement to assess significance.
400
401 *Multivariate statistical analysis*
402 A correlation matrix was calculated using the 'corrplot' function from the corrplot R package
403 (https://CRAN.R-project.org/package=corrplot) to determine which univariate physiology
404 variables were correlated and thus what to include in multivariate analyses. Gross and net
405 photosynthetic rates were highly correlated and as a result, only net photosynthetic rates were
406 used in downstream analyses as measure of symbiont photophysiology without the influence of
407 cellular respiration. Multivariate physiological matrices were centered and scaled prior to
408 principal components analyses that were performed using the 'prcomp' function from the stats
409 package in R (https://www.r-project.org/) to examine multivariate physiological states for each

410 species in the exposure period, as well as the recovery period for *M. capitata*. Permutational
411 multivariate analysis of variance (PERMANOVA) tests were used to assess significant
412 differences in multivariate physiology with time, temperature and pCO_2 as fixed effects ('adonis'
413 function in the R package vegan; https://CRAN.Rproject.org/package=vegan) separately for
414 exposure and recovery periods for each species.
415
416 *Molecular response variables*
417 Molecular sampling occurred at the following time points: 0, 6, 12 and 30 h, and 1, 2, 4,
418 6, 8, 12 and 16weeks (Fig. 1D). At each time point, one fragment was selected at random from
419 each tank of each species (n=1 per tank×3 tanks per treatment=3 fragments per treatment per
420 species) and placed in sterile whirlpak bags and snap-frozen in liquid nitrogen at 13:00 h each
421 day (with the exception of 6, 12 and 30 h time points).
422
423 *DNA and RNA Extractions*
424 DNA and RNA were extracted simultaneously from the coral fragments that had been
425 snap-frozen and stored at −80°C. A small piece (~0.5–1 cm) was clipped off using clippers
426 sterilized in 10% bleach, deionized water, isopropanol and RNAse free water, and then placed in
427 2 ml microcentrifuge tube containing 0.5 mm glass beads (Fisher Scientific, catalog no. 15-340-
428 152) with 1000 µl of DNA/RNA shield. A two-step extraction protocol was used to extract RNA
429 and DNA for RNASeq and DNA methylation, respectively, with the first step as a 'soft'
430 homogenization to reduce shearing of RNA or DNA. Tubes were vortexed at high speed for 1 and
431 2 min for *P. acuta* and *M. capitata* fragments, respectively. The supernatant was removed and
432 designated as the 'soft extraction'. In the second step, 500 µl of DNA/RNA shield was added to
433 the bead tubes and placed in a Qiagen TissueLyser for 1 min at 20 Hz. The supernatant was
434 removed and designated as the 'hard extraction'. Subsequently, 300 µl of samples from both soft
435 and hard homogenate were extracted individually with the Zymo Quick-DNA/RNA Miniprep Plus

436 Kit (Zymo Research, catalog no. D7003T) following the protocol instructions, with the following
437 modifications. For the DNA elution step, the first elution of 10 μl of warmed 10 mmol l^{-1} Tris HCl
438 was added to DNA columns for a 15 min room temperature incubation and centrifuged at 16,000
439 g for 30 s. A second elution of 100 μl of warmed 10 mmol l^{-1} Tris HCl was added for a 5 min
440 incubation and centrifuged at 16,000 g for 30 s. Broad-range DNA quantity (ng μl^{-1}) was measured
441 with a Thermo Fisher Qubit Fluorometer, and DNA quality was assessed using gel
442 electrophoresis. Only the second elution of the 'hard extraction' DNA elution was used for
443 downstream internal transcribed spacer 2 (ITS2) sequencing protocols and analysis.
444
445 *Internal Transcribed Spacer 2 (ITS2) Sequencing*
446 Custom primers were ordered from Integrated DNA Technologies with ITS2 region
447 locus-specific sequences based on Lajeunesse and Trench (2000) and Illumina adapters (in
448 italics) to create our ITS2 forward primer (5′ GAATTG CAG AAC TCC GTG TCG TCG GCA
449 GCGTCA GATGTG TATAAG AGACAG 3′) and ITS2 reverse primer (5′ GGGATC
450 CATATGCTTAAG TTCAGCGGGTGTCTCGTG GGC TCG GAG ATG TGT ATA AGA GAC AG
451 3′). PCR master mix solution included (per sample values): 16.6 μl of 2× Phusion HiFi
452 Mastermix (Thermo Scientific, catalog no. F531s), 14 μl of DNase/RNase freewater, 0.6 μl of 10
453 μmol l^{-1} ITS2 forward primer, 0.6 μl of 10 μmol l^{-1} ITS2 reverse primer and 1 μl of 10 ng μl^{-1}
454 DNA sample or 1 μl ofDNase/RNase freewater as a negative control. To avoid PCR
455 amplification bias, each sample was run in triplicate on 96-well plates with 32 μl of master mix
456 and 1 μl of 10 ng μl^{-1} DNA sample in each well. Samples were run on the following PCR
457 settings: 3 min at 95°C, then 35 cycles of 30 s at 95°C, 30 s at 52°C and 30 s at 72°C, followed
458 by 2 min at 72°C and held indefinitely at 4°C. The triplicate PCR products for each sample were
459 pooled and stored at −20°C. The PCR products were run on a 2% agarose gel to confirm 360–
460 390 bp pair fragment length (330–360 bp ITS2 region and locus-specific primers+33 bp adapter

461 length). Then, 45 µl of PCR product was sent to the RI-INBRE Molecular Informatics Core at the
462 University of Rhode Island (RI, USA) for the index PCR and sequencing. There, PCR products
463 were cleaned with NucleoMag beads (Takara Bio, catalog no. 744503) and then visualized
464 using gel electrophoresis. A second round of PCR was performed with 50 ng DNA input for 8
465 cycles to attach Nextera XT indices and adapters using the Illumina Nextera XT Index Kit
466 (Illumina, catalog no. FC-131-200×) and Phusion HF PCR master mix (Thermo Fisher Scientific,
467 catalog no. F531L). Products were then cleaned with NucleoMag beads and visualized using
468 gel electrophoresis (1.5% agarose gel, 110 V, 35 min). The quality of samples was assessed
469 using an Agilent BioAnalyzer DNA1000 chip (Agilent, catalog no. 5067-1505) and quantification
470 was performed using a Qubit fluorometer with a High Sensitivity Kit (Invitrogen, catalog no.
471 Q32584) prior to pooling all samples. The final pooled library was quantified using qPCR (Roche
472 LightCycler480) with the KAPA Biosystems Illumina Kit (KAPA Biosystems). Samples were
473 analyzed using 2×250 bp paired-end sequencing on an Illumina MiSeq (Illumina).
474
475 *Bioinformatic analysis*
476 ITS2 sequences fromrawFASTQ fileswere analyzed using SymPortal (symportal.org;
477 Hume et al., 2019) on theUniversity of Rhode Island's High Performance Cluster. This workflow
478 used Miniconda3 v4.9.2 and SymPortal v0.3.21-foss-2020b to assign sequences as defined
479 intragenomic variants (DIV) and 'ITS2 Type Profiles'. A raw counts matrix of the ITS2 Type Profile
480 output from SymPortal was exported and analyzed locally using R Software Version 4.0.3 in
481 RStudio Version 1.4.1103. Relative abundance and a Bray–Curtis distance matrix were calculated
482 using the 'vegan' package (Dixon, 2003). A PERMANOVA was performed for each species to
483 assess significant effects of time point, treatment and their interaction.

484 **Results**

At the end of the ~14-day acclimation period, 89.8% of *P. acuta* (n=405) and 97.8% of *M. capitata* (n=440) fragments were alive. During the exposures, treatments showed no significant variation in TA across the 16-week experiment (treatment P=0.776; ATAC=2159.06 ±5.88, ATHC=2162.46±0.12, HTAC=2155.58±5.25, HTHC= 2156.79±0.058; Fig. S2). Additionally, light conditions were not significantly different between treatments (treatment P=0.558; ATAC=179.70±9.97, ATHC=186.54±10.20, HTAC=176.64±10.84, HTHC=165.12±10.41; Fig. S3). High temperature treatments during the 8-week stress period were maintained above 29°C (HTAC=29.47 ±0.004, HTHC=29.59±0.004; n=7691), whereas ambient conditions, dictated by flow-through water, steadily declined from 28°C to 26°C (Fig. 1G). Recovery temperature conditions reflected natural conditions of Kāneʻohe Bay with declines from 26°C to 23°C by week 16 in mid-January (Fig. 1G,H).

High pCO_2 treatments (ATHC, HTHC) were maintained between 7.6 and 7.7 pH total scale (ATAC=8.03±0.011, ATHC=7.67±0.014, HTAC=8.01±0.011, HTHC=7.64±0.019). During the stress period, high pCO_2 treatments were characterized by significant decreases in aragonite saturation (Ω; treatment×time P<0.0001), carbonate (CO_3^{2-}; treatment×time P<0.0001) and pH (treatment×time P<0.0001), as well as increases in carbon dioxide (CO_2; treatment P<0.0001), dissolved inorganic carbon (DIC; treatment×time P<0.0001), bicarbonate (HCO^{3-}; treatment×time P<0.0001) and pCO_2 (treatment P<0.0001; Fig. 1E,F, Fig. S2). During recovery, all treatments reflected the natural conditions of Kāneʻohe Bay, ~8 pH total scale (Fig. 1E). Additional univariate figures and summary statistical tables can be found at Open Science Framework (OSF) doi:10.17605/OSF.IO/Q9HMC.

High temperature drives bleaching responses and low P. acuta survivorship

In high temperature treatments (HTAC and HTHC), both species displayed significant color change relative to ambient, starting at 4 weeks in *P. acuta* and 6 weeks in *M. capitata*. High temperature and ambient pCO_2 (HTAC) and high temperature high pCO_2 (HTHC)

511 treatments drove this decrease in color score in the exposure period in *M. capitata*
512 (time×temperature×pCO_2 P=0.0004) and *P. acuta* (time×temperature P<0.0001;
513 time×temperature×pCO_2 P<0.0001). Additionally, *P. acuta* color score decreased significantly
514 through the autumn season (time P<0.0001) and in high pCO_2 treatments over time
515 (time×pCO_2 P<0.0001; Fig. S6). Following this visual bleaching response in the exposure
516 period, both high temperature (HTHC, HTAC) and pCO_2 treatments (ATHC) elicited decreased
517 survivorship probability in both *M. capitata* (temperature P <0.0001; pCO_2 P=0.0007) and *P.*
518 *acuta* (temperature×pCO_2 P<0.0001; Fig. S5). In the recovery period, *M. capitata* fragments that
519 experienced high temperature treatments (HTHC and HTAC) increased in color score to
520 ambient values by week 16 (time×temperature×pCO_2 P=0.0124; Fig. S6). The decreases in
521 survivorship probability for *M. capitata* stopped once treatment conditions were removed.
522 However, *P. acuta* fragments did not recover color, and survivorship probability continued
523 to sharply decrease (Fig. S5).
524
525 ***High temperature decreased metabolic rates in both species, but P. acuta displays higher***
526 ***baseline photosynthetic rates***
527 There were significant decreases during the stress period (September to November)
528 regardless of treatment in both species for respiration (*M. capitata* time P=0.0005; *P. acuta* time
529 P<0.0001) and photosynthetic rates (*M. capitata* Pnet cm^{-2} time P=0.0060; *P. acuta* Pnet cm^{-2}
530 time P<0.0001; *P. acuta* Pnet cell−1 time P <0.0001). However, *P. acuta* displayed significantly
531 higher baseline (as defined by week 1) areal (Pnet cm^{-2} P=0.0002; Pgross cm^{-2} P=0.0013) and
532 per cell photosynthetic rates (Pnet $cell^{-1}$ P=0.0045), as well as higher photosynthesis:respiration
533 ratios (P:R P=0.0023) than *M. capitata* (Fig. 2). During the exposure period, high temperature,
534 rather than high pCO_2, caused a decrease in respiration rates in *M. capitata* (temperature
535 P=0.0203) and *P. acuta* (time×temperature P=0.0412). Similarly, high temperature drove
536 significant decreases in net photosynthetic rates in *M. capitata* (time×temperature P=0.0079)

537 and *P. acuta* (time×temperature P<0.0001).When net photosynthetic rates were normalized per
538 symbiont cell, treatments did not affect *M. capitata* fragments (time×temperature×pCO_2
539 P=0.1833), but *P. acuta* fragments in high temperature treatments displayed a significant
540 decrease by week 6 (time×temperature P=0.0011). Concomitantly, by week 6 (out of 8
541 exposure weeks), *P. acuta* fragments also displayed a significant decrease in P:R in high
542 temperature treatments (time×temperature P=0.0139) and overall changes in metabolic rates
543 were more drastic in *P. acuta* fragments.
544
545 ***High pCO_2 stress depresses seasonal increase in growth rates in M. capitata and high***
546 ***temperature decreases growth rates in both species***
547 In both species, growth rates (mg $CaCO_3$ cm^{-2} day^{-1}) peaked in at week 4 of exposure
548 (October) and gradually decreased by week 8 (November) of the exposure period (*M. capitata*
549 time P<0.0001; *P. acuta* time P<0.0001) regardless of treatment. High temperature treatment
550 decreased growth rates in later exposure time points (time×temperature×pCO_2 P<0.0001) in
551 both species. Similarly, both pCO_2 and temperature treatments exhibited lower growth rates
552 through the entire exposure period (time×temperature×pCO_2 P<0.0001) in *P. acuta* fragments.
553 In *M. capitata*, corals in high pCO_2 treatments displayed significantly lower growth rates over
554 time (Time× pCO_2 P=0.0003). However, during the recovery period, *M. capitata* fragments that
555 experienced only high pCO_2 (ATHC) displayed increasing growth rates through week 16 (time×
556 pCO_2 P=0.0017), whereas fragments that experienced the high temperature treatments
557 (HTAC and HTHC) gradually increased to ambient levels by week 16 (time×temperature
558 P<0.0001).
559
560 ***Host physiology: biomass remained stable while temperature stress increased TAC and***
561 ***decreased protein levels***

562 On average, *M. capitata* exhibited higher baseline TAC than *P. acuta* (P=0.0008; Fig. 2). Host
563 TAC (CRE µmol mg^{-1}) remained constant in *M. capitata* through the exposure period regardless
564 of treatment (time×temperature×pCO_2 P=0.7028) but increased by week 8 in *P. acuta* under
565 high temperature in HTAC and HTHC (time×temperature P=0.0277). During recovery, *M.*
566 *capitata* fragments previously exposed to high temperature treatments showed reduced TAC at
567 week 12, which returned to ambient treatment values by week 16 (time×temperature P=0.0237).
568 Host soluble protein (mg cm^{-2}) was not significantly different between species at baseline, week
569 1 (P=0.29), but significantly decreased through time from September to January in both *M.*
570 *capitata* (time P<0.0001) and *P. acuta* (time P<0.0001). At week 6, protein concentration in *M.*
571 *capitata* was significantly greater in both high pCO_2 treatments (pCO_2 P=0.0002) in comparison
572 to HTAC and ATAC. Additionally, corals in high temperature treatments (HTHC and HTAC in
573 comparison with ATAC and ATHC) displayed a decrease in protein over time (temperature×time
574 P=0.0463). In *P. acuta* fragments, high temperature treatments decreased in protein at week 8
575 (time×temperature P=0.0490). Host AFDW (mg cm^{-2}) was not significantly different at baseline,
576 week 1 (P=0.22), or affected by treatment, but gradually and significantly decreased throughout
577 the stress and exposure period from September to January in *M. capitata* (time P=0.0050) and
578 *P. acuta* (time P=0.0188).
579
580 ***Symbiont and holobiont physiology: stress treatments caused an increase in symbiont***
581 ***biomass but decreased chl a content and endosymbiont density***
582 Symbiont biomass (mg AFDW cm^{-2}) was unaffected by either temperature or pCO_2
583 treatment (time×temperature×pCO_2; *M. capitata* P=0.3839, *P. acuta* P=0.3790), but significantly
584 decreased through the autumn season in both *M. capitata* (P=0.0013) and *P. acuta* (P=0.0028).
585 Despite no treatment effect on symbiont and host biomass (mg AFDW cm^{-2}), for *P. acuta* the
586 symbiont:host biomass ratio significantly decreased in high temperature treatments
587 (temperature P=0.0180) and decreased also over time (Time P=0.0090). *Montipora capitata*

588 fragments exhibited significantly higher baseline week 1 biomass (mg cm^{-2} P=0.0145; mg $cell^{-1}$
589 P=0.0079; Fig. 2) than *P. acuta*. In *M. capitata*, symbiont cellular biomass (mg AFDW $cell^{-1}$)
590 significantly increased in corals in the high temperature treatments during exposure
591 (temperature×pCO_2 P=0.0133) and then returned to ambient levels by week 16
592 (time×temperature P=0.0041). In *P. acuta*, symbiont per cell biomass decreased from
593 September to January (P=0.0141), but significantly increased under both temperature and pCO_2
594 exposure (time×temperature P<0.0001; time×pCO_2 P=0.0146). Holobiont *chl a* (cm^{-2})
595 increased over the autumn season in *M. capitata* (time P=0.0003; Fig. 3G), but high
596 temperature exposure resulted in decreased *chl a* over time (time×temperature P=0.0089) that
597 remained low in the recovery period (temperature P<0.0001). In *P. acuta*, *chl a* decreased over
598 time (time P<0.0001) and in high temperature treatments over time (time×temperature
599 P<0.0001; Fig. 3H). In *M. capitata*, only time significantly affected cellular *chl a* $cell^{-1}$ (time
600 P=0.0347), and in all fragments, regardless of treatment, *chl a* $cell^{-1}$ increased from September
601 to January. However, in *P. acuta*, *chl a* per cell was significantly affected by temperature and
602 time (time×temperature P=0.0764). Endosymbiont density (cells cm^{-2}) decreased in high
603 temperature and pCO_2 treatments over time in *M. capitata* (time×temperature P=0.0100;
604 time×pCO_2 P=0.0249) and the magnitude of decline was greater in high temperature in *P. acuta*
605 (time×temperature P<0.0001). *Pocillopora acuta* endosymbiont density decreased by week 4 in
606 all treatments (time P<0.0001; Fig. 3F), but all *M. capitata* fragments displayed an increase in
607 densities in the same time period, followed decreased values by week 8 (time P<0.0001; Fig.
608 3E). By the end of the recovery period, *M. capitata* fragments that had experienced high
609 temperature treatments did not fully recover in symbiont cell densities (temperature P=0.0070),
610 despite being statistically indistinguishable in color score.
611
612 ***Multivariate physiology: high temperature exacerbates seasonal changes during stress***
613 ***and drives physiological states during recovery***

614 In both species, treatments exacerbated existing seasonal shifts in multivariate
615 physiological states (Fig. 4). In *P. acuta*, physiological state shifted over time (P<0.001) and in
616 high temperature treatments (time×temperature P<0.001). Similarly, *M. capitata* fragments
617 experienced a shift in physiological state over time (time P<0.001) owing to temperature
618 (temperature P=0.005), and this was different between pCO_2 treatments over time (time×pCO_2
619 P=0.038). PC1 explained 39.83% of the variance and separated the samples between ambient
620 temperature and high temperature for *P. acuta*, with changes in respiration rates and host TAC
621 levels contributing most strongly to the separation (Fig. 4A,B). The PC2 axis explained 18.40%
622 of the variation and the separation between treatment groups was characterized by changes in
623 endosymbiont density and cellular symbiont biomass. In *M. capitata*, the PC1 axis explained
624 30.51% of the variation and was characterized by changes in the host (protein, biomass,
625 respiration) and holobiont physiology (areal net photosynthetic rates, areal symbiont AFDW and
626 holobiont *chl a* content) that contribute to separation primarily between time points. The PC2
627 axis explained 25.81% of the variation and was characterized by symbiont functions (symbiont
628 AFDW mg $cell^{-1}$, net photosynthetic rates and *chl a* content) that separate primarily treatment
629 groups (Fig. 4C,D). During the recovery period, both time (P<0.001) and high temperature
630 treatment (P<0.001) significantly affected physiological shifts in *M. capitata* (Fig. 5C,D). PC1
631 explained 37.61% of the variation and was characterized by host (biomass, protein) and
632 holobiont traits (mg AFDW cm^{-2}, *chl a* cm^{-2}) that separate between the history of high
633 temperature treatment groups in *M. capitata*. PC2 explained 30.11% of the variation and
634 changes in endosymbiont density and symbiont traits (*chl a* $cell^{-1}$, S:H biomass ratio, biomass)
635 contributed strongly to the separation of treatment and time groups.
636
637 ***Montipora capitata and P. acuta harbor distinctly different Symbiodiniaceae community***
638 ***compositions that do not change significantly during stress or recovery***

639 The ITS2 sequencing generated 5,807,744 total raw reads from 251 samples, with an
640 average of 22,775 reads per sample. The SymPortal analysis resulted in 4,902,971 total
641 cleaned sequences, which excludes week 16 in *P. acuta* because of low sample sizes.
642 *Montipora capitata* fragments harbored mixed Symbiodiniaceae communities composed of ITS2
643 symbiont type profiles with majority sequences 'D1/D4' and variations of 'C17d/No-Name'
644 (Durusdinium and Cladocopium spp.; LaJeunesse et al., 2018; Fig. 6). *Pocillopora acuta*
645 communities were dominated by type profiles in clade C with majority groups 'C1d/C42.2' and
646 'C1d'. Endosymbiont communities were significantly different between species (PERMANOVA
647 $P<0.001$) and differed only between two time points in *M. capitata* (12 h versus 24 h $P=0.045$)
648 but did not significantly change in exposure treatments ($P=1.000$).
649
650 **Discussion**
651
652 ***Extended heatwave scenario induces species-specific mortality of corals and creates***
653 ***altered physiological legacies for the survivors***
654 Scaling up from controlled single variable lab experiments to environmentally relevant
655 multi-stressor experiments is essential to capture the effects of stressors in the context of
656 seasonal physiological and thus the time-dependent and environmentally relevant sensitivity
657 of corals to global change stressors. Our examination of the effects of high pCO_2 and an
658 extended heatwave at the peak of seasonal temperatures on *M. capitata* and *P. acuta* reinforce
659 that increased temperatures are the more substantial threat to coral physiological
660 performance (Putnam et al., 2013), survivorship (Klein et al., 2022) and physiological legacy
661 effects (Wall et al., 2021) than high pCO_2 conditions. We found that high pCO_2 concentrations
662 alone can elicit potentially beneficial effects in the more resilient *M. capitata* such as higher
663 endosymbiont density and thus higher photosynthetic rates (cm^{-2}) during exposure, and higher

664 growth rates during recovery periods. However, these effects are not seen when high pCO_2
665 conditions occur simultaneously with higher temperatures. The extent of physiological shifts,
666 decreased survival probability and increased bleaching were all greater in *P. acuta* than in *M.*
667 *capitata*, reinforcing the outcome of species-specific susceptibility and loss of corals on future
668 reefs (Loya et al., 2001; van Woesik et al., 2011). Our data indicate that a combination of
669 Symbiodiniaceae community and baseline levels of host antioxidant capacity and cellular
670 photosynthetic rates are contributing to species-specific stress responses. Further, our findings
671 of different physiology trajectories of *M. capitata* during the recovery period, specifically in those
672 exposed to high temperature, support prior work that high temperature conditions leave lasting
673 physiological legacies several months into recovery (Rodríguez-Troncoso et al., 2016; Schoepf
674 et al., 2015; Rodrigues and Grottoli, 2007), and those legacies can have cumulative effects that
675 shift physiological baselines leading into a subsequent stress event (Wall et al., 2021; Safaie et
676 al., 2018; Ainsworth et al., 2016).
677

678 ***Symbiodiniaeceae communities and high levels of antioxidants relative to cellular***
679 ***photosynthetic rates contribute to M. capitata thermal tolerance***

680 Symbiodiniaceae communities aid in a coral holobiont's tolerance and survival (Baskett,
681 et al., 2009; Oliver and Palumbi, 2011); specifically, studies have documented that the presence
682 of Durusdinium spp. (Silverstein et al., 2015; Guest et al., 2016) and/or mixed endosymbiont
683 communities (Abbott et al., 2021) can be beneficial for coral holobiont survival. Our results
684 support these hypotheses, as the mixture of Durusdinimum spp. (D1/D4; ~60–80%) and
685 Cladocopium spp. (C17/C31; ~20–40%) in *M. capitata* was associated with higher thermal
686 tolerance, compared with *P. acuta*'s Cladocopium spp. (C1; 100%) dominated communities.
687 Although there was no evidence of Symbiodiniaceae community shuffling by treatment or

688 through time, a holobiont's community prior to an exposure event likely plays a crucial role in
689 their ability to handle changing environmental conditions. Through these community
690 composition differences, symbiont physiology influences holobiont tolerance (Hoadley et al.,
691 2019; Ziegler et al., 2015), thus indicating that both the host and symbiont physiological states
692 are critical to understanding the stress response of the holobiont (Bellantuono et al., 2012).
693 Differential photophysiology, carbon assimilation and translocation to the host (Stat et al., 2008)
694 and metabolite profiles (Matthews et al., 2017, 2018) have been seen between
695 Symbiodiniaceae genera and thus influence holobiont tolerance (Wall et al., 2020; Matthews et
696 al., 2018; Roach et al., 2021).

697 For both host and symbiont partners, a core physiological response to stress is the
698 activity of antioxidant systems to neutralize ROS molecules that build up during daily
699 metabolism and in response to stressful conditions such as increased temperature (Baird et al.,
700 2009; Downs et al., 2000). These excess ROS molecules can leak into the host to cause a
701 downstream cascade of cellular damage and eventually coral bleaching and apoptosis (Weis,
702 2008). A mismatch between the amount of symbiont-derived ROS molecules and the host's
703 antioxidant capacity may lead to higher susceptibility for coral bleaching (e.g. Cunning and
704 Baker, 2013). We hypothesize that *P. acuta*'s naturally higher cellular photosynthetic rates, but
705 lower host antioxidant capacity per unit protein, may lead to a faster build-up of ROS damage
706 and consequently higher mortality rates. Thus, *P. acuta* are challenged under thermal stress
707 because the symbiotic community is operating closer to the threshold between productivity and
708 damage. In comparison, *M. capitata*'s naturally lower photosynthetic rates and higher host
709 antioxidant capacity levels may be providing a greater buffer, allowing them capacity to support
710 and balance their higher endosymbiont densities during November (Fig. 3), resulting in a more
711 muted bleaching response when faced with stressful conditions. Further, *M. capitata* have the
712 benefit of thicker tissues (Loya et al., 2001; Magnusson et al., 2007) with greater energy

713 reserves (Rodrigues and Grottoli, 2007) in addition to their symbiont community composition. By
714 the end of the exposure period, *P. acuta* host antioxidant capacity levels increased, and cellular
715 photosynthetic rates decreased, but visual bleaching responses preceded this cellular
716 physiological change, indicating that the response was insufficient. *Montipora capitata* may be
717 well equipped to acclimatize to changing environmental conditions because of baseline
718 holobiont physiological states and existing Symbiodiniaceae communities.
719

720 ***Thermal exposure influences bleaching recovery trajectories in M. capitata***

721 Recent studies have emphasized the importance of recovery time in between marine
722 heatwaves (Osborne et al., 2017; Neal et al., 2017; Grottoli et al., 2014). Recovery time can be
723 highly variable, with species taking anywhere from 1.5 months (Rodrigues and Grottoli, 2007), 2
724 months (Cunning et al., 2016), 3 months (Wall et al., 2019) up to 2 years (Matsuda et al., 2020).
725 We found that in our experimental recovery period of 2 months following exposure, physiological
726 metrics that decreased in chronic high temperature conditions stabilized as *M. capitata* fragments
727 began to recover pigmentation (color score, symbiont density and *chl a*). Despite full recovery in
728 color score and growth rates by week 16, *chl a* and endosymbiont densities did not fully recover
729 to the same extent as the ambient condition corals, with differential physiological states and
730 trajectories throughout the recovery period (Fig. 5). Our results indicate that extended high
731 temperature exposure at the peak of seasonal temperature leaves a physiological legacy that
732 lasts beyond 2 months. Even in this resistant and resilient species, legacy effects of bleaching on
733 organismal state can be as long as 1–2 years (Wall et al., 2019, Roach et al., 2021; Thomas and
734 Palumbi, 2017).

735 These legacy effect results are consistent with those of other studies that suggest that
736 environmental conditions shift coral phenotypes, ultimately eliciting a lasting legacy that could

737 have either a beneficial or detrimental priming effect for response in future stress events (Wall et
738 al., 2021; Hackerott et al., 2021; Putnam et al., 2017; Brown et al., 2000). However, recovery time
739 is imperative to understand whether the lasting effects of prior thermal events can be beneficial.
740 Sublethal temperatures that induce a bleaching response 10 days prior to a larger intensity
741 bleaching event have been shown to be beneficial (termed a 'protective trajectory'; Ainsworth et
742 al., 2016). Although beneficial effects were documented in long-term recovery periods of 11
743 months (Schoepf et al., 2015) following thermal perturbation, not all species recovery is on the
744 same timeline, with Porites divaricata and Orbicella faveolata recovering faster than Porites
745 astreoides (Schoepf et al., 2015). This potential for 'environmental memory' based on previous
746 environmental conditions is clear in corals (Brown et al., 2000, 2022). Utilizing this to elicit
747 purposeful stress hardening or environmental priming (Hackerott et al., 2021; Putnam et al., 2017;
748 Brown et al., 2000; DeMerlis et al., 2022) is a proposed restoration technique (van Oppen et al.,
749 2015), but it is clear there are limits of recovery time. *Montipora capitata* is likely to survive future
750 thermal stress events, but back-to-back bleaching events and decreased recovery time may
751 reduce their buffer and push their physiology closer to a threshold. More multi-year studies to
752 track differential bleaching patterns over time are needed to elucidate the threshold between
753 eliciting beneficial 'environmental memory' versus accumulated physiological damage and
754 energetic deficits (Schoepf et al., 2015).

755

756 **Conclusion**

757 This study highlighted the divergent thermal tolerance and recovery potential of *M.*
758 *capitata* and *P. acuta*, indicating a potential for species-specific susceptibility to stress and loss
759 of corals in future, more frequent and higher intensity bleaching events. *Montipora capitata*

elevated stress tolerance may be due in part to mixed Cladocopium and Durusdinium Symbiodiniaceae communities, higher antioxidant capacity and elevated photosynthetic rates at baseline, and stability of metabolic and symbiont physiology during chronic high temperature conditions. In the 2 months of ambient recovery conditions that followed 2 months of elevated temperature and pCO_2 conditions, *M. capitata* multivariate physiology did not fully recover. High temperature treatment history elicited a lasting multivariate physiological legacy that set recovering *M. capitata* on a different trajectory than those that experienced ambient conditions. This study illuminates and emphasizes the importance of environmentally and seasonally realistic time-series experiments to further understand the impacts of pre-existing seasonal dynamics on thermal stress response. Multi-year repeated bleaching event studies are needed to disentangle howa physiological legacy may be adaptive or maladaptive under predicted climate change scenarios.

Contributions

Conceptualization: E.L.S., H.M.P.; Methodology: E.L.S., K.H.W., A.F., S.G., A.M., H.M.P.; Software: E.L.S., H.M.P.; Validation: E.L.S., H.M.P.; Formal analysis: E.L.S., H.M.P.; Investigation: E.L.S., H.M.P.; Resources: E.L.S., H.M.P.; Data curation: E.L.S., K.H.W., A.F., S.G., A.M., H.M.P.; Writing - original draft: E.L.S., H.M.P.; Writing - review & editing: E.L.S., K.H.W., A.F., S.G., A.M., H.M.P.; Visualization: E.L.S., H.M.P.; Supervision: E.L.S., H.M.P.; Project administration: E.L.S., H.M.P.; Funding acquisition: H.M.P.

Data Availability

All data and code used to produce results and complete analyses are available at https://github.com/hputnam/Acclim_Dynamics. Laboratory protocols and processing can be found on Emma Strand's Open Laboratory Notebook at

https://emmastrand.github.io/EmmaStrand_Notebook/. ITS2 Sequencing FASTQ files are uploaded to NCBI under Project #PRJNA761780.

Acknowledgements

We thank the Hawai‘i Institute of Marine Biology and the Coral Resilience Laboratory for hosting us to conduct the experiment on Coconut Island, and Chris Suchoki and Adam Helbig for assistance with field work. Ariana Huffmyer provided valuable feedback on an earlier version of the manuscript. As guests, we recognize and give thanks for the land and water resources of the ‘ā ina and the traditional owners of the land, kānaka ‘ō iwi, on which this experimental work was conducted in the Kāne‘ohe Ahupua’a and the islands of Hawai’i. The authors acknowledge use of the computational resources of the URI Center for Computational Research for this work.

References

Abbott, E., Dixon, G. and Matz, M. (2021). Shuffling between Cladocopium and Durusdinium extensively modifies the physiology of each symbiont without stressing the coral host. Mol. Ecol. 30, 6585-6595. doi:10.1111/mec.16190

Ainsworth, T. D., Heron, S. F., Ortiz, J. C., Mumby, P. J., Grech, A., Ogawa, D., Mark Eakin, C. and Leggat, W. (2016). Climate change disables coral bleaching protection on the Great Barrier Reef. Science 352, 338-342. doi:10.1126/science.aac7125

Anthony, K. R. N. and Hoegh-Guldberg, O. (2003). Variation in coral photosynthesis, respiration and growth characteristics in contrasting light microhabitats: an analogue to plants in forest gaps and understoreys? Funct. Ecol. 17, 246-259. doi:10.1046/j.1365-2435.2003.00731.x

Bahr, K. D., Jokiel, P. L. and Rodgers, K. S. (2015). The 2014 coral bleaching and freshwater flood events in Kāne’ohe Bay, Hawai’i. PeerJ 3, e1136. doi:10.7717/peerj.1136

Bahr, K. D., Jokiel, P. L. and Rodgers, K. S. (2016). Relative sensitivity of five Hawaiian coral species to high temperature under high-pCO_2 conditions. Coral Reefs 35, 729-738. doi:10.1007/s00338-016-1405-4

Baird, A. H., Bhagooli, R., Ralph, P. J. and Takahashi, S. (2009). Coral bleaching: the role of the host. Trends Ecol. Evol. 24, 16-20. doi:10.1016/j.tree.2008.09.005

Barshis, D. J., Ladner, J. T., Oliver, T. A., Seneca, F. O., Traylor-Knowles, N. and Palumbi, S. R. (2013). Genomic basis for coral resilience to climate change. Proc. Natl. Acad. Sci. U.S.A. 110, 1387-1392. doi:10.1073/pnas.1210224110

Baskett, M. L., Gaines, S. D. and Nisbet, R. M. (2009). Symbiont diversity may help coral reefs survive moderate climate change. Ecol. Appl. 19, 3-17. doi:10.1890/08-0139.1

Bates, D., Ma¨ chler, M., Bolker, B. and Walker, S. (2015). Fitting linear mixed effects models using lme4. J. Stat. Softw. 67, 1-48. doi:10.18637/jss.v067.i01

Bellantuono, A. J., Hoegh-Guldberg, O. and Rodriguez-Lanetty, M. (2012). Resistance to thermal stress in corals without changes in symbiont composition. Proc. Biol. Sci. R. Soc. 279, 1100-1107. doi:10.1098/rspb.2011.1780

Boilard, A., Dube´, C. E., Gruet, C., Mercie`re, A., Hernandez-Agreda, A. and Derome, N. (2020). Defining coral bleaching as a microbial dysbiosis within the coral holobiont. Microorganisms 8, 1682. doi:10.3390/microorganisms8111682

Bourne, D. G., Morrow, K. M. and Webster, N. S. (2016). Insights into the coral microbiome: underpinning the health and resilience of reef ecosystems. Annu. Rev. Microbiol. 70, 317-340. doi:10.1146/annurev-micro-102215-095440

Brown, B. E., Dunne, R. P., Goodson, M. S. and Douglas, A. E. (2000). Bleaching patterns in reef corals. Nature 404, 142-143. doi:10.1038/35004657

Brown, K. T., Mello-Athayde, M. A., Sampayo, E. M., Chai, A., Dove, S. and Barott, K. L. (2022). Environmental memory gained from exposure to extreme pCO variability promotes coral cellular acid-base homeostasis. Proc. Biol. Sci. R. Soc. 289, 20220941. doi:10.1098/rspb.2022.0941

Claar, D. C., Starko, S., Tietjen, K. L., Epstein, H. E., Cunning, R., Cobb, K. M., Baker, A. C., Gates, R. D. and Baum, J. K. (2020). Dynamic symbioses reveal pathways to coral survival through prolonged heatwaves. Nat. Commun. 11, 6097. doi:10.1038/s41467-020-19169-y

Cunning, R. and Baker, A. C. (2013). Excess algal symbionts increase the susceptibility of reef corals to bleaching. Nat. Clim. Change. 3, 259-262. doi:10.1038/nclimate1711

Cunning, R., Ritson-Williams, R. and Gates, R. D. (2016). Patterns of bleaching and recovery of *Montipora capitata* in Kāne'ohe Bay, Hawai'i, USA. Mar. Ecol. Prog. Ser. 551, 131-139. doi:10.3354/meps11733

Cziesielski, M. J., Schmidt-Roach, S. and Aranda, M. (2019). The past, present, and future of coral heat stress studies. Ecol. Evol. 9, 10055-10066. doi:10.1002/ece3.5576

Davies, S. P. (1989). Short-term growth measurements of corals using an accurate buoyant weighing technique. Mar. Biol. 101, 389-395.

DeMerlis, A., Kirkland, A., Kaufman, M. L., Mayfield, A. B., Formel, N., Kolodziej, G., Manzello, D. P., Lirman, D., Traylor-Knowles, N. and Enochs, I. C. (2022). Pre-exposure to a variable temperature treatment improves the response of Acropora cervicornis to acute thermal stress. Coral Reefs. 41, 435-445. doi:10.1007/s00338-022-02232-z

Dickson, A. G. (1990). Standard potential of the reaction: AgCl(s)+12H2(g)=Ag(s)+HCl(aq), and the standard acidity constant of the ion HSO4 − in synthetic sea water from 273.15 to 318.15 K. J. Chem. Thermodyn. 22, 113-127. doi:10.1016/0021-9614(90)90074-Z

870
871 Dickson, A. G., Sabine, C. L. and Christian, J. R. (ed.) (2007). Guide to Best Practices for
872 Ocean CO2 Measurements. PICES Special Publication 3. Sidney, BC: North Pacific Marine
873 Science Organization.
874
875 Dixon, P. (2003). VEGAN, a package of R functions for community ecology. J. Veg. Sci. 14,
876 927-930. doi:10.1111/j.1654-1103.2003.tb02228.x
877
878 Downs, C. A., Mueller, E., Phillips, S., Fauth, J. E. and Woodley, C. M. (2000). A molecular
879 biomarker system for assessing the health of coral (Montastraea faveolate) during heat stress.
880 Mar. Biotechnol. 2, 533-544. doi:10.1007/s101260000038
881
882 Drupp, P., De Carlo, E. H., Mackenzie, F. T., Bienfang, P. and Sabine, C. L. (2011). Nutrient
883 inputs, phytoplankton response, and CO2 variations in a semienclosed subtropical embayment,
884 Kaneohe Bay, Hawaii. Aquat. Geochem. 17, 473-498. doi:10.1007/s10498-010-9115-y
885
886 Dufault, A. M., Cumbo, V. R., Fan, T. Y. and Edmunds, P. J. (2012). Effects of diurnally
887 oscillating pCO_2 on the calcification and survival of coral recruits. Proc. R. Soc. B 279, 2951-
888 2958. doi:10.1098/rspb.2011.2545
889
890 Edmunds, P. J. and Davies, P. S. (1988). Post-illumination stimulation of respiration rate in the
891 coral Porites porites. Coral Reefs 7, 7-9. doi:10.1007/BF00301975
892
893 Edmunds, P. J. and Putnam, H. M. (2020). Science-based approach to using growth rate to
894 assess coral performance and restoration outcomes. Biol. Lett. 16, 20200227.
895 doi:10.1098/rsbl.2020.0227
896
897 Edmunds, P. J., Gates, R. D. and Gleason, D. F. (2003). The tissue composition of Montastraea
898 franksi during a natural bleaching event in the Florida Keys. Coral Reefs 22, 54-62.
899 doi:10.1007/s00338-003-0278-5
900
901 Gardner, S. G., Raina, J.-B., Nitschke, M. R., Nielsen, D. A., Stat, M., Motti, C. A., Ralph, P. J.
902 and Petrou, K. (2017). A multi-trait systems approach reveals a response cascade to bleaching
903 in corals. BMC Biol. 15, 117. doi:10.1186/s12915-017-0459-2
904
905 Gates, R. D., Baghdasarian, G. and Muscatine, L. (1992). Temperature stress causes host cell
906 detachment in symbiotic cnidarians: implications for coral bleaching. Biol. Bull. 182, 324-332.
907 doi:10.2307/1542252
908
909 Gattuso, J.-P., Magnan, A., Bille´, R., Cheung, W. W. L., Howes, E. L., Joos, F., Allemand, D.,
910 Bopp, L., Cooley, S. R., Eakin, C. M. et al. (2015). Contrasting futures for ocean and society
911 from different anthropogenic CO2 emissions scenarios. Science 349, 6243.
912 doi:10.1126/science.aac4722
913
914 Gibbin, E. M., Putnam, H. M., Davy, S. K. and Gates, R. D. (2014). Intracellular pH and its
915 response to CO2-driven seawater acidification in symbiotic versus nonsymbiotic coral cells. J.
916 Exp. Biol. 217, 1963-1969. doi:10.1242/jeb.099549
917
918 Gibbin, E. M., Putnam, H. M., Gates, R. D., Nitschke, M. R. and Davy, S. K. (2015). Species-
919 specific differences in thermal tolerance may define susceptibility to intracellular acidosis in reef
920 corals. Mar. Biol. 162, 717-723. doi:10.1007/s00227-015-2617-9

Grottoli, A. G., Warner, M. E., Levas, S. J., Aschaffenburg, M. D., Schoepf, V., McGinley, M., Baumann, J. and Matsui, Y. (2014). The cumulative impact of annual coral bleaching can turn some coral species winners into losers. Glob. Change Biol. 20, 3823-3833. doi:10.1111/gcb.12658

Guadayol, O., Silbiger, N. J., Donahue, M. J. and Thomas, F. I. (2014). Patterns in temporal variability of temperature, oxygen and pH along an environmental gradient in a coral reef. PLoS ONE 9, e85213. doi:10.1371/journal.pone.0085213

Guest, J. R., Low, J., Tun, K., Wilson, B., Ng, C., Raingeard, D., Ulstrup, K. E., Tanzil, J. T. I., Todd, P. A., Toh, T. C. et al. (2016). Coral community response to bleaching on a highly disturbed reef. Sci. Rep. 6, 20717. doi:10.1038/srep20717

Hackerott, S., Martell, H. A. and Eirin-Lopez, J. M. (2021). Coral environmental memory: causes, mechanisms, and consequences for future reefs. Trends Ecol. Evol. 36, 1011-1023. doi:10.1016/j.tree.2021.06.014

Heberling, J. M. and Fridley, J. D. (2013). Resource-use strategies of native and invasive plants in eastern North American forests. New Phytol. 200, 523-533. doi:10.1111/nph.12388

Heron, S. F., Maynard, J. A., van Hooidonk, R. and Mark Eakin, C. (2016). Warming trends and bleaching stress of the World's coral reefs 1985–2012. Sci. Rep. 6, 1-14. doi:10.1038/s41598-016-0001-8

Hoadley, K. D., Lewis, A. M., Wham, D. C., Tye Pettay, D., Grasso, C., Smith, R., Kemp, D. W., LaJeunesse, T. C. and Warner, M. E. (2019). Host–symbiont combinations dictate the photo-physiological response of reef-building corals to thermal stress. Sci. Rep. 9, 9985. doi:10.1038/s41598-019-46412-4

Hume, B. C. C., Smith, E. G., Ziegler, M., Warrington, H. J. M., Burt, J. A., LaJeunesse, T. C., Wiedenmann, J. and Voolstra, C. R. (2019). SymPortal: A novel analytical framework and platform for coral algal symbiont next-generation sequencing ITS2 profiling. Mol. Ecol. Res. 19, 1063-1080. doi:10.1111/1755-0998.13004

IPCC (2018). Summary for policymakers. In: Global Warming of 1.5°C. An IPCC Special Report on the Impacts of Global Warming of 1.5°C above Pre-Industrial Levels and Related Global Greenhouse Gas Emission Pathways, in the Context of Strengthening the Global Response to the Threat of Climate Change, Sustainable Development, and Efforts to Eradicate Poverty (ed. Masson-Delmotte, T. W. V., Zhai, P., Pö rtner, H. O., Roberts, D., Skea, J., Shukla, P. R., Pirani, A. et al.), pp. 3-24. Cambridge University Press. doi:10.1017/9781009157940.001

Jeffrey, S. W. and Humphrey, G. F. (1975). New spectrophotometric equations for determining chlorophylls a, b, c1 and c2 in higher plants, algae and natural phytoplankton. Biochem. Physiol. Pflanzen 167, 191-194. doi:10.1016/s0015-3796(17)30778-3

Jokiel, P. L., Maragos, J. E. and Franzisket, L. (1978). Coral growth: buoyant weight technique. In Coral Reefs: Research Methods (ed. D. R. Stoddart and R. E. Johannes), pp. 529-541. Paris: UNESCO.

Jurriaans, S. and Hoogenboom, M. O. (2020). Seasonal acclimation of thermal performance in two species of reef-building corals. Mar. Ecol. Prog. Ser. 635, 55-70. doi:10.3354/meps13203

Jury, C. P., Thomas, F. I. M., Atkinson, M. J. and Toonen, R. J. (2013). Buffer capacity, ecosystem feedbacks, and seawater chemistry under global change. WATER 5, 1303-1325. doi:10.3390/w5031303

Klein, S. G., Geraldi, N. R., Anton, A., Schmidt-Roach, S., Ziegler, M., Cziesielski, M. J., Martin, C., Ra¨decker, N., Fro¨ licher, T. L., Mumby, P. J. et al. (2022). Projecting coral responses to intensifying marine heatwaves under ocean acidification. Glob. Change Biol. 28, 1753-1765. doi:10.1111/gcb.15818

Kugler, K. C., Dziak, J. J. and Trail, J. (2018). Coding and interpretation of effects in analysis of data from a factorial experiment. In Optimization of Behavioral, Biobehavioral, and Biomedical Interventions. Statistics for Social and Behavioral Sciences (ed. L. Collins and K. Kugler), pp. 175-205. Cham: Springer. doi:10.1007/978-3-319-91776-4_6

Lajeunesse, T. C. and Trench, R. K. (2000). Biogeography of two species of Symbiodinium (Freudenthal) Inhabiting the intertidal sea anemone Anthopleura elegantissima (Brandt). Biol. Bull. 199, 126-134. doi:10.2307/1542872

LaJeunesse, T. C., Parkinson, J. E., Gabrielson, P. W., Jeong, H. J., Reimer, J. D., Voolstra, C. R. and Santos, S. R. (2018). Systematic revision of Symbiodiniaceae highlights the antiquity and diversity of coral endosymbionts. Curr. Biol. 28, 2570-2580. doi:10.1016/j.cub.2018.07.008

Le Nohaïc, M., Ross, C. L., Cornwall, C. E., Comeau, S., Lowe, R., McCulloch, M. T. and Schoepf, V. (2017). Marine heatwave causes unprecedented regional mass bleaching of thermally resistant corals in Northwestern Australia. Sci. Rep. 7, 14999. doi:10.1038/s41598-017-14794-y

Lesser, M. P. (2004). Experimental biology of coral reef ecosystems. J. Exp. Mar. Biol. Ecol. 300, 217-252. doi:10.1016/j.jembe.2003.12.027

Lesser, M. P. (2011). Coral bleaching: causes and mechanisms. In Coral Reefs: An Ecosystem in Transition (ed. Z. Dubinsky and N. Stambler). Dordrecht: Springer. doi:10.1007/978-94-007-0114-4_23

Loya, Y., Sakai, K., Yamazato, K., Nakano, Y., Sambali, H. and van Woesik, R. (2001). Coral bleaching: the winners and the losers. Ecol. Lett. 4, 122-131. doi:10.1046/j.14610248.2001.00203.x

Lueker, T. J., Dickson, A. G. and Keeling, C. D. (2000). Ocean pCO_2 calculated from dissolved inorganic carbon, alkalinity, and equations for K1 and K2: validation based on laboratory measurements of CO2 in gas and seawater at equilibrium. Mar. Chem. 70, 105-119. doi:10.1016/S0304-4203(00)00022-0

Magnusson, S. H., Fine, M. and Ku¨ hl, M. (2007). Light microclimate of endolithic phototrophs in the scleractinian corals Montipora monasteriata and Porites cylindrica. Mar. Ecol. Prog. Ser. 332, 119-128. doi:10.3354/meps332119

1021 Marshall, B. and Biscoe, P. V. (1980). A model for C3 leaves describing the dependence of net
1022 photosynthesis on irradiance. J. Exp. Bot. 31, 29-39. doi:10.1093/jxb/31.1.29
1023
1024 Matsuda, S., Huffmyer, A., Lenz, E. A., Davidson, J., Hancock, J., Przybylowski, A., Innis, T.,
1025 Gates, R. D. and Barott, K. L. (2020). Coral bleaching susceptibility is predictive of subsequent
1026 mortality within but not between coral species. Front. Ecol. Evol. 8, 178.
1027 doi:10.3389/fevo.2020.00178
1028
1029 Matthews, J. L., Crowder, C. M., Oakley, C. A., Lutz, A., Roessner, U., Meyer, E., Grossman, A.
1030 R., Weis, V. M. and Davy, S. K. (2017). Optimal nutrient exchange and immune responses
1031 operate in partner specificity in the cnidarian–dinoflagellate symbiosis. Proc. Natl. Acad. Sci.
1032 U.S.A. 114, E11058.
1033
1034 Matthews, J. L., Oakley, C. A., Lutz, A., Hillyer, K. E., Roessner, U., Grossman, A. R., Weis, V.
1035 M. and Davy, S. K. (2018). Partner switching and metabolic flux in a model cnidarian–
1036 dinoflagellate symbiosis. Proc. R. Soc. B 285, 20182336. doi:10.1098/rspb.2018.2336
1037
1038 McLachlan, R. H., Price, J. T., Solomon, S. L. and Grottoli, A. G. (2020). Thirty years of coral
1039 heat-stress experiments: a review of methods. Coral Reefs 39, 885-902. doi:10.1007/s00338-
1040 020-01931-9
1041
1042 McLachlan, R. H., Price, J. T., Mun˜oz-Garcia, A., Weisleder, N. L., Jury, C. P., Toonen, R. J.
1043 and Grottoli, A. G. (2021). Environmental gradients drive physiological variation in Hawaiian
1044 corals. Coral Reefs 40, 1505-1523. doi:10.1007/s00338-021-02140-8
1045
1046 Mollica, N. R., Guo, W., Cohen, A. L., Huang, K.-F., Foster, G. L., Donald, H. K. and Solow, A.
1047 R. (2018). Ocean acidification affects coral growth by reducing skeletal density. Proc. Natl.
1048 Acad. Sci. U.S.A. 115, 1754-1759. doi:10.1073/pnas.1712806115
1049
1050 Mydlarz, L. D., McGinty, E. S. and Drew Harvell, C. (2010). What are the physiological and
1051 immunological responses of coral to climate warming and disease? J. Exp. Biol. 213, 934-945.
1052 doi:10.1242/jeb.037580
1053
1054 Neal, B. P., Khen, A., Treibitz, T., Beijbom, O., O'Connor, G., Coffroth, M. A., Knowlton, N.,
1055 Kriegman, D., Greg Mitchell, B. and Kline, D. I. (2017). Caribbean massive corals not recovering
1056 from repeated thermal stress events during 2005–2013. Ecol. Evol. 7, 1339-1353.
1057
1058 Oakley, C. A. and Davy, S. K. (2018). Cell biology of coral bleaching. In Coral Bleaching.
1059 Ecological Studies, vol. 233 (ed. M. van Oppen and J. Lough). Cham: Springer.
1060 doi:10.1007/978-3-319-75393-5_8
1061
1062 Olito, C., White, C. R., Marshall, D. J. and Barneche, D. R. (2017). Estimating monotonic rates
1063 from biological data using local linear regression. J. Exp. Biol. 220, 759-764.
1064 doi:10.1242/jeb.148775
1065
1066 Oliver, T. A. and Palumbi, S. R. (2011). Many corals host thermally resistant symbionts in high-
1067 temperature habitat. Coral Reefs 30, 241-250. doi:10.1007/s00338-010-0696-0
1068
1069 Oliver, E. C. J., Donat, M. G., Burrows, M. T., Moore, P. J., Smale, D. A., Alexander, L. V.,
1070 Benthuysen, J. A., Feng, M., Sen Gupta, A., Hobday, A. J. et al. (2018). Longer and more

frequent marine heatwaves over the past century. Nat. Commun. 9, 1324. doi:10.1038/s41467-018-03732-9

Oliver, E. C. J., Benthuysen, J. A., Darmaraki, S., Donat, M. G., Hobday, A. J., Holbrook, N. J., Schlegel, R. W. and Gupta, A. S. (2021). Marine heatwaves. Ann. Rev. Mar. Sci. 13, 313-342. doi:10.1146/annurev-marine-032720-095144

Osborne, K., Thompson, A. A., Cheal, A. J., Emslie, M. J., Johns, K. A., Jonker, M. J., Logan, M., Miller, I. R. and Sweatman, H. P. A. (2017). Delayed coral recovery in a warming ocean. Glob. Change Biol. 23, 3869-3881. doi:10.1111/gcb.13707

Pendleton, L. H., Hoegh-Guldberg, O., Langdon, C. and Comte, A. (2016). Multiple stressors and ecological complexity require a new approach to coral reef research. Front. Mar. Sci. 3, 36. doi:10.3389/fmars.2016.00036

Perez, F. F. and Fraga, F. (1987). Association constant of fluoride and hydrogen ions in seawater. Mar. Chem. 21, 161-168. doi:10.1016/0304-4203(87)90036-3

Putnam, H. M. (2021). Avenues of reef-building coral acclimatization in response to rapid environmental change. J. Exp. Biol. 224, jeb239319. doi:10.1242/jeb.239319

Putnam, H. M. and Edmunds, P. J. (2011). The physiological response of reef corals to diel fluctuations in seawater temperature. J. Exp. Mar. Biol. Ecol. 396, 216-223. doi:10.1016/j.jembe.2010.10.026

Putnam, H. M., Mayfield, A. B., Fan, T. Y., Chen, C. S. and Gates, R. D. (2013). The physiological and molecular responses of larvae from the reef-building coral Pocillopora damicornis exposed to near-future increases in temperature and pCO_2. Mar. Biol. 160, 2157-2173. doi:10.1007/s00227-012-2129-9

Putnam, H. M., Barott, K. L., Ainsworth, T. D. and Gates, R. D. (2017). The vulnerability and resilience of reef-building corals. Curr. Biol. 27, R528-R540. doi:10.1016/j.cub.2017.04.047

Roach, T. N., Dilworth, J., Jones, A. D., Quinn, R. A. and Drury, C. (2021). Metabolomic signatures of coral bleaching history. Nature Ecol. Evol. 54, 495-503.doi:10.1038/s41559-020-01388-7

Rodrigues, L. J. and Grottoli, A. G. (2007). Energy reserves and metabolism as indicators of coral recovery from bleaching. Limnol. Oceanogr. 52, 1874-1882. doi:10.4319/lo.2007.52.5.1874

Rodrıdguez-Troncoso, A. P., Carpizo-Ituarte, E. and Cupul-Magan˜a, A. L. (2016). Physiological response to high temperature in the tropical Eastern Pacific coral Pocillopora verrucosa. Mar. Ecol. 10, 1212717. doi:10.3389/fmars.2023.1212717

Rohwer, F., Seguritan, V., Azam, F. and Knowlton, N. (2002). Diversity and distribution of coral-associated bacteria. Mar. Ecol. Prog. Ser. 243, 1-10. doi:10.3354/meps243001

Safaie, A., Silbiger, N. J., McClanahan, T. R., Pawlak, G., Barshis, D. J., Hench, J. L., Rogers, J. S., Williams, G. J. and Davis, K. A. (2018). High frequency temperature variability reduces the risk of coral bleaching. Nat. Commun. 9, 1671. doi:10.1038/s41467-018-04074-2

Scheufen, T., Kra¨mer, W. E., Iglesias-Prieto, R. and Enrı´quez, S. (2017). Seasonal variation modulates coral sensibility to heat-stress and explains annual changes in coral productivity. Sci. Rep. 7, 4937. doi:10.1038/s41598-017-04927-8

Schoepf, V., Grottoli, A. G., Levas, S. J., Aschaffenburg, M. D., Baumann, J. H., Matsui, Y. and Warner, M. E. (2015). Annual coral bleaching and the long-term recovery capacity of coral. Proc. R. Soc. B 282, 20151887. doi:10.1098/rspb.2015.1887

Schoepf, V., Sanderson, H. and Larcombe, E. (2022). Coral heat tolerance under variable temperatures: effects of different variability regimes and past environmental history vs. current exposure. Limnol.Oceanogr. 67, 404-418. doi:10.1002/lno.12000

Shaw, E. C., Hamylton, S. M. and Phinn, S. R. (2016). Incorporating benthic community changes into hydrochemical-based projections of coral reef calcium carbonate production under ocean acidification. Coral Reefs 35, 739-750. doi:10.1007/s00338-016-1407-2

Silverstein, R. N., Cunning, R. and Baker, A. C. (2015). Change in algal symbiont communities after bleaching, not prior heat exposure, increases heat tolerance of reef corals. Glob. Change Biol. 21, 236-249. doi:10.1111/gcb.12706

Stat, M., Morris, E. and Gates, R. D. (2008). Functional diversity in coral–dinoflagellate symbiosis. Proc. Natl Acad. Sci. USA 105, 9256-9261. doi:10.1073/pnas.0801328105

Sweet, M. J. and Brown, B. E. (2016). Coral responses to anthropogenic stress in the twenty-first century: an ecophysiological perspective. Oceanogr. Mar. Biol. Ann. Rev. 54, 271-314.

Therneau, T. M., and Grambsch, P. M. (2013). Modeling Survival Data: Extending the Cox Model. Springer Science & Business Media.

Thomas, L. and Palumbi, S. R. (2017). The genomics of recovery from coral bleaching. Proc. Biol. Sci. R. Soc. 284, 20171790. doi:10.1098/rspb.2017.1790

Thornhill, D. J., Rotjan, R. D., Todd, B. D., Chilcoat, G. C., Iglesias-Prieto, R., Kemp, D.W., LaJeunesse, T. C., Reynolds, J. M. C., Schmidt, G.W., Shannon, T. et al. (2011). A connection between colony biomass and death in caribbean reef-building corals. PloS One 6, e29535. doi:10.1371/journal.pone.0029535

Tresguerres, M., K. L. Barott, M. E. Barron, D. D. Deheyn, D. I. Kline, and Linsmayer, L. B. (2017). Cell biology of reef-building corals: ion transport, acid/ base regulation, and energy metabolism. In Acid-Base Balance and Nitrogen Excretion in Invertebrates: Mechanisms and Strategies in Various Invertebrate Groups with Considerations of Challenges Caused by Ocean Acidification (ed. Dirk Weihrauch and Michael O'Donnell), 193-218. Cham: Springer International Publishing.

van Oppen, M. J. H. and Lough, J. M. (2018). Coral Bleaching: Patterns, Processes, Causes and Consequences. Springer. Veal, C. J., Carmi, M., Fine, M. and Hoegh-Guldberg, O. (2010). Increasing the accuracy of surface area estimation using single wax dipping of coral fragments. Coral Reefs 29, 893-897. doi:10.1007/s00338-010-0647-9

Wall, C. B., Ritson-Williams, R., Popp, B. N. and Gates, R. D. (2019). Spatial variation in the biochemical and isotopic composition of corals during bleaching and recovery. Limnol. Oceanogr. 64, 2011-2028. doi:10.1002/lno.11166

Wall, C. B., Kaluhiokalani, M., Popp, B. N., Donahue, M. J. and Gates, R. D. (2020). Divergent symbiont communities determine the physiology and nutrition of a reef coral across a light-availability gradient. ISME J. 14, 945-958. doi:10.1038/s41396-019-0570-1

Wall, C. B., Ricci, C. A., Wen, A. D., Ledbetter, B. E., Klinger, D. E., Mydlarz, L. D., Gates, R. D. and Putnam, H. M. (2021). Shifting baselines: physiological legacies contribute to the response of reef corals to frequent heatwaves. Funct. Ecol. 35, 1366-1378. doi:10.1111/1365-2435.13795

Weis, V. M. (2008). Cellular mechanisms of cnidarian bleaching: stress causes the collapse of symbiosis. J. Exp. Biol. 211, 3059-3066. doi:10.1242/jeb.009597

van Oppen, M. J., Oliver, J. K., Putnam, H. M. and Gates, R. D. (2015). Building coral reef resilience through assisted evolution. Proc. Natl. Acad. Sci. USA 112, 2307-2313. doi:10.1073/pnas.1422301112

van Woesik, R. and Kratochwill, C. (2022). A global coral-bleaching database, 19802020. Sci. Data 9, 20. doi:10.1038/s41597-022-01121-y

vanWoesik, R., Sakai, K., Ganase, A. and Loya, Y. (2011). Revisiting the winners and the losers a decade after coral bleaching. Mar. Ecol. Prog. Ser. 434, 67-76. doi:10.3354/meps09203

van Woesik, R., Shlesinger, T., Grottoli, A. G., Toonen, R. J., Thurber, R. V., Warner, M. E., Hulver, A. M., Chapron, L., McLachlan, R. H., Albright, R. et al. (2022). Coral-bleaching responses to climate change across biological scales. Glob. Change Biol. 28, 4229-4250. doi:10.1111/gcb.16192

Ziegler, M., Anton, A., Klein, S. G., Ra¨decker, N., Geraldi, N. R., Schmidt-Roach, S., Saderne, V., Mumby, P. J., Cziesielski, M. J., Martin, C. et al. (2021). Integrating environmental variability to broaden the research on coral responses to future ocean conditions. Glob. Change Biol. 27, 5532-5546. doi:10.1111/gcb.15840

Ziegler, M., Roder, C. M., Bu¨ chel, C. and Voolstra, C. R. (2015). Mesophotic coral depth acclimatization is a function of host-specific symbiont physiology. Front. Mar. Sci. 2, 4. doi:10.3389/fmars.2015.00004

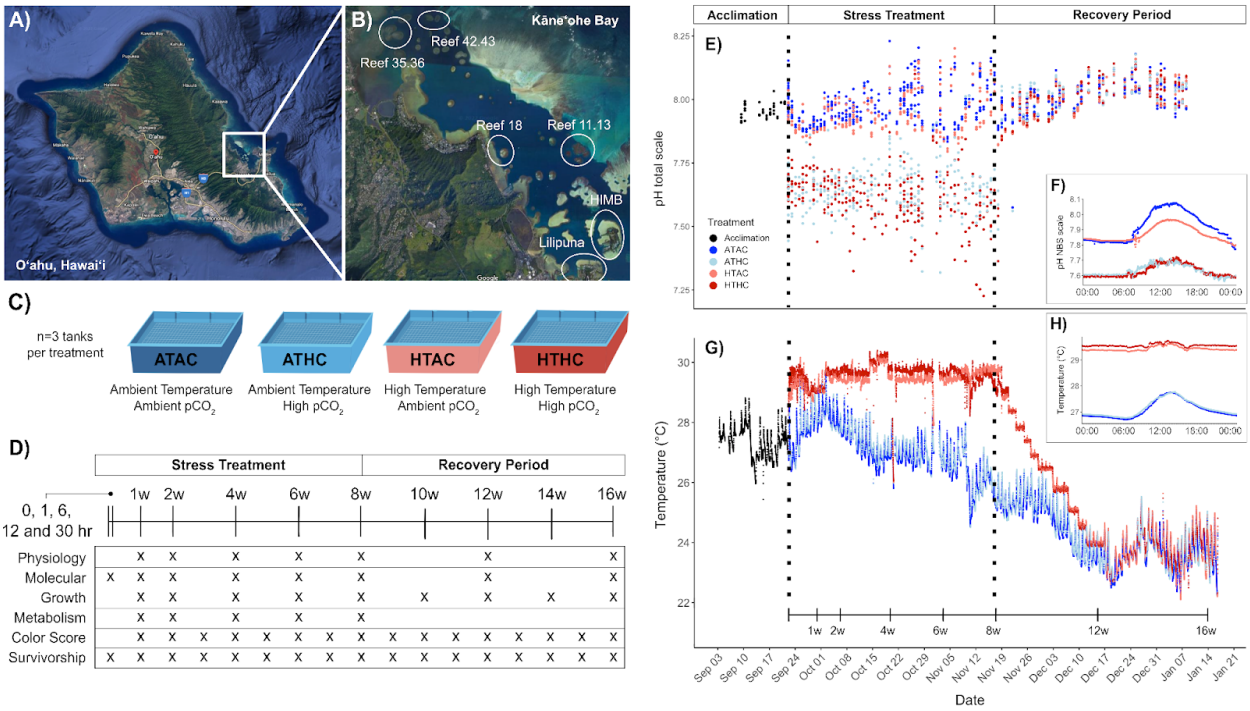

Fig. 1. Experimental design for an environmentally and seasonally realistic extended heatwave scenario. (A) A map of O'ahu, Hawai'i, with a highlight box around the study site. (B) A map of Kāne'ohe Bay with six circled collection sites. (C) Twelve tanks (n=3 per treatment) were assigned a treatment with the following color and acronym code: ATAC (dark blue), ATHC (light blue), HTAC (light red), HTHC (dark red). (D) Sampling timeline with an 'x' to indicate when sampling occurred for each response category (n=6 physiology; n=3 molecular per species per treatment). Physiology includes antioxidant capacity, soluble protein, ash-free dry weight (AFDW), chlorophyll a (*chl a*) content and endosymbiont density. Metabolism includes photosynthetic and respiration rates. (E) Discrete measurements for pH treatment conditions (pH total scale) for the full experimental period. (F) Average daily pH treatment conditions modeled after natural fluctuations that occur in Kāne'ohe Bay. Data come from continuous measurements from an Apex System set up during the first 2 weeks of the exposure period. (G) Discrete measurements for temperature treatment conditions (°C) for the full experimental period. A timeline of physiological sampling dates is indicated above the x-ais. (H) Average daily temperature treatment conditions modeled after natural fluctuations that occur in Kāne'ohe Bay.

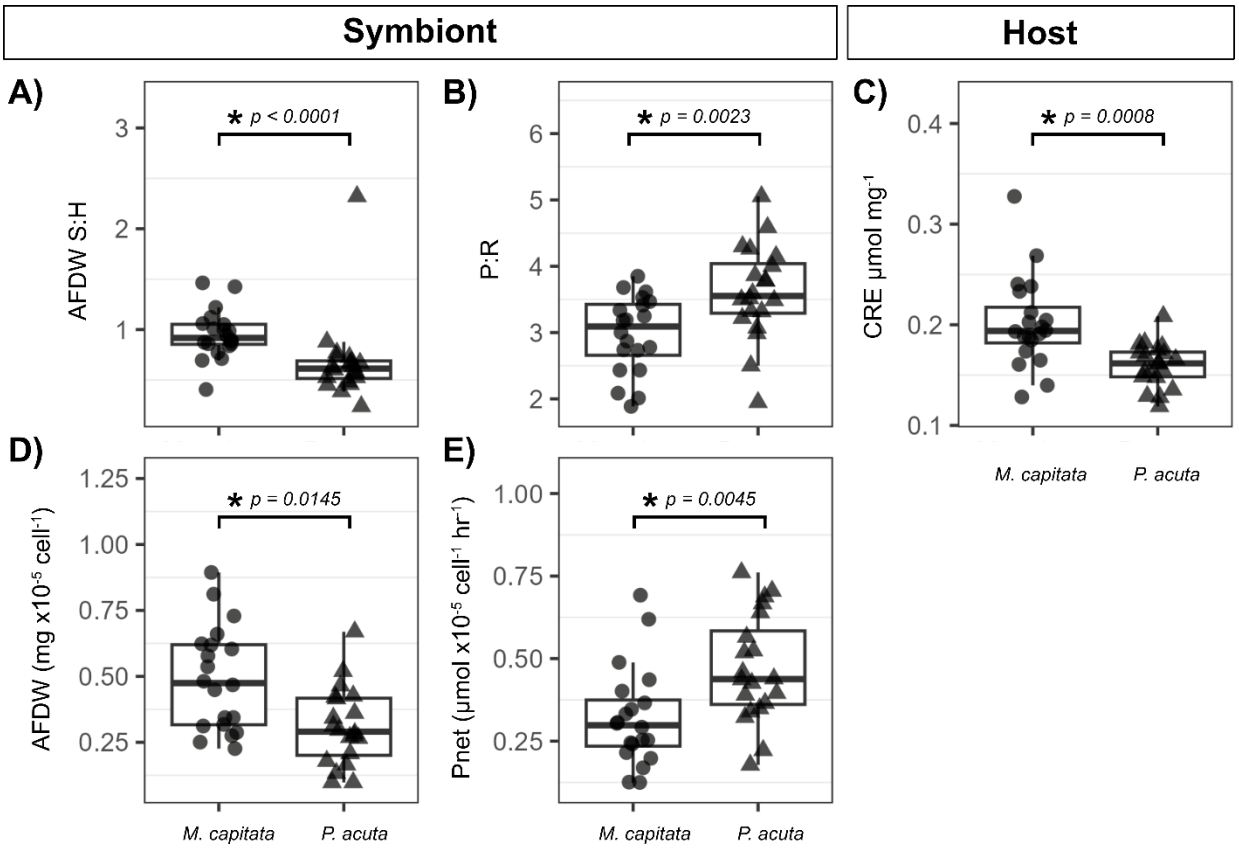

Fig. 2. *Montipora capitata* and *Pocillopora acuta* baseline physiological measurements measured at week 1. (A) AFDW symbiont:host (S:H) ratio, (B) photosynthesis:respiration (P:R) ratio, (C) host total antioxidant capacity (CRE µmol mg−1), (D) symbiont cellular AFDW (×10−5 mg cell−1) and (E) cellular net photosynthetic rates (Pnet; ×10−5 µmol O2 cell−1 h−1).

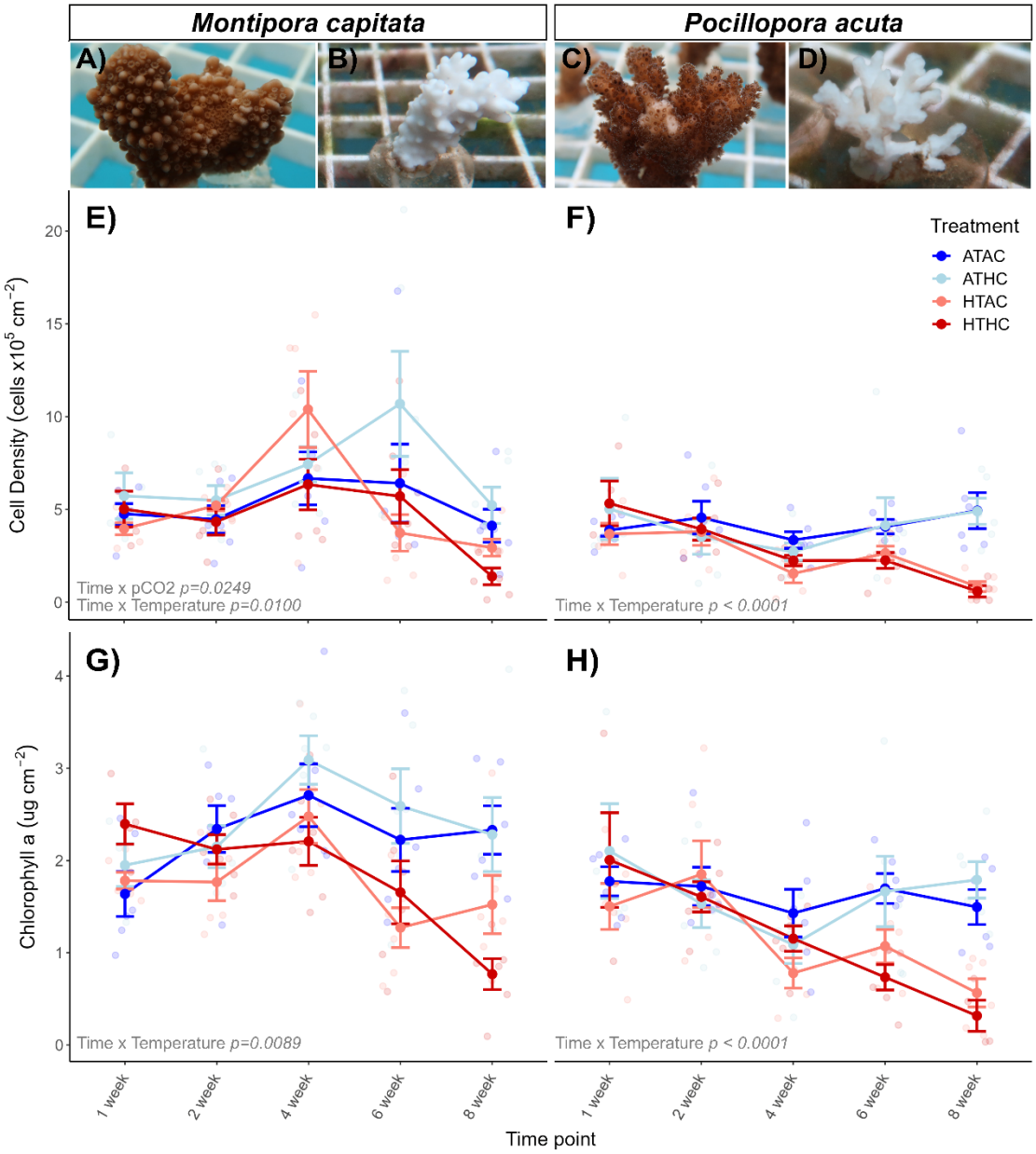

Fig. 3. Holobiont chlorophyll a content (µg cm−2) and endosymbiont cell density (×105 cells cm−2) levels during the exposure period (weeks 1–8). The x-axis of E–H is time in weeks with sampling at 1, 2, 4, 6 and 8 weeks. Color indicates the four treatments. Points represent means±s.e.m., and significant effects from Type III ANOVA of linear mixed models for each response are labeled with corresponding P-value. (A–D) Examples of (A,C) healthy and (B,D) bleached *M. capitata* and *P. acuta* fragments. (E,F) Cell density levels (×105 cells cm−2) of (E) *M. capitata* and (F) *P. acuta*. (G) *Chl a* content (µg cm−2) of (G) *M. capitata* and (H) *P. acuta*.

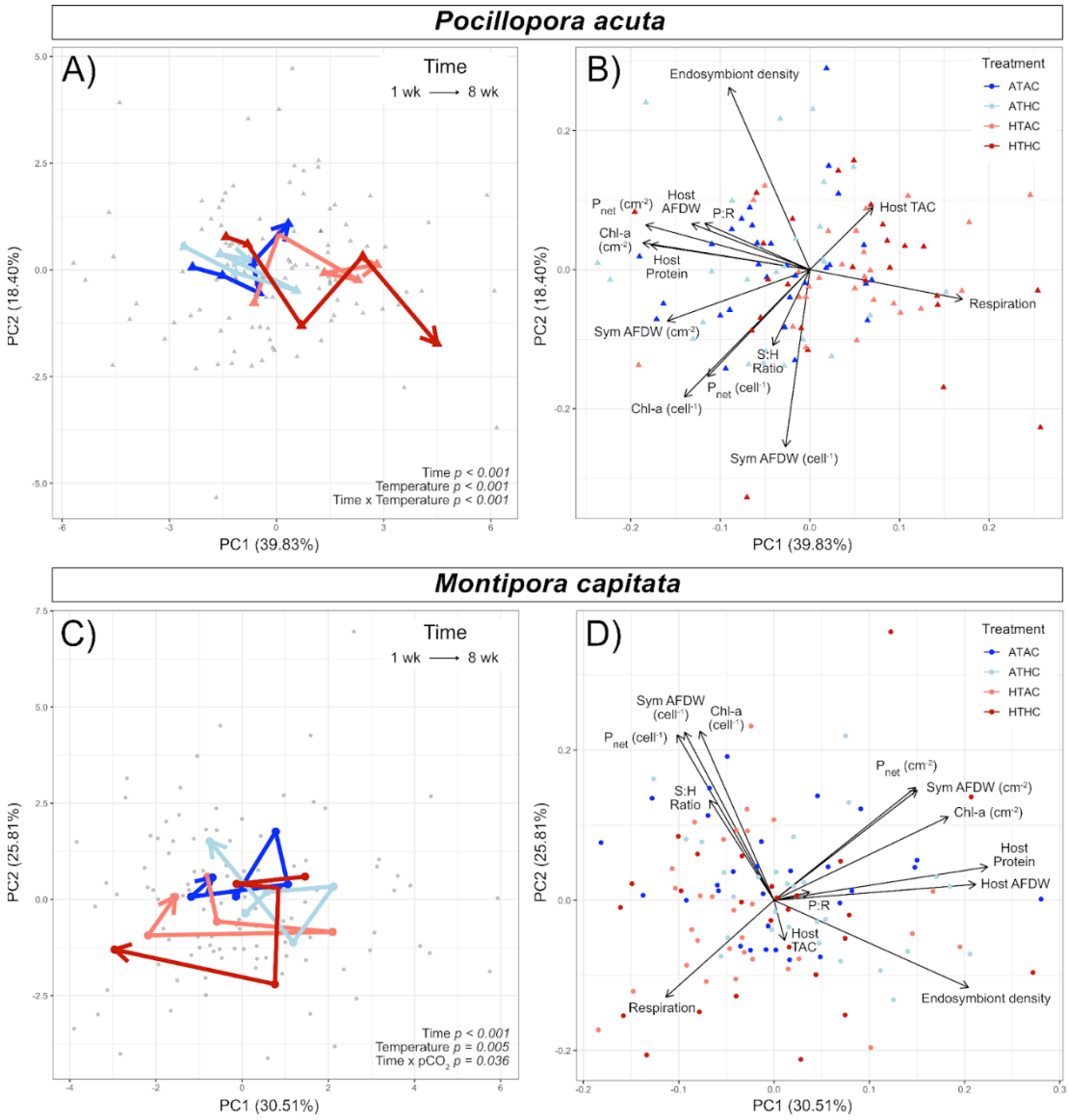

Fig. 4. Principal component analyses of multivariate physiological state during the exposure period (weeks 1–8) for both species. (A,B) *Pocillopora acuta* fragments. (C,D) *Montipora capitata* fragments. Each point represents an individual coral fragment's multivariate physiological state composed of 13 host and symbiont response variables and colored by treatment. Significant effects from PERMANOVA tests for each species are included within A and C (bottom right of each panel). PC axis labels indicate the percent variance explained by that axis. (A,C) Centroid multivariate state for each treatment at each time period is indicated by a bold, treatment-colored point. All mean points are connected within each treatment to show the shifts through time (week 1→8). (B,D) Biplots of the response variables are shown on the multivariate plots. Each black arrow represents a physiological response variable. The direction and length of each arrow indicates the relative strength of that variable to the PC axes.

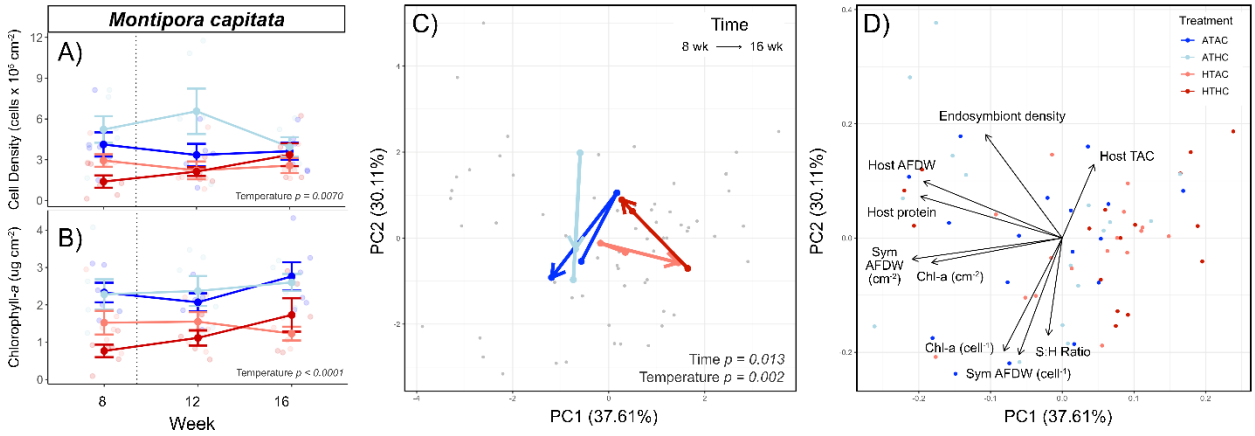

Fig. 5. Bleaching assessment and principal components analysis for multivariate physiological state of *M. capitata* fragments during the recovery period (weeks 8–16). (A) Endosymbiont densities (×105 cells cm−2) and (B) Holobiont *chl a* content (µg cm−2) for the recovery period. (C,D) Each point represents an individual fragment's multivariate physiological state composed of nine host and symbiont response variables (respiration and photosynthetic rates were not measured during the recovery period). (C) Centroid multivariate physiological state through time (week 8→16). (D) Biplot of individual physiological variable contributions to PCA separation. Each point (individual fragment) is colored by treatment. Significant effects from PERMANOVA tests for each species are indicated in gray text.

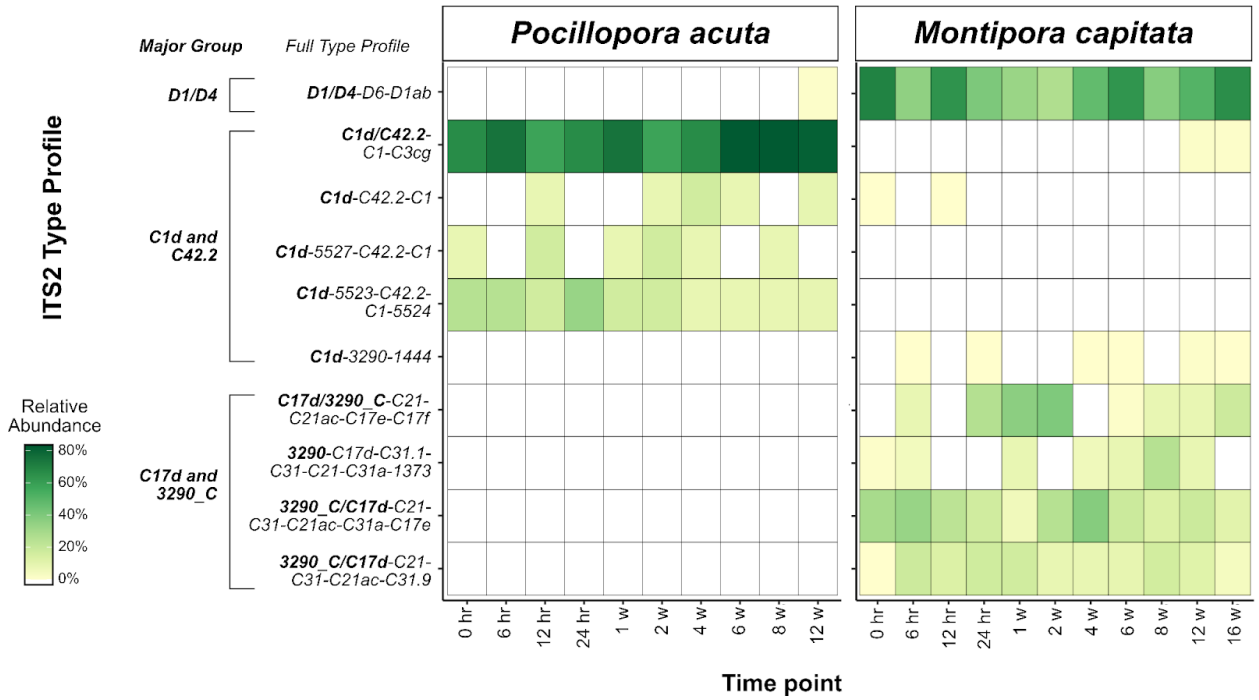

Fig. 6. Relative abundance of Symbiodiniaceae 'type profiles' identified by ITS2 sequencing for both species during exposure and recovery periods. The y-axis includes each type profile, composed of a major sequence ID (in bold) and subsequent full type profile ID. Relative abundance is indicated by 0–100% continuous color scale, with the darkest green coloring indicating 100% abundance of that full type profile. The exposure period includes 0, 6 and 12 h, and 1, 2, 4, 6 and 8 weeks. The recovery period includes 12 and 16 weeks, but there was not a high enough sample size for *P. acuta* fragments at 16 weeks.

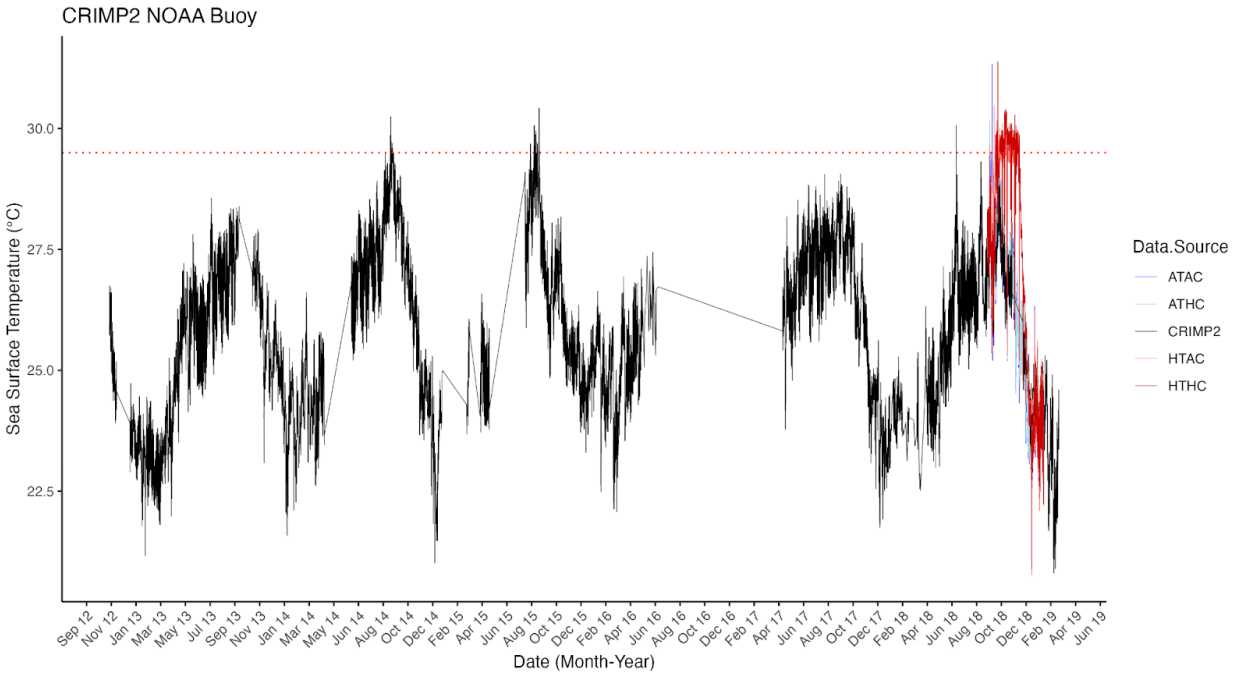

Fig. S1. NOAA Moku o Lo‘e Buoy data (CRIMP2) from September 2012 - June 2019 with treatment conditions overlayed. CRIMP2 buoy data (sea surface temperature °C) was used to determine an environmentally realistic range of temperatures for the experimental exposure period. The red dotted line represents the average high temperature treatment condition. CRIMP2 information can be found at https://www.ndbc.noaa.gov/station_page.php?station=mokh1.

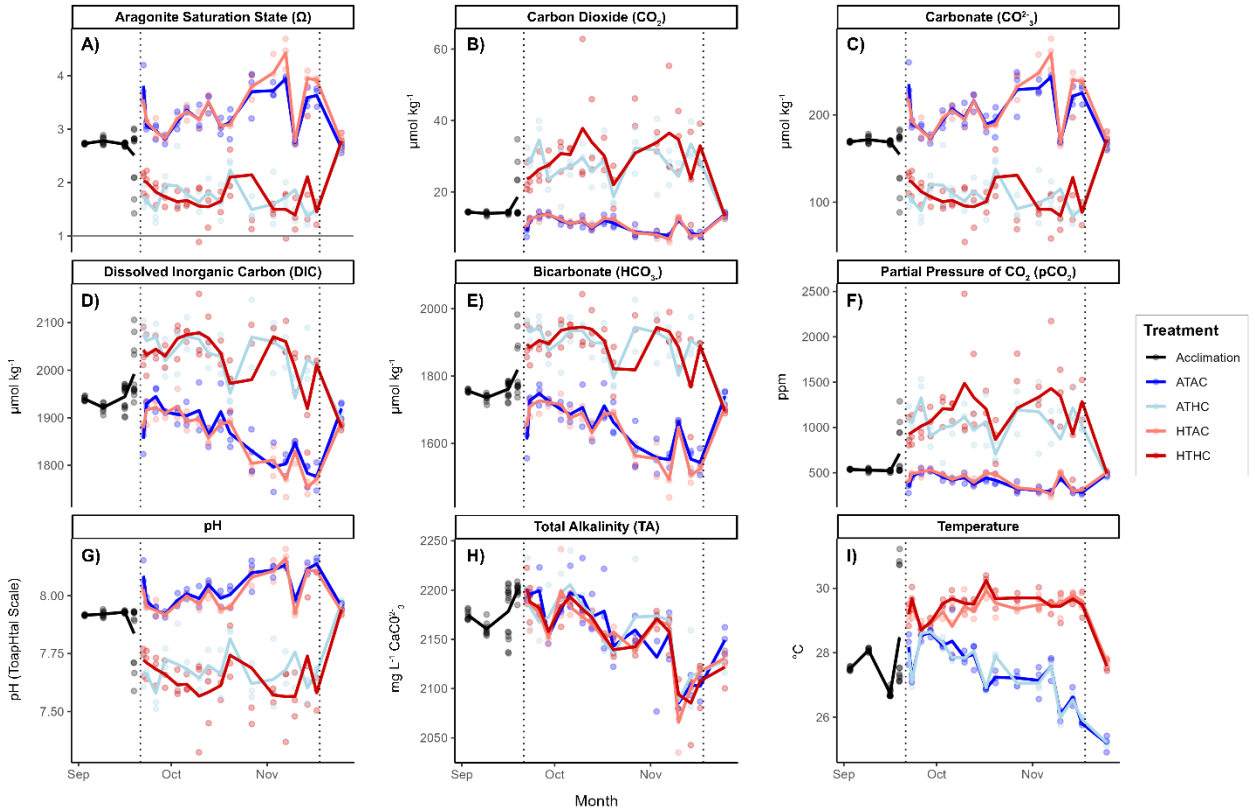

Fig. S2. Carbonate chemistry parameters during the acclimation, exposure, and beginning of the recovery period for all treatments. Treatment is indicated by color and vertical dotted lines mark the start and end of the treatment period. All x-axes represent time by month. Parameters include the following: (A) Aragonite Saturation State (Ω). (B) Carbon dioxide (CO_2; µmol kg^{-1}). (C) Carbonate (CO^{2-}_3; µmol kg^{-1}). (D) Dissolved inorganic carbon (DIC; µmol kg^{-1}). (E) Bicarbonate (HCO_3^-; µmol kg^{-1}). (F) Partial pressure of CO_2 (pCO_2; ppm). (G) pH (total scale). (H) Total alkalinity (TA; mg L^{-1} $CaCO_3$) (I). Temperature (°C).

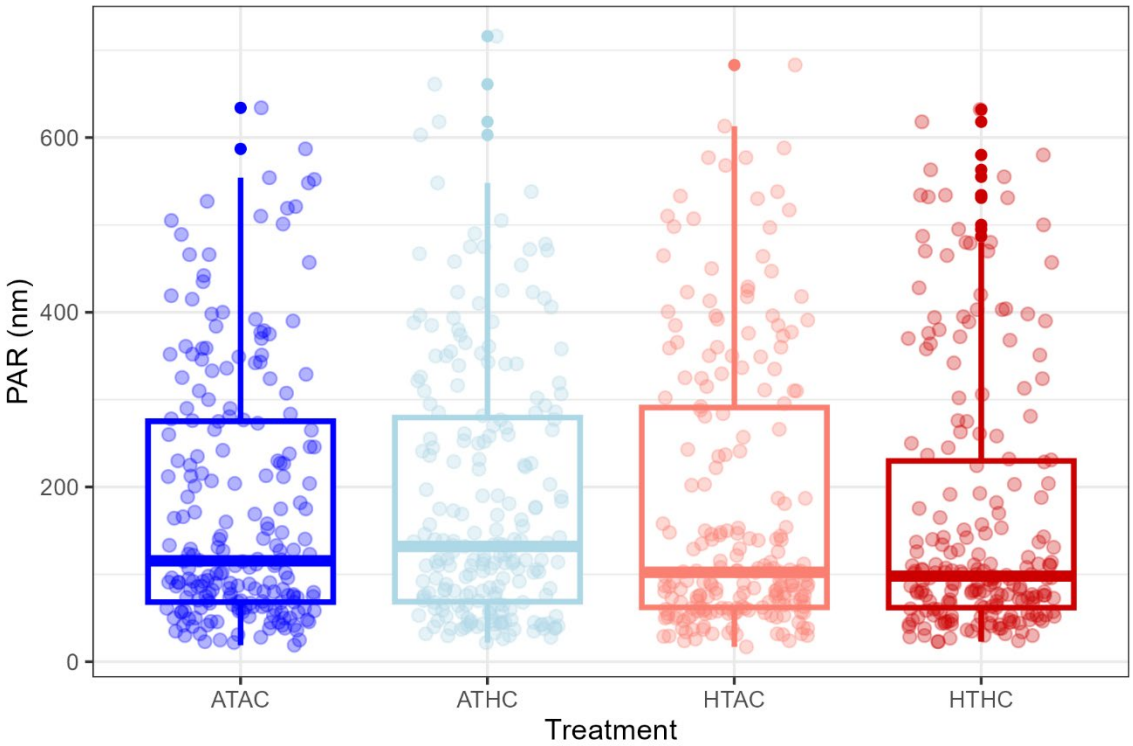

Fig. S3. Light data from the exposure period for all treatments. Light reported in PAR (nm) measured with a LICOR-193 as described in methods. Color indicates treatment (dark blue = ATAC, light blue = ATHC, light red = HTAC, and dark red = HTHC).

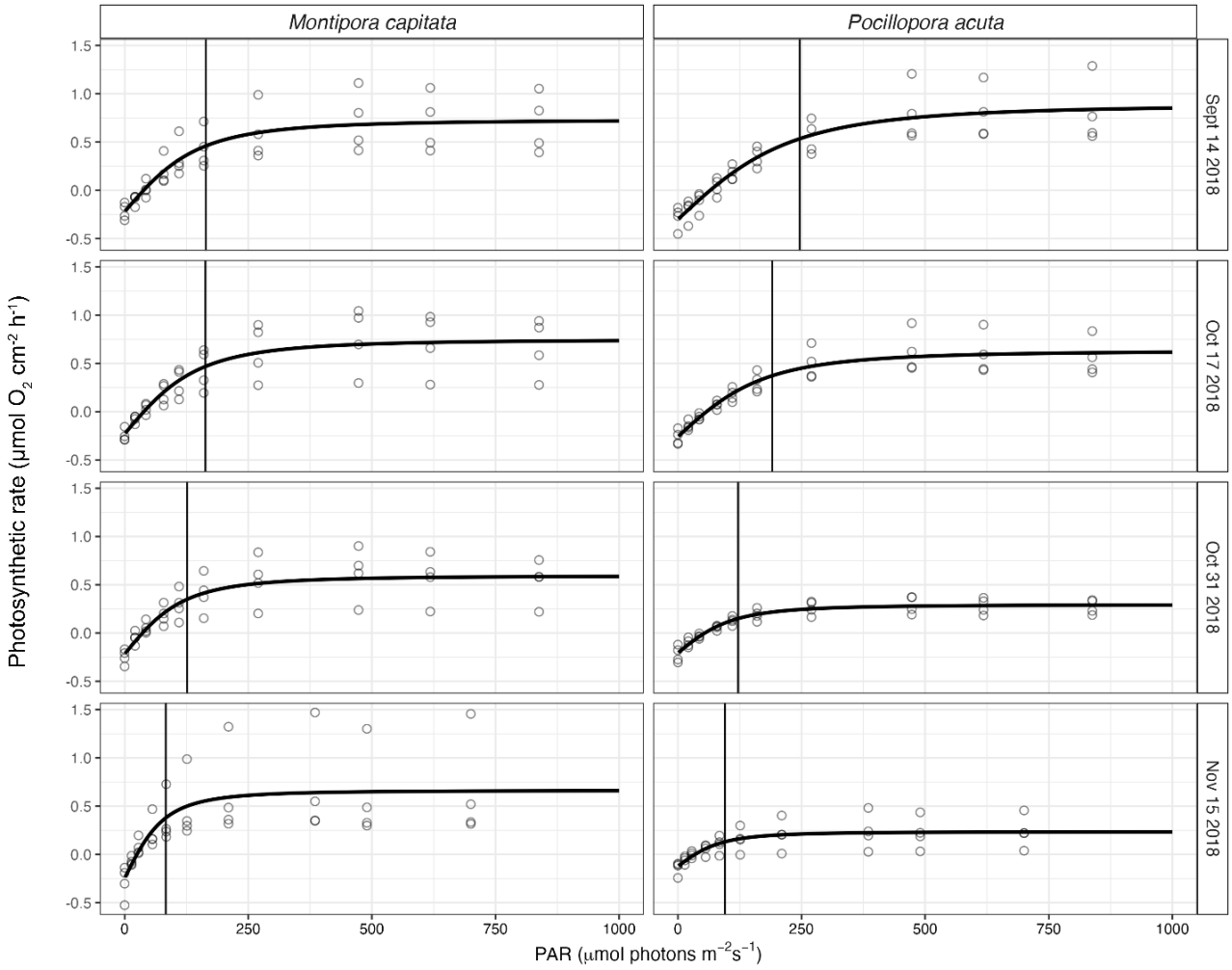

Fig. S4. Photosynthetic Irradiance (PI) Curves for four time points during the exposure period for both species. Photosynthetic rates (µmol O_2 cm^{-2} h^{-1}) measured at a range of irradiance (µmol photons m^{-2} s^{-1}) levels plotted for four time points: September 14 2018, October 17 2018, October 31 2018, and November 15 2018. PI curves were conducted to identify saturating irradiance (I_k; solid vertical line in each plot) and ensure coral fragments were not reaching photoinhibition during respiration and photosynthesis measurements.

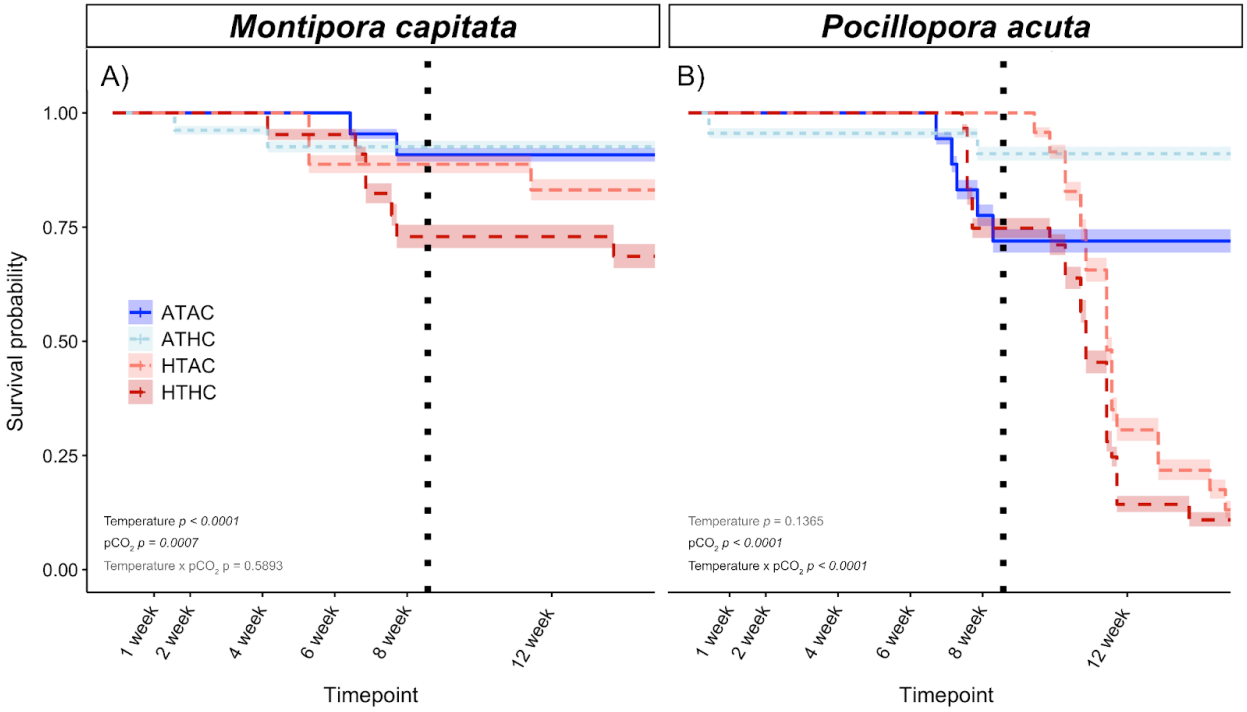

Fig. S5. Survival probability calculated from a cox-mixed effects model for each species. Treatment is indicated by color, significant effects are in black text, and non-significant effects are in gray text. The dotted line is the point when all treatment returns to ambient level conditions. Survival probability is on a scale of 0-1.00 for both (A) *Montipora capitata* fragments. (B) *Pocillopora acuta* fragments across both exposure (day 1 - week 8) and recovery (week 8-16) periods.

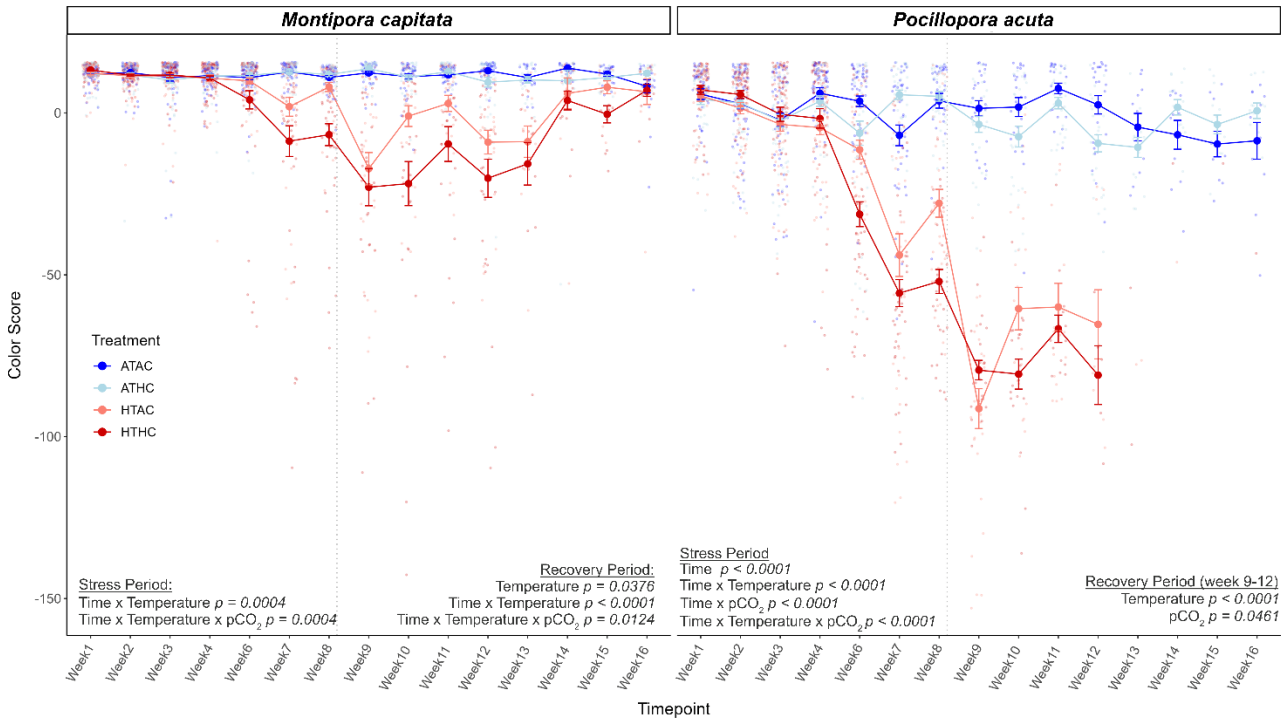

Fig. S6. Mean ± s.e.m. weekly color score measurements through both exposure (week 1-8) and recovery (week 9-16) periods for each species. As coral bleaches, color score decreases into negative values. (A) *M. capitata* fragments. (B) *P. acuta* fragments. Significant effects from the Type III ANOVA of linear mixed model outputs are listed on each panel. Treatments are indicated by colored mean points for each time point. The dotted line is when treatment conditions return to fully ambient values (week 9).

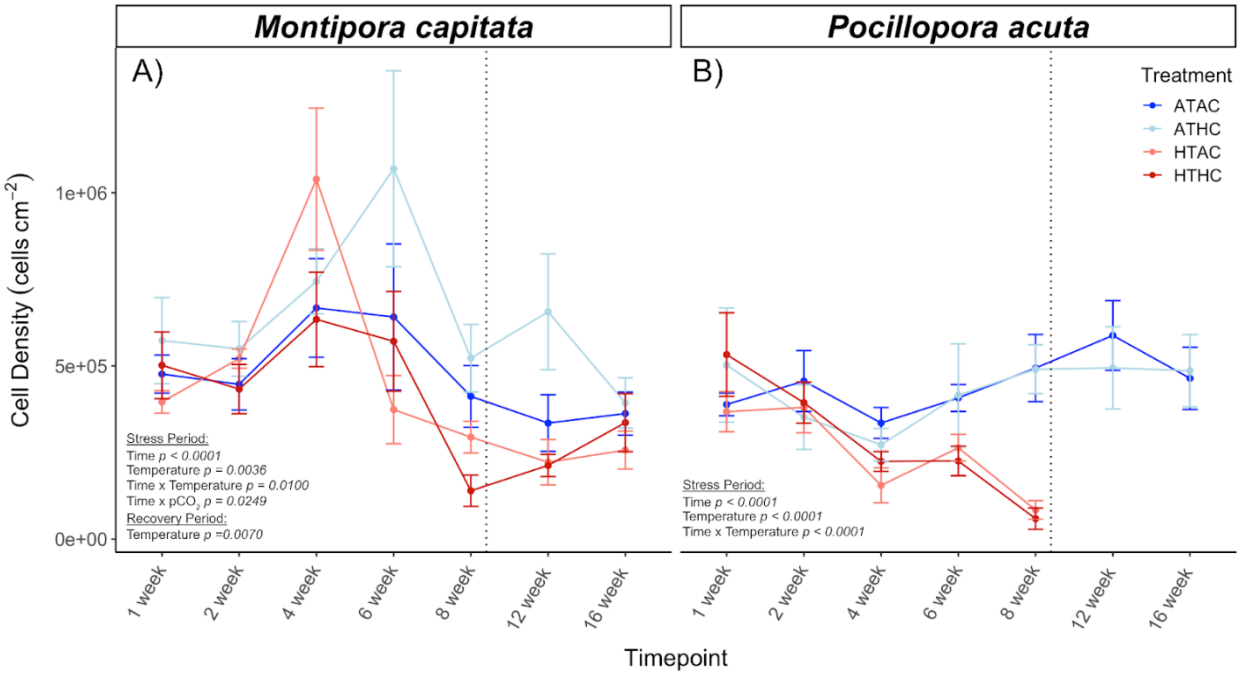

Fig. S7. Mean endosymbiont cell density levels (cells cm^{-2}) through both exposure and recovery periods for (A) *M. capitata* and (B) *P. acuta*. Treatments are indicated by color and significant effects for each species are labeled on the corresponding panel. The dotted line marks when all treatments returned to ambient level conditions at week 9. In *P. acuta*, high temperature treatments did not yield enough sample sizes to complete physiological measurements for weeks 12 and 16.

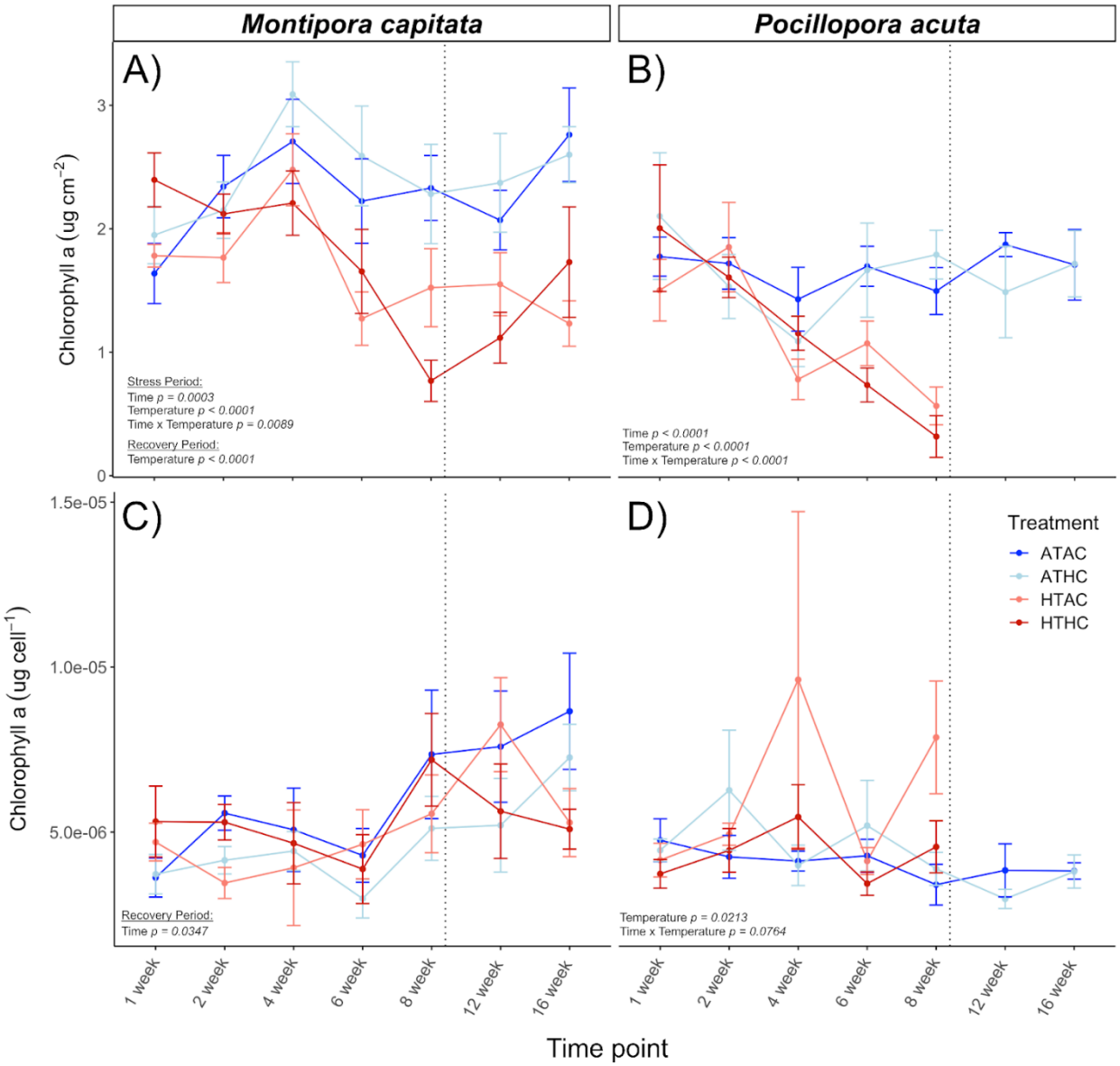

Fig. S8. Mean chlorophyll-a-a content levels normalized to both surface area (µg cm^{-2}) and endosymbiont cell density (µg cell^{-1}) for (A, C) *M. capitata* and (B, D) *P. acuta*. Treatments are indicated by color and significant effects for each species are labeled on the corresponding panel. The dotted line marks when all treatments returned to ambient level conditions at week 9. In all *P. actua* panels, high temperature treatments did not yield enough sample sizes to complete physiological measurements for weeks 12 and 16.

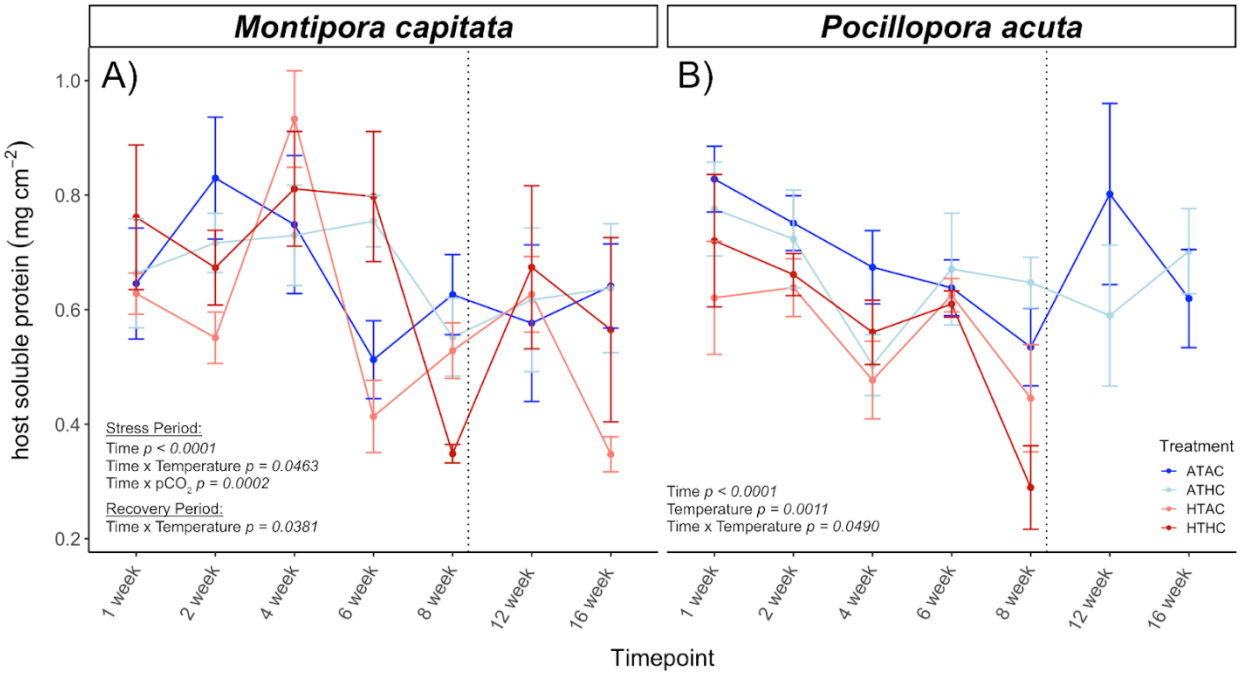

Fig. S9. Mean host soluble protein levels normalized to surface area (mg cm^{-2}) for both (A) *M. capitata* and (B) *P. acuta* in exposure and recovery periods. Treatments are indicated by color and significant effects for each species are labeled on the corresponding panel. The dotted line marks when all treatments returned to ambient level conditions at week 9. In *P. acuta*, high temperature treatments did not yield enough sample sizes to complete physiological measurements for weeks 12 and 16.

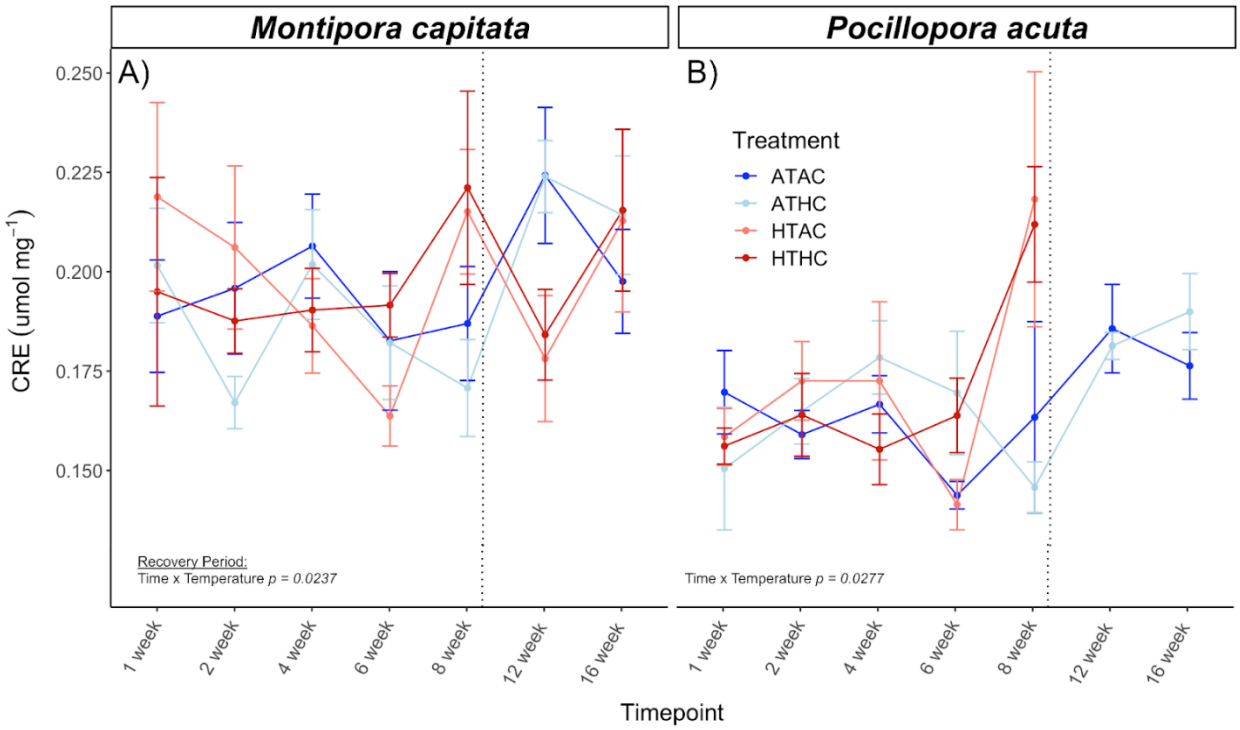

Fig. S10. Mean host total antioxidant capacity (TAC) levels normalized to host soluble protein (CRE µmol mg^{-1}) for both (A) *M. capitata* and (B) *P. acuta* through exposure and recovery periods. Treatments are indicated by color and significant effects for each species are labeled on the corresponding panel. The dotted line marks when all treatments returned to ambient level conditions at week 9. In *P. acuta*, high temperature treatments did not yield enough sample sizes to complete physiological measurements for weeks 12 and 16.

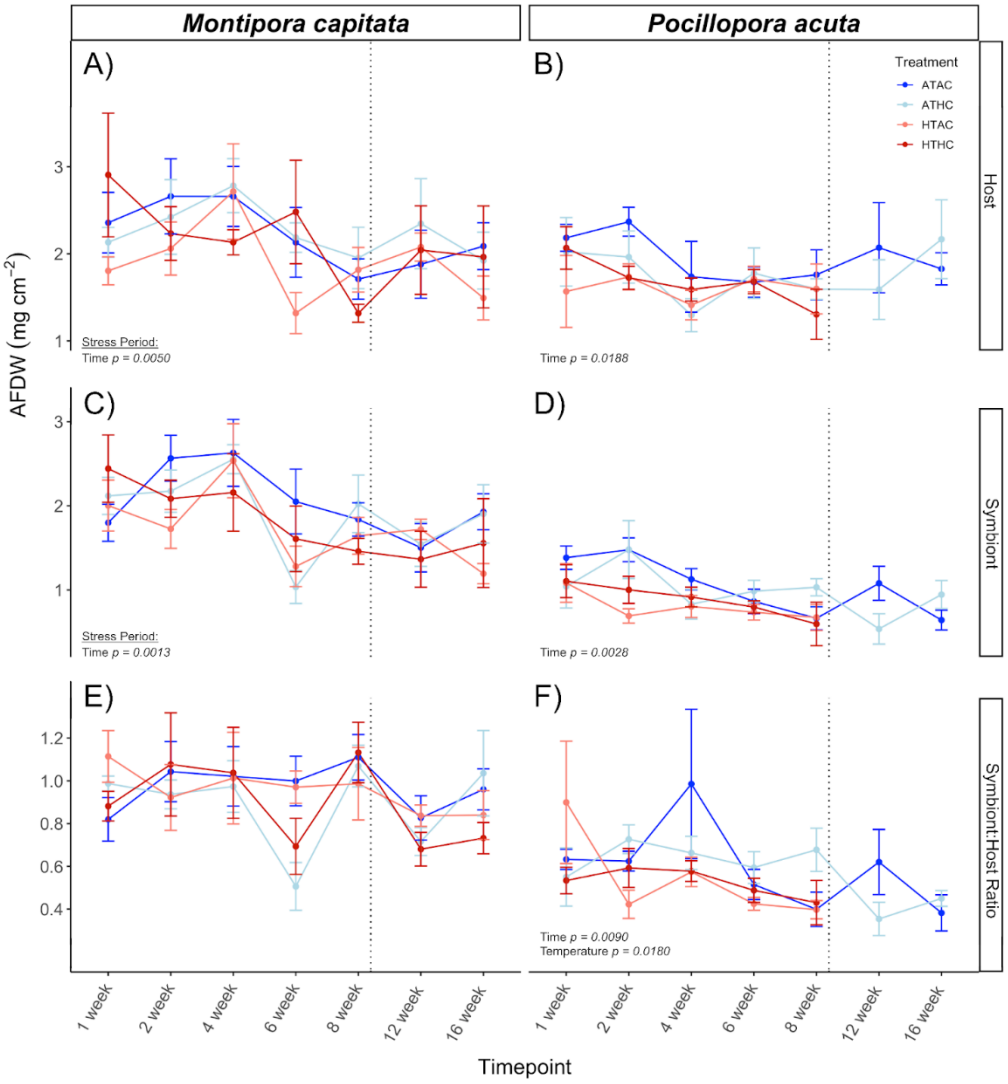

Fig. S11. Mean tissue biomass levels measured in Ash-Free Dry Weight normalized to surface area (AFDW mg cm^{-2}) for host, symbiont, and the ratio of symbiont:host for both (A, C, E) *M. capitata* and (B, D, F) *P. acuta*. Treatments are indicated by color and significant effects are labeled on the corresponding panel. The dotted line represents when treatments returned to ambient level conditions. (A,B) Host AFDW (mg cm^{-2}). (C,D) Symbiont AFDW (mg cm^{-2}). (E,F) Symbiont:Host AFDW Ratio. For all *P. acuta* panels, high temperature treatments did not yield enough sample sizes to complete physiological measurements for weeks 12 and 16.

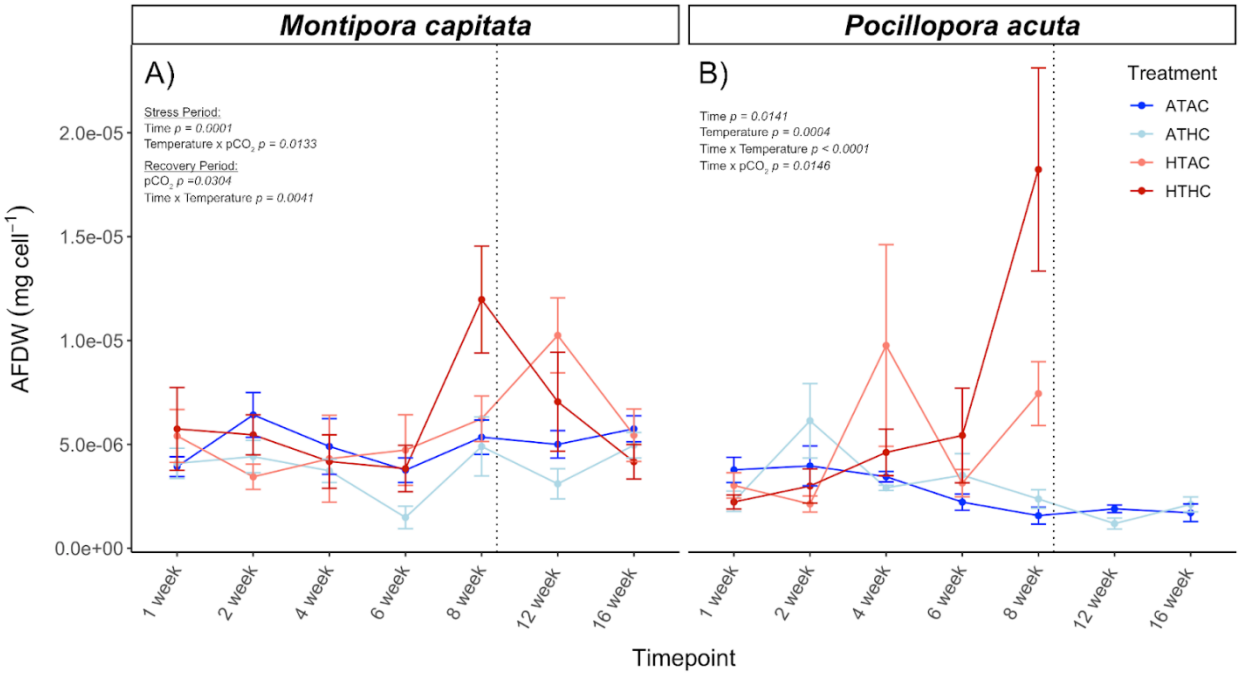

Fig. S12. Mean symbiont cellular Ash-Free Dry Weight levels normalized to cell densities (AFDW; mg cell^{-1}) for (A) *M. capitata* and (B) *P. acuta*. Treatments are indicated by color and significant effects are labeled on the corresponding panel. The dotted line represents when treatments returned to ambient level conditions. In *P. acuta*, high temperature treatments did not yield enough sample sizes to complete physiological measurements for weeks 12 and 16.

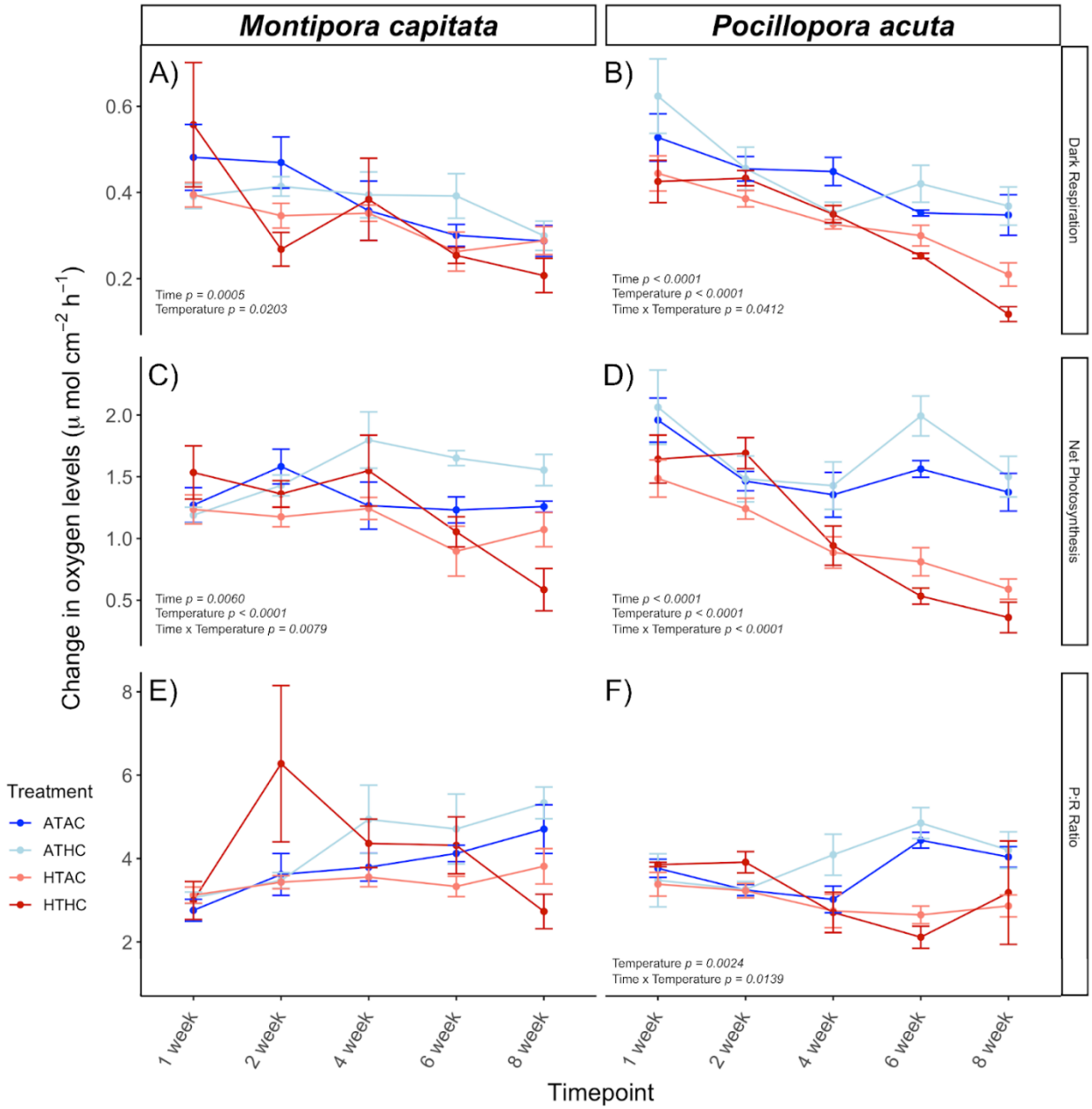

Fig. S13. Mean dark respiration and net photosynthetic rates during the exposure period for both (A, C, E) *M. capitata* and (B, D, F) *P. acuta*. Treatments are indicated by color and significant effects are labeled on the corresponding panel. Both respiration (A,B) and photosynthetic rates (C,D) are reported in units of change in oxygen levels (μmol cm^{-2} hr^{-1}). Respiration rates are the absolute value of the rate of change so that a decrease in rates is equal to lower respiration happening within the coral holobiont. Both respiration and photosynthetic rates were not measured for the recovery period. (E,F) Net photosynthetic rates (μmol cm^{-2} hr^{-1}) to dark respiration rates (μmol cm^{-2} hr^{-1}) ratio reported in unitless values.

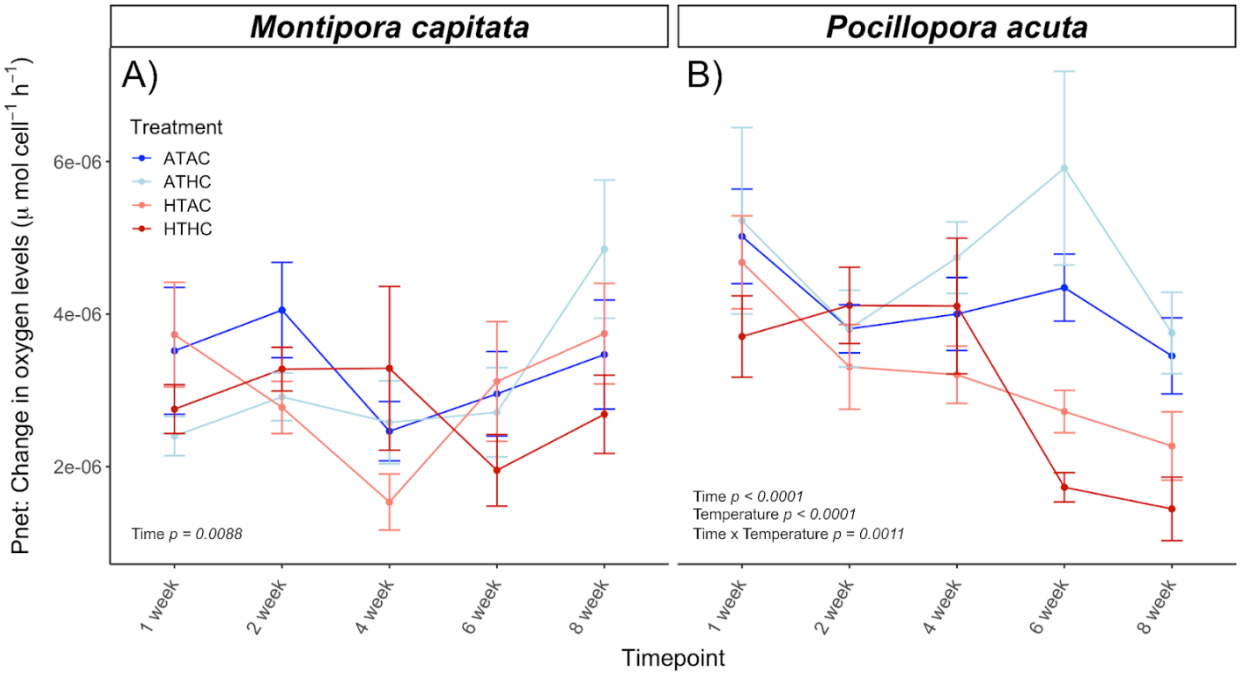

Fig. S14. Mean cellular net photosynthetic rates measured via change in oxygen levels µmol cell^{-1} hr^{-1}) and normalized to cell densities for each species (A) *M. capitata*. (B) *P. acuta*. Treatments are indicated by color and significant effects are labeled on the corresponding panel. Both respiration and photosynthetic rates were not measured for the recovery period.

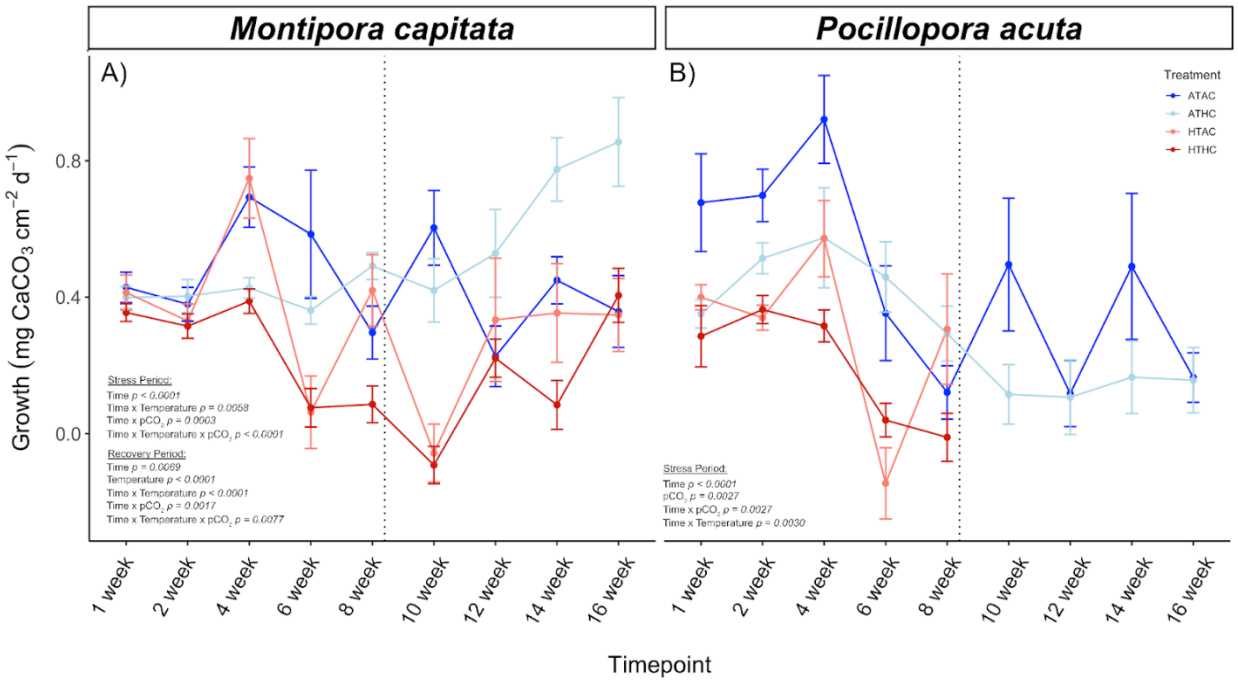

Fig. S15. Weekly mean holobiont growth rates measured in mg $CaCO_3$ cm^{-2} d^{-1} for both (A) *M. capitata* and (B) *Pocilopora acuta*. Treatments are indicated by color and significant effects are labeled on the corresponding panel. The dotted line indicates when treatment returned to ambient levels. *P. acuta* fragments did not survive in enough quantities for sufficient sample sizes during the recovery period.

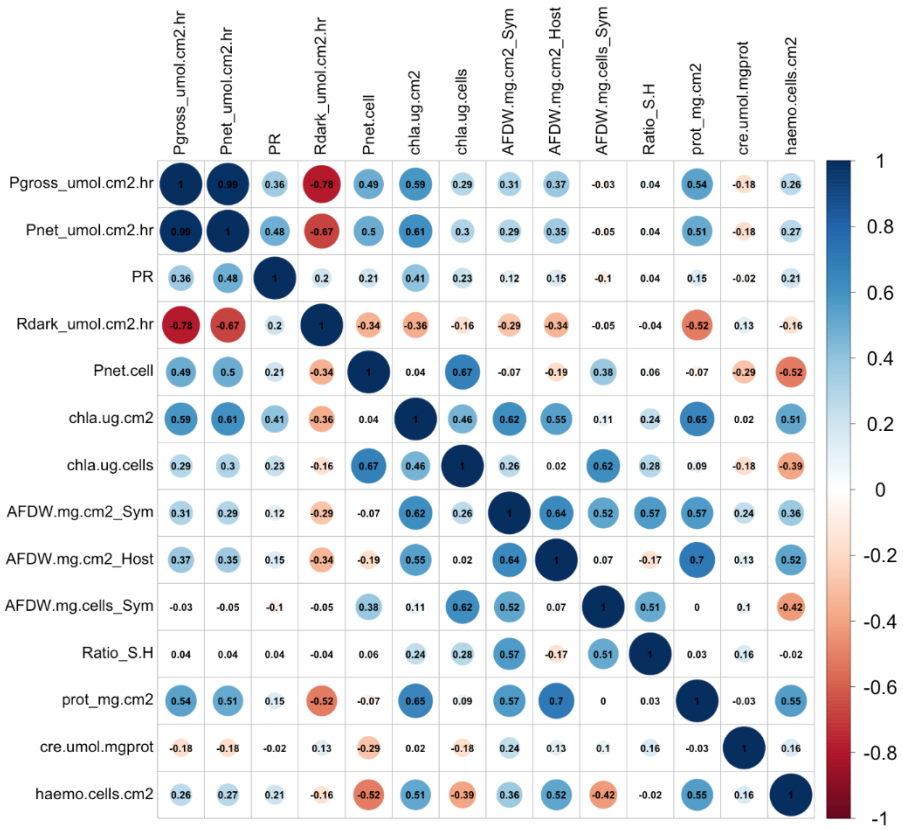

Fig. S16. Correlation plot between all measured physiological variables (14 total). All treatments, species, and timepoints are collapsed into one figure to assess which variables are highly correlated and redundant to include in multivariate analyses. Dark blue indicates highly positively correlated (value of 1) and dark red indicates highly negatively correlated (value of -1). The size of the dot in each cell indicates the degree of correlation so that a larger dot is a higher correlation. Gross photosynthetic rates and net photosynthetic rates were highly positively correlated and therefore only net photosynthetic rates were included in multivariate analyses.

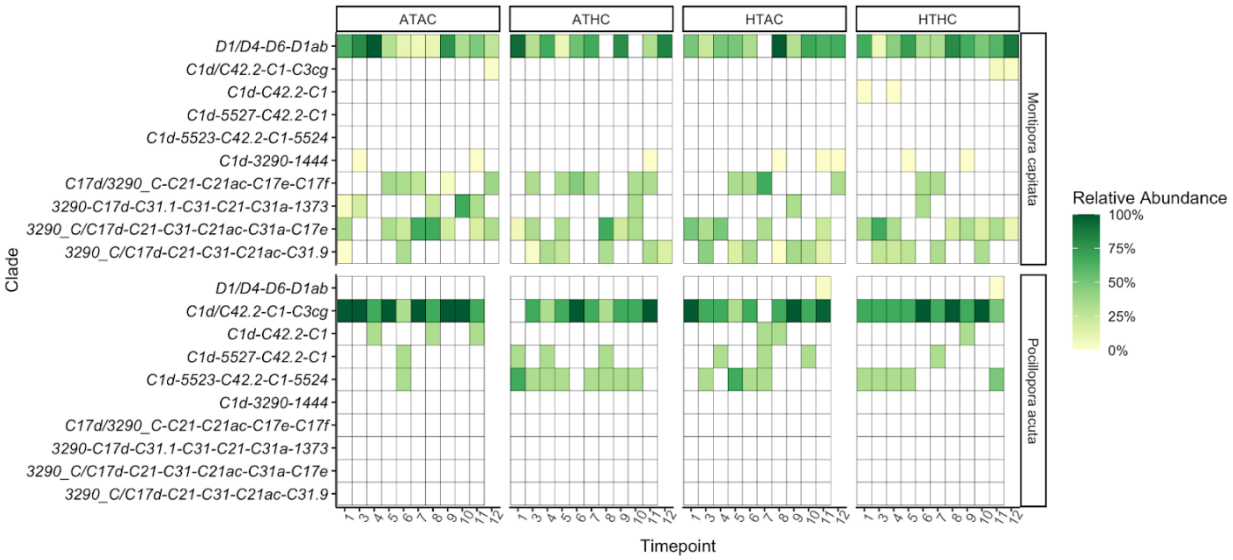

Fig. S17. Relative abundance (%) of ITS2 Symbiodiniaceae Type Profiles. Each individual square is the average percent relative abundance per treatment per time point per species (n=3). The four column sections indicate treatments (ATAC, ATHC, HTAC, and HTHC) and the two row sections indicate host species (*Montipora capitata* and *Pocillopora acuta*). The following time points are included in the exposure period: 0 hour, 6 hour, 12 hour, 30 hour, 1, 2, 4, 6, and 8 weeks. The vertical dotted line indicates the start of the recovery period, which includes 12 and 16 weeks. *P. acuta* samples were only collected through week 12. Each square is colored by percentage relative abundance, with 100% as the darkest green and 0% as white. In the ITS2 Type Profile name, the major sequence is bolded, followed by the rest of the full type profile name.

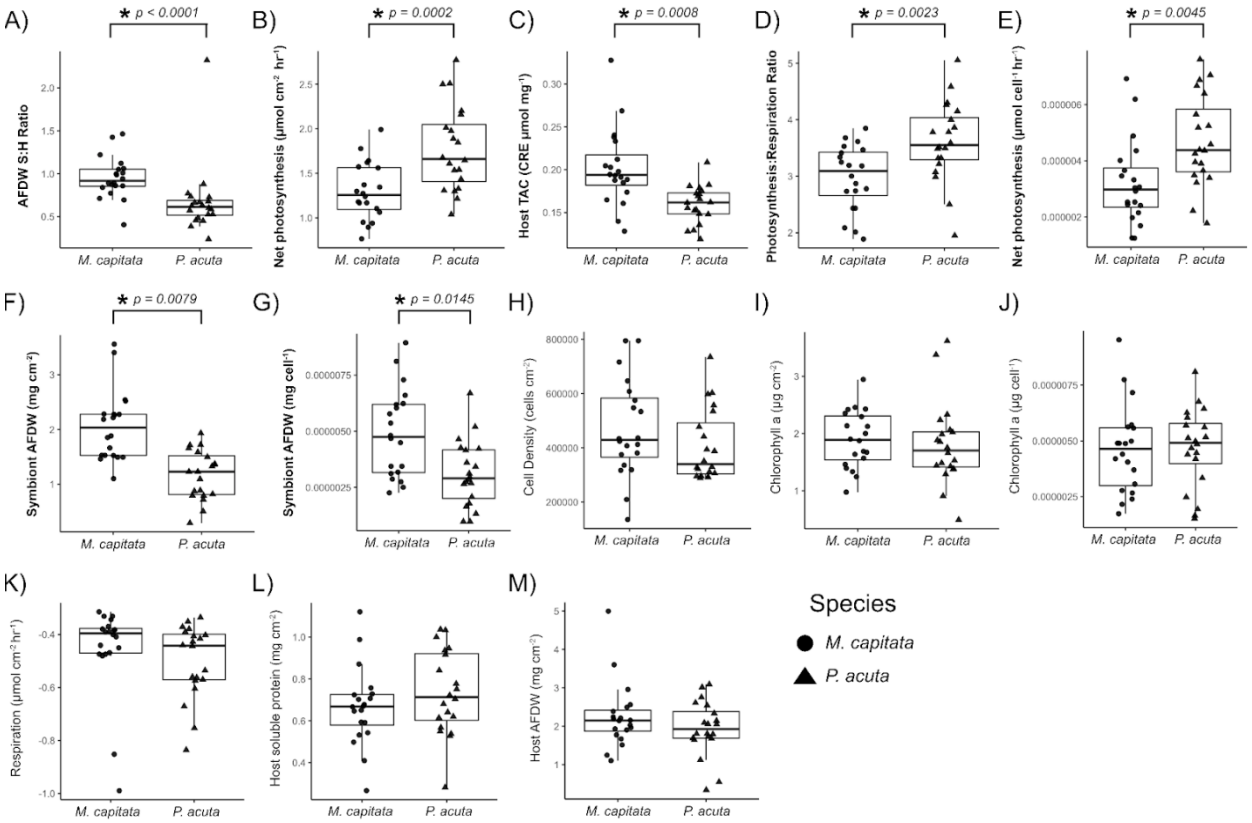

Fig S18. Baseline physiological measurements from week 1 ordered by most significant differences to least. (A) Ash-free dry weight symbiont:host ratio, (B) Holobiont net photosynthetic rates (µmol cm^{-2} hr^{-1}), (C) Host total antioxidant capacity (CRE µmol mg^{-1}), (D) Photosynthesis:Respiration ratio, (E) Cellular net photosynthetic rates (µmol $cell^{-1}$ hr^{-1}), (F) Symbiont AFDW (mg cm^{-2}), (G) Symbiont cellular AFDW (mg $cell^{-1}$), (H) Endosymbiont cell density (cells cm^{-2}), (I) Holobiont chlorophyll-a-a content (µg cm^{-2}), (J) Symbiont cellular chlorophyll-a-a content (µg $cell^{-1}$), (K) Host respiration rates (µmol cm^{-2} hr^{-1}), (L) Host soluble protein (mg cm^{-2}), (M) Host AFDW (mg cm^{-2}). *M. capitata* indicated by circles and *P. acuta* samples indicated by triangles.

Total Alkalinity: Stress Period

Treatment	*N*	*Mean*	*St. Error*
ATAC	48	2159.06	5.89
ATHC	48	2162.74	5.49
HTAC	48	2155.58	5.25
HTHC	48	2156.79	5.31

*Timepoint * Treatment + (1 | Tank)*

Effect	X^2	*df*	*P*
Timepoint	170.0467	15	**< 0.0001**
Treatment	1.1034	3	0.7762
Timepoint:Treatment	43.8277	45	0.5126

Table S1. Total Alkalinity sample size (N), mean, and standard error (St. Error) output from the exposure period for each treatment. A linear mixed model was run to determine the effects of treatment and time point on tank conditions.

*aov: PAR ~ Position * Tank*

Effect	*df*	*Sum of Sq*	*Mean Sq*	*F*	*Pr(>F)*
Position	5	23764	4753	0.155	0.978
Tank	11	498085	45280	1.475	0.143
Position:Tank	55	120265	2187	0.071	1.000

Light Summary Data: Stress Period

Treatment	*N*	*Mean*	*St. Error*
ATAC	212	179.70	9.97
ATHC	211	186.54	10.20
HTAC	210	176.64	10.84
HTHC	211	165.12	10.41

lmer: Treatment + (1 | Date) + (1 | Tank)

Effect	X^2	*df*	*P*
Treatment	2.0687	3	0.5583

Table S2. Light (PAR) output: sample size (N), mean, and standard error (St. Error) output from the exposure period for each treatment. A linear mixed model was run to determine the effects of treatment on tank conditions.

Stress Treatment Period

Montipora capitata

Dependent Variable	Effect	X^2	*df*	*P*
Respiration	**Timepoint**	19.7897	4	**0.0005**
(µmol cm^{-2} h^{-1})	**Temperature**	5.3829	1	**0.0203**
	CO2	0.2874	1	0.5919
	Timepoint:Temperature	3.5403	4	0.4718
	Timepoint:CO2	2.8987	4	0.5749
	Temperature:CO2	0.1348	1	0.7135
	Timepoint:Temperature:CO2	3.7495	4	0.4410
Net Photosynthesis	**Timepoint**	14.4620	4	**0.0060**
(µmol cm^{-2} h^{-1})	**Temperature**	18.1524	1	**< 0.0001**
	CO2	1.9896	1	0.1584
	Timepoint:Temperature	13.8077	4	**0.0079**
	Timepoint:CO2	9.1105	4	0.0584
	Temperature:CO2	1.5185	1	0.2178
	Timepoint:Temperature:CO2	9.0938	4	0.0588
Net Photosynthesis	**Timepoint**	13.5702	4	**0.0088**
(µmol cell^{-1} h^{-1})	Temperature	1.8312	1	0.1760
	CO2	0.3743	1	0.5407
	Timepoint:Temperature	1.6383	4	0.8019
	Timepoint:CO2	4.1280	4	0.3890
	Temperature:CO2	0.0064	1	0.9360
	Timepoint:Temperature:CO2	6.2204	4	0.1833
Gross Photosynthesis	**Timepoint**	21.1984	4	**0.0003**
(µmol cm^{-2} h^{-1})	**Temperature**	22.3058	1	**< 0.0001**
	CO2	0.3925	1	0.5310
	Timepoint:Temperature	15.5217	4	**0.0037**
	Timepoint:CO2	11.9872	4	**0.0174**
	Temperature:CO2	2.2441	1	0.1341
	Timepoint:Temperature:CO2	11.0932	4	**0.0255**
P:R Ratio	Timepoint	8.5378	4	0.0738
	Temperature	0.0187	1	0.8913
	CO2	3.4479	1	0.0633
	Timepoint:Temperature	2.2871	4	0.6831
	Timepoint:CO2	0.3761	4	0.9844
	Temperature:CO2	0.3484	1	0.5550
	Timepoint:Temperature:CO2	1.0685	4	0.8992

Pocillopora acuta

Dependent Variable	Effect	X^2	*df*	*P*
Respiration	**Timepoint**	87.4169	4	**< 0.0001**
(µmol cm^{-2} h^{-1})	**Temperature**	40.3078	1	**< 0.0001**
	CO2	0.3721	1	0.5419
	Timepoint:Temperature	9.9564	4	**0.0412**
	Timepoint:CO2	2.2023	4	0.6986
	Temperature:CO2	0.4268	1	0.5136
	Timepoint:Temperature:CO2	7.8998	4	0.0953
Net Photosynthesis	**Timepoint**	51.8737	4	**< 0.0001**
(µmol cm^{-2} h^{-1})	**Temperature**	61.5502	1	**< 0.0001**
	CO2	0.0146	1	0.9038
	Timepoint:Temperature	34.5005	4	**< 0.0001**
	Timepoint:CO2	2.3684	4	0.6684
	Temperature:CO2	0.7537	1	0.3853
	Timepoint:Temperature:CO2	7.6865	4	0.1038
Net Photosynthesis	**Timepoint**	29.9940	4	**< 0.0001**
(µmol cell^{-1} h^{-1})	**Temperature**	29.7790	1	**< 0.0001**
	CO2	2.8160	1	0.5957
	Timepoint:Temperature	18.3100	4	**0.001073**
	Timepoint:CO2	3.7644	4	0.4388
	Temperature:CO2	2.4520	1	0.1174
	Timepoint:Temperature:CO2	5.6688	4	0.2253
Gross Photosynthesis	**Timepoint**	58.0206	4	**< 0.0001**
(µmol cm^{-2} h^{-1})	**Temperature**	60.0036	1	**< 0.0001**
	CO2	0.3337	1	0.5635
	Timepoint:Temperature	24.9031	4	**< 0.0001**
	Timepoint:CO2	1.7910	4	0.7741
	Temperature:CO2	0.3442	1	0.5574
	Timepoint:Temperature:CO2	7.1393	4	0.1287
P:R Ratio	Timepoint	1.8573	4	0.7620
	Temperature	9.1988	1	**0.0024**
	CO2	0.8475	1	0.3573
	Timepoint:Temperature	12.5200	4	**0.0139**
	Timepoint:CO2	0.5815	4	0.9651
	Temperature:CO2	0.0370	1	0.8475
	Timepoint:Temperature:CO2	2.3578	4	0.6703

Table S3. Statistical output for metabolic (photosynthetic and respiration) rates normalized to both surface area (cm^{-2}) and cell density (cell^{-1}). Left: *M. capitata*. Right: *P. acuta*.

Stress Treatment Period

Montipora capitata

Dependent Variable	Effect	X^2	*df*	*P*
Host soluble protein	**Timepoint**	28.6767	4	**< 0.0001**
mg cm^{-2}	Temperature	1.6554	1	0.1982
	CO2	1.4948	1	0.2215
	Timepoint:Temperature	9.6751	4	**0.0463**
	Timepoint:CO2	22.1155	4	**0.0002**
	Temperature:CO2	0.2089	1	0.6476
	Timepoint:Temperature:CO2	3.8747	4	0.4232
Host total antioxidant capacity (TAC)	Timepoint	3.3971	4	0.4937
	Temperature	1.2026	1	0.2728
CRE µmol (mg prot)$^{-1}$	CO2	0.2111	1	0.6459
	Timepoint:Temperature	5.7398	4	0.2194
	Timepoint:CO2	2.3971	4	0.6632
	Temperature:CO2	0.2418	1	0.6229
	Timepoint:Temperature:CO2	2.1796	4	0.7028
Chlorophyll-a	**Timepoint**	21.1924	4	**0.0003**
ug cm^{-2}	**Temperature**	15.8058	1	**< 0.0001**
	CO2	0.7297	1	0.3930
	Timepoint:Temperature	13.5381	4	**0.0089**
	Timepoint:CO2	5.0723	4	0.2800
	Temperature:CO2	0.1355	1	0.7128
	Timepoint:Temperature:CO2	3.5923	4	0.4640
Chlorophyll-a	Timepoint	7.2542	4	0.1231
ug $cell^{-1}$	Temperature	3.0607	1	0.0802
	CO2	2.2806	1	0.1310
	Timepoint:Temperature	4.2774	4	0.3698
	Timepoint:CO2	1.9902	4	0.7376
	Temperature:CO2	0.2751	1	0.5999
	Timepoint:Temperature:CO2	4.2725	4	0.3704
Endosymbiont density	**Timepoint**	34.9996	4	**< 0.0001**
cells cm^{-2}	**Temperature**	8.4654	1	**0.0036**
	CO2	0.0533	1	0.8173
	Timepoint:Temperature	13.2732	4	**0.0100**
	Timepoint:CO2	8.4822	4	0.0754
	Temperature:CO2	5.0336	1	**0.0249**
	Timepoint:Temperature:CO2	5.3255	4	0.2555

Pocillopora acuta

Dependent Variable	Effect	X^2	*df*	*P*
Host soluble protein	**Timepoint**	31.4707	4	**< 0.0001**
mg cm^{-2}	**Temperature**	10.7168	1	**0.0011**
	CO2	0.1423	1	0.7060
	Timepoint:Temperature	9.5372	4	**0.0490**
	Timepoint:CO2	0.6262	4	0.9601
	Temperature:CO2	0.0761	1	0.7827
	Timepoint:Temperature:CO2	8.6149	4	0.0715
Host total antioxidant capacity (TAC)	Timepoint	5.5116	4	0.2387
	Temperature	1.5631	1	0.2387
CRE µmol (mg prot)$^{-1}$	CO2	0.0277	1	0.8679
	Timepoint:Temperature	11.2675	4	**0.0237**
	Timepoint:CO2	2.9275	4	0.5700
	Temperature:CO2	0.0066	1	0.9351
	Timepoint:Temperature:CO2	1.3579	4	0.8515
Chlorophyll-a	**Timepoint**	27.8694	4	**< 0.0001**
ug cm^{-2}	**Temperature**	18.5191	1	**< 0.0001**
	CO2	0.6615	1	0.4160
	Timepoint:Temperature	25.1913	4	**< 0.0001**
	Timepoint:CO2	2.8095	4	0.5902
	Temperature:CO2	0.1432	1	0.7051
	Timepoint:Temperature:CO2	6.3085	4	0.1773
Chlorophyll-a	Timepoint	9.3925	4	0.0520
ug $cell^{-1}$	**Temperature**	5.3056	1	**0.0213**
	CO2	0.1696	1	0.6804
	Timepoint:Temperature	8.4497	4	**0.0764**
	Timepoint:CO2	1.9180	4	0.7508
	Temperature:CO2	0.0055	1	0.9408
	Timepoint:Temperature:CO2	1.8844	4	0.7570
Endosymbiont density	**Timepoint**	28.9709	4	**< 0.0001**
cells cm^{-2}	**Temperature**	25.8864	1	**< 0.0001**
	CO2	0.0001	1	0.9905
	Timepoint:Temperature	36.2584	4	**< 0.0001**
	Timepoint:CO2	3.6063	4	0.4619
	Temperature:CO2	0.7820	1	0.3765
	Timepoint:Temperature:CO2	4.6170	4	0.3289

Recovery Period

Montipora capitata

Dependent Variable	Effect	X^2	*df*	*P*
Host soluble protein	Timepoint	1.2029	1	0.2727
mg cm^{-2}	Temperature	1.2085	1	0.2716
	CO2	0.4967	1	0.4810
	Timepoint:Temperature	4.3028	1	**0.0381**
	Timepoint:CO2	0.1406	1	0.7077
	Temperature:CO2	0.2735	1	0.6010
	Timepoint:Temperature:CO2	0.4454	1	0.5045
Host total antioxidant capacity (TAC)	Timepoint	0.446	1	0.5043
	Temperature	2.7182	1	0.0992
CRE µmol (mg prot)$^{-1}$	CO2	0.4044	1	0.5248
	Timepoint:Temperature	4.8473	1	**0.0277**
	Timepoint:CO2	0.0354	1	0.8507
	Temperature:CO2	0.0317	1	0.8586
	Timepoint:Temperature:CO2	0.2589	1	0.6109
Chlorophyll-a	Timepoint	1.7639	1	0.1841
ug cm^{-2}	**Temperature**	20.1042	1	**< 0.0001**
	CO2	0.0496	1	0.8237
	Timepoint:Temperature	0.458	1	0.4986
	Timepoint:CO2	0.2575	1	0.6118
	Temperature:CO2	0.0059	1	0.9389
	Timepoint:Temperature:CO2	2.2585	1	0.1329
Chlorophyll-a	**Timepoint**	4.4612	1	**0.0347**
ug $cell^{-1}$	Temperature	0.869	1	0.3512
	CO2	2.2783	1	0.1312
	Timepoint:Temperature	0.929	1	0.3351
	Timepoint:CO2	0.7022	1	0.4020
	Temperature:CO2	0.0001	1	0.9907
	Timepoint:Temperature:CO2	0.2732	1	0.6012
Endosymbiont density	Timepoint	1.5153	1	0.2183
cells cm^{-2}	**Temperature**	7.2667	1	**0.0070**
	CO2	2.2871	1	0.1305
	Timepoint:Temperature	1.3407	1	0.2469
	Timepoint:CO2	0.1552	1	0.6936
	Temperature:CO2	0.1244	1	0.7244
	Timepoint:Temperature:CO2	0.9057	1	0.3413

Table S4. Statistical output for host soluble protein, host total antioxidant capacity, chlorophyll-a-a content, and endosymbiont densities during the exposure period for both *M. capitata* and *P. acuta* and the recovery period for *M. capitata.*

Stress Treatment Period

Montipora capitata

Dependent Variable	Effect	X^2	*df*	*P*
Host AFDW	**Timepoint**	14.8616	4	**0.0050**
mg cm^{-2}	Temperature	1.9343	1	0.1643
	CO2	0.6814	1	0.4091
	Timepoint:Temperature	1.0511	4	0.9020
	Timepoint:CO2	4.3846	4	0.3564
	Temperature:CO2	0.7694	1	0.3804
	Timepoint:Temperature:CO2	7.4577	4	0.1136
Symbiont AFDW	**Timepoint**	17.8198	4	**0.0013**
mg cm^{-2}	Temperature	1.2744	1	0.2589
	CO2	0.0635	1	0.8010
	Timepoint:Temperature	2.2496	4	0.6900
	Timepoint:CO2	2.105	4	0.7165
	Temperature:CO2	0.8867	1	0.3464
	Timepoint:Temperature:CO2	4.1668	4	0.3839
Symbiont AFDW	**Timepoint**	23.2685	4	**0.0001**
mg $cell^{-1}$	Temperature	2.064	1	0.1508
	CO2	0.6042	1	0.4370
	Timepoint:Temperature	8.7003	4	0.0690
	Timepoint:CO2	8.6447	4	0.0706
	Temperature:CO2	6.1314	1	**0.0133**
	Timepoint:Temperature:CO2	1.9128	4	0.7518
Symbiont:Host Ratio	Timepoint	9.1648	4	0.0571
	Temperature	0.3193	1	0.5720
	CO2	1.2031	1	0.2727
	Timepoint:Temperature	0.4943	4	0.9741
	Timepoint:CO2	6.4993	4	0.1648
	Temperature:CO2	0.2733	1	0.6011
	Timepoint:Temperature:CO2	3.1485	4	0.5333

Pocillopora acuta

Dependent Variable	Effect	X^2	*df*	*P*
Host AFDW	**Timepoint**	11.8141	4	**0.0188**
mg cm^{-2}	Temperature	3.3048	1	0.0691
	CO2	0.4392	1	0.5075
	Timepoint:Temperature	2.2453	4	0.6907
	Timepoint:CO2	1.8383	4	0.7655
	Temperature:CO2	1.6816	1	0.1947
	Timepoint:Temperature:CO2	2.5394	4	0.6376
Symbiont AFDW	**Timepoint**	16.1781	4	**0.0028**
mg cm^{-2}	Temperature	1.5581	1	0.2120
	CO2	1.6089	1	0.2046
	Timepoint:Temperature	6.0128	4	0.1982
	Timepoint:CO2	5.5813	4	0.2327
	Temperature:CO2	0.9101	1	0.3401
	Timepoint:Temperature:CO2	4.2046	4	0.3790
Symbiont AFDW	**Timepoint**	12.4879	4	**0.0141**
mg $cell^{-1}$	**Temperature**	12.4936	1	**0.0004**
	CO2	1.2175	1	0.2699
	Timepoint:Temperature	54.2688	4	**< 0.0001**
	Timepoint:CO2	12.4029	4	**0.0146**
	Temperature:CO2	0.0764	1	0.7822
	Timepoint:Temperature:CO2	1.0241	4	0.9061
Symbiont:Host Ratio	**Timepoint**	13.5081	4	**0.0090**
	Temperature	5.5936	1	**0.0180**
	CO2	0.3185	1	0.5725
	Timepoint:Temperature	4.2439	4	0.3740
	Timepoint:CO2	6.6815	4	0.1537
	Temperature:CO2	0.2966	1	0.5860
	Timepoint:Temperature:CO2	4.1574	4	0.3851

Recovery Period

Montipora capitata

Dependent Variable	Effect	X^2	*df*	*P*
Host AFDW	Timepoint	0.5857	4	0.4441
mg cm^{-2}	Temperature	0.3283	1	0.5666
	CO2	0.4115	1	0.5212
	Timepoint:Temperature	0.1518	4	0.6968
	Timepoint:CO2	0.0118	4	0.9136
	Temperature:CO2	0.0139	1	0.9061
	Timepoint:Temperature:CO2	0.9804	4	0.3221
Symbiont AFDW	Timepoint	3.0004	4	0.0832
mg cm^{-2}	Temperature	2.3528	1	0.1251
	CO2	1.0417	1	0.3074
	Timepoint:Temperature	1.8469	4	0.1741
	Timepoint:CO2	0.6433	4	0.4225
	Temperature:CO2	0.6127	1	0.4338
	Timepoint:Temperature:CO2	0.2205	4	0.6386
Symbiont AFDW	Timepoint	0.3926	4	0.5309
mg $cell^{-1}$	Temperature	2.8253	1	0.0928
	CO2	4.6844	1	**0.0304**
	Timepoint:Temperature	8.2396	4	**0.0041**
	Timepoint:CO2	1.0486	4	0.3058
	Temperature:CO2	0.0088	1	0.9254
	Timepoint:Temperature:CO2	0.1601	4	0.6891
Symbiont:Host Ratio	Timepoint	0.2829	4	0.5948
	Temperature	1.5012	1	0.2205
	CO2	0.0007	1	0.9794
	Timepoint:Temperature	1.7413	4	0.1870
	Timepoint:CO2	0.5863	4	0.4438
	Temperature:CO2	0.0001	1	0.9926
	Timepoint:Temperature:CO2	0.8463	4	0.3576

Table S5. Statistical output for tissue biomass measurements: host AFDW, symbiont AFDW normalized to both surface area (cm^{-2}) and cell density ($cell^{-1}$), and symbiont:host AFDW Ratio for both species during the exposure and the recovery period for *M. capitata*.

Buoyant Weight

Montipora capitata

Time Period	Effect	X^2	*df*	*P*
Stress	**Timepoint**	32.815	4	**< 0.0001**
	Temperature	0.2465	1	0.6195
	CO2	0.0469	1	0.8285
	Timepoint:Temperature	14.516	4	**0.0058**
	Timepoint:CO2	21.1175	4	**0.0003**
	Temperature:CO2	0.022	1	0.8820
	Timepoint:Temperature:CO2	32.3638	4	**< 0.0001**
Recovery	**Timepoint**	12.1538	4	**0.0069**
	Temperature	12.1538	1	**< 0.0001**
	CO2	1.1876	1	0.2758
	Timepoint:Temperature	28.2451	4	**< 0.0001**
	Timepoint:CO2	15.1806	4	**0.0017**
	Temperature:CO2	1.9284	1	0.1649
	Timepoint:Temperature:CO2	11.9167	4	**0.0077**

Pocillopora acuta

Time Period	Effect	X^2	*df*	*P*
Stress	**Timepoint**	47.5441	4	**< 0.0001**
	Temperature	3.2183	1	0.0728
	CO2	9.0017	1	**0.0027**
	Timepoint:Temperature	16.0271	4	**0.0030**
	Timepoint:CO2	16.2463	4	**0.0027**
	Temperature:CO2	2.3846	1	0.1225
	Timepoint:Temperature:CO2	4.5003	4	0.3425

Color Score

Montipora capitata

Time Period	Effect	X^2	*df*	*P*
Stress	Timepoint	3.3689	7	0.8489
	Temperature	0.0019	1	0.9655
	CO2	0.0001	1	0.9916
	Timepoint:Temperature	26.3114	7	**0.0004**
	Timepoint:CO2	1.8481	7	0.9678
	Temperature:CO2	0.0753	1	0.7837
	Timepoint:Temperature:CO2	26.5600	7	**0.0004**
Recovery	Timepoint	4.4963	3	0.7212
	Temperature	4.3216	1	**0.0376**
	CO2	0.0016	1	0.9680
	Timepoint:Temperature	87.9628	3	**< 0.0001**
	Timepoint:CO2	10.1081	3	0.1825
	Temperature:CO2	3.242	1	0.0718
	Timepoint:Temperature:CO2	17.8984	3	**0.0124**

Pocillopora acuta

Time Period	Effect	X^2	*df*	*P*
Stress	**Timepoint**	41.936	7	**< 0.0001**
	Temperature	0.0074	1	0.9312
	CO2	0.052	1	0.8196
	Timepoint:Temperature	57.1031	7	**< 0.0001**
	Timepoint:CO2	95.8169	7	**< 0.0001**
	Temperature:CO2	0.0231	1	0.8792
	Timepoint:Temperature:CO2	49.8236	7	**< 0.0001**
Recovery *(week 9-12)*	Timepoint	5.8895	3	0.1171
	Temperature	34.8274	1	**< 0.0001**
	CO2	3.9797	1	**0.0461**
	Timepoint:Temperature	1.2276	3	0.7464
	Timepoint:CO2	6.781	3	0.0792
	Temperature:CO2	0.0042	1	0.9485
	Timepoint:Temperature:CO2	0.509	3	0.9169

Table S6. Statistical output for calcification growth rates and color score for both species during the exposure and recovery period.

Survivorship Probability

Montipora capitata

Type III Anova	Effect	*df*	X^2	*P*
	Temperature	1	21.004	**< 0.0001**
	CO2	1	11.4891	**0.0007**
	Temperature:CO2	1	0.2914	0.5893

Cox mixed-effects model fit by maximum likelihood	Effect	*coef*	*exp(coef)*	*se(coef)*	*z*	*p*
Surv(lifespan, status) ~ Temperature * CO2 + (1|PLUG.ID/Tank)	**High Temperature**	1.1421189	3.133401	0.2492068	4.58	**< 0. 0001**
	High CO2	0.7981529	2.221434	0.2354737	3.39	**0.0007**
	High Temp: High CO2	0.1732892	1.18921	0.3210069	0.54	0.5900

	NULL	*Integrated*	*Fitted*
Log-likelihood	-7359.299	-5183.304	-4472.52

Pocillopora

Type III Anova	Effect	*df*	X^2	*P*
	Temperature	1	2.2173	0.1365
	CO2	1	40.5412	**< 0.0001**
	Temperature:CO2	1	79.9506	**< 0.0001**

Cox mixed-effects model fit by maximum likelihood	Effect	*coef*	*exp(coef)*	*se(coef)*	*z*	*p*
Surv(lifespan, status) ~ Temperature * CO2 + (1|PLUG.ID/Tank)	**High Temperature**	-0.9585059	0.383	0.6436949	-1.49	**0.1400**
	High CO2	-4.4442835	0.012	0.6979973	-6.37	**< 0.0001**
	High Temp: High CO2	7.8613358	2594.984	0.8791956	8.94	**< 0.0001**

	NULL	*Integrated*	*Fitted*
Log-likelihood	-24130.77	NaN	-18100.5

Table S7. Statistical output from survival probability models for both *M. capitata* and *P. acuta* throughout the entire experiment.

Species Comparison (all samples at Week 1)

Dependent Variable	*t*	*df*	*P*
Host total antioxidant capacity (TAC) CRE µmol (mg prot)$^{-1}$	3.7566	27.413	**0.0008**
Host soluble protein mg cm^{-2}	-1.0843	37.811	0.2851
Respiration (µmol cm^{-2} h^{-1})	1.2234	44.266	0.2276
Gross Photosynthesis (µmol cm^{-2} h^{-1})	-3.4385	44.001	**0.0013**
Net Photosynthesis (µmol cm^{-2} h^{-1})	-4.0388	40.851	**0.0002**
Net Photosynthesis (µmol cell^{-1} h^{-1})	-3.0230	37.777	**0.0045**
P:R Ratio	-3.2361	45.631	**0.0023**
Endosymbiont Density cells cm^{-2}	1.8842	229.730	0.0608
Chlorophyll-a concentration ug cm^{-2}	0.4576	33.717	0.6502
Chlorophyll-a concentration ug cell^{-1}	-0.1252	37.549	0.9011
Host AFDW mg cm^{-2}	1.2561	36.851	0.2170
Symbiont AFDW mg cell^{-1}	2.5909	30.642	**0.0145**
Symbiont AFDW mg cm^{-2}	2.8515	28.989	**0.0079**
Symbiont:Host Ratio AFDW	5.0694	34.066	**< 0.0001**

Table S8. Statistical output for baseline physiological measurement comparison between *M. capitata* and *P. acuta* fragments at the initial week 1 measurement.

STRESS PERIOD

PERMANOVA: Timepoint * Temperature * CO2 * Species

Effect	df	Sum of Squares	R2	F	Pr(>F)
Timepoint	4	203.56	0.07022	5.4788	**0.001**
Temperature	1	130.16	0.04490	14.0127	**0.001**
CO2	1	13.74	0.00474	1.4789	0.166
Species	1	298.93	0.10311	32.1831	**0.001**
Timepoint:Temperature	4	115.98	0.04001	3.1218	**0.001**
Timepoint:CO2	4	69.68	0.02404	1.8755	**0.008**
Temperature:CO2	1	9.13	0.00315	0.9830	0.403
Timepoint:Species	4	145.09	0.05005	3.9051	**0.001**
Temperature:Species	1	21.56	0.00744	2.3213	**0.029**
CO2:Species	1	13.25	0.00457	1.4270	0.209
Timepoint:Temperature:CO2	4	62.88	0.02169	1.6926	**0.033**
Timepoint:Temperature:Species	4	32.22	0.01111	0.8672	0.652
Timepoint:CO2:Species	4	36.75	0.01268	0.9892	0.456
Temperature:CO2:Species	1	3.11	0.00107	0.3350	0.936
Timepoint:Temperature:CO2:Species	4	33.88	0.01169	0.9119	0.545

Montipora capitata PERMANOVA: Timepoint * Temperature * CO2

Effect	df	Sum of Squares	R2	F	Pr(>F)
Timepoint	4	184.65	0.12682	4.2291	**0.001**
Temperature	1	39.29	0.02699	3.5995	**0.005**
CO2	1	20.27	0.01393	1.8574	0.091
Timepoint:Temperature	4	60.73	0.04171	1.3909	0.099
Timepoint:CO2	4	71.81	0.04932	1.6447	**0.036**
Temperature:CO2	1	5.78	0.00397	0.5298	0.792
Timepoint:Temperature:CO2	4	58.28	0.04003	1.3349	0.135

Pocillopora acuta PERMANOVA: Timepoint * Temperature * CO2

Effect	df	Sum of Squares	R2	F	Pr(>F)
Timepoint	4	171.63	0.12002	4.3344	**0.001**
Temperature	1	139.81	0.09777	14.1231	**0.001**
CO2	1	4.67	0.00326	0.4716	0.824
Timepoint:Temperature	4	117.25	0.082	2.9611	**0.001**
Timepoint:CO2	4	42.69	0.02985	1.0781	0.377
Temperature:CO2	1	8.25	0.00577	0.8334	0.487
Timepoint:Temperature:CO2	4	44.86	0.03137	1.133	0.314

RECOVERY PERIOD

Montipora capitata PERMANOVA: Timepoint * Temperature * CO2

Effect	df	Sum of Squares	R2	F	Pr(>F)
Timepoint	4	40.95	0.0711	2.5587	**0.013**
Temperature	1	46.70	0.0811	5.8358	**0.002**
CO2	1	5.56	0.0097	0.6945	0.621
Timepoint:Temperature	4	29.98	0.0521	1.8732	0.060
Timepoint:CO2	4	14.18	0.0246	0.8861	0.507
Temperature:CO2	1	2.39	0.0042	0.2987	0.921
Timepoint:Temperature:CO2	4	12.08	0.0210	0.7550	0.661

Table S9. Statistical output from a permutational multivariate ANOVA (PERMANOVA) on the multivariate physiology states for each species during the exposure and the recovery period for *M. capitata*.

ITS2

PERMANOVA: Timepoint * Temperature * CO2 * Species

Effect	*df*	*Sum of Squares*	*R2*	*F*	*Pr(>F)*
Timepoint	10	119.18	0.04767	1.3438	**0.023**
Temperature	1	4.44	0.00178	0.5008	0.898
CO2	1	9.38	0.00375	1.0575	0.394
Species	1	329.71	0.13188	37.1762	**0.001**
Timepoint:Temperature	10	92.17	0.03687	1.0392	0.384
Timepoint:CO2	10	81.46	0.03258	0.9184	0.699
Temperature:CO2	1	13.62	0.00545	1.5361	0.121
Timepoint:Species	10	95.53	0.03821	1.1968	0.119
Temperature:Species	1	4.52	0.00181	0.5100	0.859
CO2:Species	1	9.32	0.00373	1.0505	0.407
Timepoint:Temperature:CO2	10	45.77	0.01831	0.5160	1.000
Timepoint:Temperature:Species	10	88.20	0.03528	1.1050	0.230
Timepoint:CO2:Species	10	69.92	0.02797	0.8760	0.776
Temperature:CO2:Species	1	13.35	0.00534	1.5057	0.138
Timepoint:Temperature:CO2:Species	10	42.32	0.01693	0.5302	1.000

Montipora capitata PERMANOVA: Timepoint * Temperature * CO2

Effect	*df*	*Sum of Squares*	*R2*	*F*	*Pr(>F)*
Timepoint	10	107.80	0.10286	1.3377	**0.030**
Temperature	1	7.88	0.00752	0.9782	0.457
CO2	1	6.37	0.00608	0.7903	0.593
Timepoint:Temperature	10	94.42	0.09010	1.1717	0.161
Timepoint:CO2	10	68.68	0.06554	0.8523	0.810
Temperature:CO2	1	10.94	0.01044	1.3573	0.215
Timepoint:Temperature:CO2	10	42.76	0.04080	0.5306	1.000

Pocillopora acuta PERMANOVA: Timepoint * Temperature * CO2

Effect	*df*	*Sum of Squares*	*R2*	*F*	*Pr(>F)*
Timepoint	10	44.00	0.07458	0.9719	0.501
Temperature	1	2.25	0.00381	0.4469	0.795
CO2	1	7.63	0.01292	1.5159	0.191
Timepoint:Temperature	10	55.42	0.09394	1.2242	0.177
Timepoint:CO2	10	40.50	0.06865	0.8946	0.630
Temperature:CO2	1	10.59	0.01795	2.1055	0.068
Timepoint:Temperature:CO2	10	32.21	0.05460	0.7115	0.916

Table S10. Statistical output from a permutational multivariate ANOVA (PERMANOVA) on the ITS2 full type profiles for each species for the entire time series.

Species	Metric	Sept 18 2018	Oct 17 2018	Oct 31 2018	Nov 15 2018
Montipora capitata	Am	0.95 ± 0.196	0.98 ± 0.178	0.81 ± 0.150	0.91 ± 0.328
	AQY	0.01 ± 0.001	0.01 ± 0.001	0.01 ± 0.001	0.01 ± 0.003
	Ic	40.40 ± 5.467	40.96 ± 5.092	38.02 ± 5.459	25.38 ± 2.962
	Ik	164.08 ± 14.970	163.35 ± 22.658	126.51 ± 6.308	83.19 ± 7.270
	Rd	0.22 ± 0.041	0.23 ± 0.028	0.22 ± 0.034	0.25 ± 0.066
Pocillopora acuta	Am	1.19 ± 0.257	0.89 ± 0.144	0.50 ± 0.079	0.36 ± 0.120
	AQY	0.005 ± 0.001	0.005 ± 0.001	0.004 ± 0.001	0.004 ± 0.001
	Ic	64.40 ± 8.240	58.28 ± 4.172	54.16 ± 4.208	50.12 ± 20.932
	Ik	246.29 ± 26.716	190.53 ± 9.757	121.90 ± 5.651	95.21 ± 7.303
	Rd	0.30 ± 0.069	0.26 ± 0.038	0.21 ± 0.040	0.12 ± 0.031

Table S11. Photosynthetic curve output (mean ± standard error, n=4) for maximal photosynthetic rate (Am; µmol O_2 cm^{-2} h^{-1}), apparent quantum yield (AQY, ф; mol O_2 mol $photons^{-1}$), Compensation irradiance (IC; PAR), saturating irradiance (I_k; PAR), and light enhanced dark respiration rate (Rd; µmol O_2 cm^{-2} h^{-1}).